EXPERIMENTAL AND ANALYTICAL INVESTIGATIONS ON THE TORSIONAL BEHAVIOUR OF GLASS FIBRE - REINFORCED CONCRETE PONTOON DECKS

A Thesis submitted by

Xian Yang

MEngSci (Civil), BEng (Naval Architecture and Marine Engineering)

For the award of

Doctor of Philosophy

2024

THIS PAGE INTENTIONALLY LEFT BLANK

THIS PAGE INTENTIONALLY LEFT BLANK

ABSTRACT

This comprehensive research delves into the use of glass fibre - reinforced polymer (GFRP) bars as internal reinforcements in concrete pontoon decks, particularly in marine environments, to counter the corrosion issues of traditional steel reinforcements. Recognizing the gap in understanding the torsional behaviour of GFRP-reinforced structures, the study systematically investigates their response, especially under wave-induced torsional loads. Key findings from the first part of the study reveal that factors such as edge cutout, bar distribution, and rotation direction influence the torsional capacity and failure behaviour of GFRP-reinforced concrete structures (GFRP-RC) pontoon decks. Notably, double-layer reinforcement demonstrates better control over crack growth post-cracking compared to single-layer reinforcement, and edge cutout reduce cracking torque by around 17%. The study also finds that the ACI 318-19 equation accurately predicts the decks' torsional behaviour during the cracking stage. Further investigation highlights the role of diagonal bars, reinforcement arrangement, and grid spacing. It shows that diagonal reinforcements in double-layer setups and denser grids considerably improve both pre- and post-cracking torsional behaviour, with some configurations matching the torsional resistance of solid decks. The third research includes extensive finite element (FE) analyses validated by large-scale laboratory tests, covering aspects like concrete strength, cutout geometry, and reinforcement configurations. These analyses underscore the critical impact of concrete strength and reinforcement configuration on torsional behaviour, while the influence of cutout geometry is less pronounced. Predictive equations developed for torsional rigidity and cracking torque show a good correlation with FE results. Overall, this study offers vital insights for the design and optimization of GFRP-reinforced concrete pontoon decks, emphasizing the importance of strategic reinforcement configurations and deck geometries. These findings are crucial for enhancing the structural integrity and durability of such decks against the challenges posed by wave-induced torsion.

Key words: GFRP, reinforced concrete pontoon decks, torsion, cutout, concrete compressive strength, reinforcement configurations, torsional rigidity, cracking torque, failure, finite element analysis, parametric study, design equation.

CERTIFICATION OF THESIS

I, Xian Yang, declare that the PhD Thesis entitled *"Experimental and analytical investigations on the torsional behaviour of glass fibre - reinforced concrete pontoon decks"* is not more than 100,000 words in length including quotes and exclusive of tables, figures, appendices, bibliography, references, and footnotes.

This Thesis is the work of Xian Yang except where otherwise acknowledged, with the majority of the contribution to the papers presented as a Thesis by Publication undertaken by the student. The work is original and has not previously been submitted for any other award, except where acknowledged.

Signed:

Xian Yang Date: 05/01/2024

Endorsed by:

Prof. Allan Manalo

Principal Supervisor

Dr. Omar Saleh Awad Alajarmeh

Associate Supervisor

Dr. Zahra Gharineiat

Associate Supervisor

Student and supervisors' signatures of endorsement are held at the University.

STATEMENT OF CONTRIBUTION

The articles produced from this study were a joint contribution of the authors. The details of the scientific contribution of each author are provided below:

Manuscript 1:

Xian Yang, Omar Alajarmeh, Allan Manalo, Brahim Benmokrane, Zahra Gharineiat, Shahrad Ebrahimzadeh, Charles-Dean Sorbello, and Senarath Weerakoon, *Torsional behaviour of GFRP-reinforced concrete pontoon decks with and without an edge cutout*. Marine Structures, 2023. 88: p. 103345. (Impact factor: 3.9; Cite Score 7.6)

DOI: https://doi.org/10.1016/j.marstruc.2022.103345

The overall contribution of Xian Yang was 60% related to the data collection, critical review of related literature, analysis and interpretation of data, drafting and revising the final submission. Allan Manalo, Omar Alajarmeh, Brahim Benmokrane, Zahra Gharineiat, Shahrad Ebrahimzadeh, Charles-Dean Sorbello, and Senarath Weerakoon contributed to structuring of the manuscript, analysis and interpretation of data, editing and providing important technical inputs.

Manuscript 2:

Xian Yang, Omar Alajarmeh, Allan Manalo, Brahim Benmokrane, Zahra Gharineiat, Shahrad Ebrahimzadeh, Charles-Dean Sorbello, and Senarath Weerakoon, *Torsional Behavior of GFRP-RC Pontoon Decks with an Edge Cutout and Diagonal Reinforcements.* Structures. (Under review) STRUCTURES-D-23-05265 (Impact factor: 4.1; Cite Score 4.7)

The overall contribution of Xian Yang was 65% related to the data collection, critical review of related literature, analysis and interpretation of data, drafting and revising

the final submission. Allan Manalo, Omar Alajarmeh, Brahim Benmokrane, Zahra Gharineiat, Shahrad Ebrahimzadeh, Charles-Dean Sorbello, and Senarath Weerakoon contributed to the structuring of the manuscript, analysis and interpretation of data, editing and providing important technical inputs.

Manuscript 3:

Xian Yang, Omar Alajarmeh, Allan Manalo, Brahim Benmokrane, Zahra Gharineiat, Shahrad Ebrahimzadeh, Charles-Dean Sorbello, and Senarath Weerakoon, *Torsional behavior in GFRP-RC pontoon decks with edge cutout - Study of critical design parameters.* Engineering Structures (submitted). ENGSTRUCT-D-24-00096. (Impact factor: 9.2; Cite Score 5.5)

The overall contribution of Xian Yang was 70% related to the data collection, critical review of related literature, analysis and interpretation of data, drafting and revising the final submission. Omar Alajarmeh, Allan Manalo, Brahim Benmokrane, Zahra Gharineiat, Shahrad Ebrahimzadeh, Charles-Dean Sorbello, and Senarath Weerakoon contributed to the structuring of the manuscript, analysis and interpretation of data, editing and providing important technical inputs.

ACKNOWLEDGEMENTS

Reflecting on my Ph.D. journey, I am filled with immense gratitude for those who have played a pivotal role in this endeavour. Foremost, I thank my parents, whose unwavering love and support have been fundamental to my achievements. Your constant encouragement and strength have been invaluable, making this accomplishment as much yours as mine.

I owe a deep sense of gratitude to my principal supervisor, Allan Manalo, for his indispensable guidance, patience, and expertise. Your mentorship has significantly shaped my academic and professional growth. My associate supervisors, Omar Alajarmeh and Zahra Gharineiat, and external mentor, Prof Brahim Benmokrane, have provided invaluable insights and feedback, contributing greatly to the refinement and success of my research.

Special appreciation is extended to my industry supervisors, Charles-Dean Sorbello and Senarath Weerakoon. Your practical insights and expertise have crucially linked academic research with real-world applications, enhancing the quality and relevance of my work.

I am also deeply thankful to our industrial partners, including the Queensland Department of Transport and Main Roads (DTMR), the Advance Queensland Industry Research Fellowship Program (AQIRF 119-2019RD2), and the Natural Science and Engineering Research Council (NSERC) of Canada. Their generous financial support has been pivotal in advancing our research. Sustainable Alliance Pty Ltd (Inconmat) and Jetty Specialist have been keying in providing essential materials and expertise.

Further, I acknowledge my colleagues, technicians, and students at the Centre for Future Material. Your collaboration, dedication, and enthusiasm have been indispensable, greatly enriching my research experience.

In conclusion, this Ph.D. journey has been a collaborative effort, made successful by the collective wisdom, support, and cooperation of everyone involved. I am profoundly grateful to all for making this journey both memorable and successful.

TABLE OF CONTENTS

LIST OF TABLES

Note: Tables that appear in the thesis chapters of published/submitted papers are **not** included.

LIST OF FIGURES

Note: Figures that appear in the thesis chapters of published/submitted papers are **not** included.

CHAPTER 1: INTRODUCTION

1.1. Background and motivation

Reinforced concrete (RC) structures, widely used in Australia and globally in various environments including marine settings, require detailed design to guarantee safety and longevity. However, challenges such as inadequate concrete cover, subpar design or workmanship, along with environmental aggressors like seawater, high moisture, and temperature, contribute to concrete cracking and steel reinforcement corrosion. A notable report by Shayan and Xu (2016) revealed a significant reduction in the service life of RC bridges and other infrastructures, dropping to just 30 years due to these issues, despite being originally designed for at least a century of service. Particularly in coastal regions, corrosion of internal steel reinforcements (refer to Figure 1.1) poses a severe problem for steel RC structures. For instance, in Queensland, the annual cost for repairing, rehabilitating, and maintaining boating infrastructure damaged by corrosion is approximately AU$10 million (Manalo et al. 2021). This underscores the critical need for constructing highly durable reinforced concrete structures that can maintain their safety and functionality throughout their intended service lives.

Figure 1.1. Reinforcement corrosion of marine infrastructures (Ramesht & Tavasani 2013)

Over recent decades, fibre-reinforced polymer (FRP) has emerged as an effective substitute for traditional steel bars in reinforcing concrete structures, thanks to its high strength, lightweight, and non-corrosive properties. Among FRP materials, glass fibre-reinforced polymer (GFRP) composites are particularly favoured in civil infrastructure due to their cost-effectiveness compared to other types, such as carbon, aramid, and basalt (Mohamed & Benmokrane 2015). Numerous field applications have successfully demonstrated the efficiency of GFRP bars in various reinforced concrete structures, including bridge decks, road pavements, and storage tanks (Ahmed et al. 2014; Mohamed & Benmokrane 2014; Benmokrane et al. 2020). In Australia, transport authorities and asset owners are increasingly recognizing the significant benefits of utilizing GFRP bars in concrete structures situated in marine environments (Manalo et al. 2021). Consequently, there is a growing need for innovative developments and applications to demonstrate the sustainable advantages of using GFRP bars as reinforcements in concrete boating and marine infrastructure.

Floating walkway modules, extensively utilized in boating tourism across Queensland and Australia, have significantly advanced the industry. These modules typically function as landing decks alongside other boating facilities or operate independently. As they float on the sea surface, piles are inserted through edge cutout on the concrete decks for stabilization. According to design criteria set by Department of Transportation and Main Road (DTMR 2015), it is mandatory for piles to be situated within flotation modules, making edge cutout on the concrete decks an essential feature of their design.

The concrete decks of these floating modules are increasingly reinforced with GFRP bars, but proprietary designs by pontoon suppliers have led to variations in their performance and durability. Torsional stress becomes a significant factor in reinforced

concrete decks under concentrated loads or when reaction forces are at the corners (Lopes et al. 2014). Precast reinforced concrete pontoon decks, typically exposed to wave actions and other service loads, often experience torsion. This torsion leads to a rotation in the cross-section, causing inclined cracks that usually start from the edge cutout on the concrete surface. While the use of non-corrosive reinforcements like GFRP bars can prevent corrosion from seawater ingress through these cracks, there is currently no design methodology specifically addressing the torsional behaviour of pontoon decks reinforced with GFRP bars.

Research on torsional behaviour in rectangular RC structures, particularly GFRP-reinforced concrete beams and steel-reinforced slabs, has shown a link with concrete strength, reinforcement configuration, and cross-sectional aspect ratio (Lopes & Bernardo 2009; Lee & Kim 2010; Lopes et al. 2014; Derkowski & Surma 2015; Mohamed et al. 2015; Mohamed & Benmokrane 2016; Mostafa et al. 2023). While reinforcement has limited impact on pre-cracking behaviour, similar to plain concrete where cracking torque depends on concrete strength and aspect ratio, it significantly influences post-cracking behaviour. Torsional failures in beams vary from brittle and ductile to crushing of concrete compressive struts, based on reinforcement quantity (Joh et al. 2019; Ju et al. 2020). Ibrahim et al. (2020) noted that beams with thick concrete cover fail mainly due to spalling, with ultimate capacity close to the initial crack. Torsional cracks often originate from edge cutouts in pontoon decks, especially near marine piles (see Figure 1.2), and occur earlier in decks with edge cutouts. In steel-reinforced concrete structures, diagonal reinforcements around cutouts can control these cracks (Mansur et al. 1983; Popescu et al. 2017), but the effectiveness of this method in GFRP-reinforced decks under torsion remains unexplored. Moreover, the crack initiation and propagation varied due to different rotation direction as the

deck with cutout has unsymmetrical geometry. A detailed study of all those factors is essential to understand in depth knowledge of torsional behaviour of GFRP-reinforced pontoon decks.

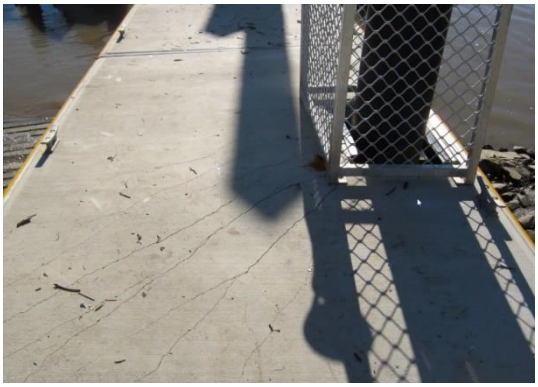

Figure 1.2. Torsional damages initiated from cutout

In this study, the behaviour of precast reinforced concrete (RC) pontoon decks using GFRP bars under torsion was investigated experimentally and numerically. Large-scale precast concrete pontoon deck specimens for floating walkway modules were tested to investigate the effect of pontoon deck geometry (cut-outs for marine piles) and reinforcement configurations (single/double layers, and diagonal bars as reinforcement). The effect of these parameters on the torsional capacity and stiffness, cracking propagation and failure behaviour were evaluated. Finite element analysis (FEA) was then implemented to simulate the behaviour of the tested pontoon decks, which was extended to conduct a parametric study on the effect of critical design parameters including concrete compressive strength, cutout geometry, and reinforcement configuration. Design equations to reliably predict the torsional behaviour of GFRP-RC pontoon deck were also developed. The knowledge and data that generated from this study are useful in the effective design and in the development of specifications for GFRP reinforcements required for concrete decks of floating walkway modules subject to wave loading actions.

1.2. Objectives

The main objective of this research is to investigate the behaviour of GFRP-reinforced precast concrete pontoon decks with edge cut out under pure torsional load. It focuses on identifying the effects of geometric parameters and reinforcement details on the torsional behaviour of the pontoon decks. It also aims to develop a procedure for the safe and reliable design of GFRP-RC pontoon decks under torsion. The specific objectives of the study were identified to achieve the main aim of the study:

1. To experimentally investigate the effect of a square edge cut out, reinforcement distribution and rotation direction on torsional behaviour of GFRP-RC pontoon decks.
2. To experimentally evaluate the effect of reinforcement arrangement on the torsional behaviour of GFRP-RC pontoon decks with edge cut out and diagonal reinforcement bars.
3. To numerically discover the effects of critical design parameters on torsional behaviour of GFRP-RC pontoon decks and to develop simplified design equations that can reliably describe the torsional resistance in GFRP-RC pontoon decks.

1.3. Study limitations

This study investigated the torsional behaviour of GFRP-RC pontoon decks with and without cutout. The design of the pontoon decks followed the Queensland's Departments of Transport and Main Road's (TMR) design criteria for floating walkways and pontoons (DTMR 2015) with a fixed dimension of 1500mm wide, 2400mm long, and 125mm thick. A 300mm square cutout was centrally located on the longer side. The reinforcements used in this study are high modulus sand-coated GFRP

reinforcements made by pultrusion process same as the production used by AlAjarmeh et al. (2019) and investigated by Benmokrane et al. (2017). All decks were manufactured using normal strength concrete containing Ordinary Portland Cement, and fine and coarse aggregates. They were casted in TMR-approved pontoon supplier, Jetty Specialist, in Sunshine Coast, Australia. All mechanical properties of the materials used, and the test methods are detailed in each study.

The data from these tests, conducted in the mechanical test laboratory of the Centre for Future Material, was bound to the test conditions and evaluated in accordance with relevant test standards. For instance, the maximum twist in the specimens reached 0.075 rad/m, limited by the 85mm stroke of the hydraulic jack. Yet, this range was sufficient to cover both pre-cracking and post-cracking stages of the decks' torsion-twist response. To ensure accurate deflection recording, three measurement methods were employed: LVDT, laser measurer, and digital image correlation. Therefore, despite these limitations, the results obtained are reliable and provide valuable insights that can be applied to future studies.

1.4 Thesis organisation

This thesis comprises 6 chapters as follows:

- **Chapter 1** is the general **Introduction** for the background and motivation of all the works done in this thesis.
- **Chapter 2** provides an extensive **Literature review** throughout the field of torsional behaviour of reinforced concrete structures and identifies the research gap.

- **Chapter 3** is the first technical chapter in which the torsional behaviour of GFRP-RC pontoon deck with and without an edge cutout was physically tested and reported.
- **Chapter 4** is the second technical chapter in which the effect of reinforcement arrangement on the torsional behaviour of GFRP-RC pontoon deck with an edge cutout and diagonal reinforcement bars was analysed experimentally.
- **Chapter 5** is the third technical chapter in which a parametric study for torsional behaviour of GFRP-RC pontoon deck was conducted based on a finite element model and validated with experimental data. Design equations to reliably describe the torsional behaviour of GFRP-RC pontoon deck was established.
- **Chapter 6** is the **Conclusion** of the thesis, reviewing the work has been done by the authors, and highlighting the significant findings from the research work. Suggestions for future work on this topic was provided.

The outcomes of this thesis contributed to the publication of three journal articles in high-quality (first quartile Q1) international journals. The three journal articles are published or are currently under review as listed below. In addition, the candidate published and presented conference papers that reflect the research's impact and scope in national and international conference. Moreover, the candidate contributed to two publication papers that related to the thesis's scope as co-authors. The Abstracts of the conference papers and publications are provided for further reference in Appendix B.

Manuscript 1:

Xian Yang, Omar Alajarmeh, Allan Manalo, Brahim Benmokrane, Zahra Gharineiat, Shahrad Ebrahimzadeh, Charles-Dean Sorbello, and Senarath Weerakoon, *Torsional*

behaviour of GFRP-reinforced concrete pontoon decks with and without an edge cutout. Marine Structures, 2023. 88: p. 103345. (Impact factor: 3.9; Cite Score 7.6)

DOI: https://doi.org/10.1016/j.marstruc.2022.103345

This manuscript addressed the first objective of this thesis where the effect of edge cutout, reinforcement distribution and rotation direction on the torsional behaviour of the GFRP-RC pontoon decks are evaluated. It details experimental analyses of five GFRP-RC pontoon decks, focusing on pre-cracking torsional rigidity, cracking torque, post-cracking torsional rigidity, and maximum torsional strength. Comparisons are made to existing design equations for cracking torque from the literature and current standards. Additionally, this study proposes a simplified approach for predicting the post-cracking torsional response of GFRP-RC pontoon decks. Findings confirm the negative impact of edge cutout on the torsional performance and show that double-layer mesh reinforcement enhances crack control and post-cracking performance. Rotation direction is a neglectable factor in the torsional behaviour. Furthermore, it identifies simple equations for estimating the cracking torque and post-cracking torsional rigidity.

Manuscript 2:

Xian Yang, Omar Alajarmeh, Allan Manalo, Brahim Benmokrane, Zahra Gharineiat, Shahrad Ebrahimzadeh, Charles-Dean Sorbello, and Senarath Weerakoon, *Torsional Behavior of GFRP-RC Pontoon Decks with an Edge Cutout and Diagonal Reinforcements.* Structures (under review). STRUCTURES-D-23-05265. (Impact factor: 4.1; Cite Score 4.7)

This manuscript addressed the second objective of this thesis by evaluating the impact of diagonal reinforcement around edge cutouts, bar arrangement, and grid spacing in

GFRP-bar-reinforced concrete pontoon decks. Through experimental investigation, the study tested large-scale pontoon decks with edge cutouts to observe the effects of these variables. The data showed that diagonal reinforcement significantly improves pre-cracking torsional stiffness, particularly when applied in a double-layered reinforcement scheme. Notably, when the reinforcement grid spacing was reduced to 100 mm, the post-cracking torsional rigidity surged by 137% compared to decks with a 250 mm grid spacing, aligning the performance of these decks with that of double-layered reinforced solid decks. The study introduces predictive equations that effectively estimate cracking torque and post-cracking torsional behavior, taking into account the effective width from diagonal bars and the longitudinal GFRP bars' contributions.

Manuscript 3:

Xian Yang, Omar Alajarmeh, Allan Manalo, Brahim Benmokrane, Zahra Gharineiat, Shahrad Ebrahimzadeh, Charles-Dean Sorbello, and Senarath Weerakoon, *Torsional behaviour in GFRP-RC pontoon decks with edge cutout - Study of critical design parameters.* Engineering Structures (submitted). ENGSTRUCT-D-24-00096. (Impact factor: 9.2; Cite Score 5.5)

This manuscript addressed the third objective of this thesis by numerically explored the effect of various design parameters, including concrete compressive strength, cutout geometry, reinforcement configuration both within the deck and the cutout on the torsional behaviour of GFRP-RC pontoon decks. A total of 27 finite element models simulating GFRP-RC pontoon decks with various design parameters in torsion were built and analysed. The pre-cracking torsional behaviour of the deck is significantly affected by the levels of concrete compressive strength with the reinforcement configuration influenced to some degree the cracking torque. The cutout geometry has

no effect of the pre-cracking torsional behaviour. The GFRP reinforcement has only a minor effect on the first cracking torque but more than four sets diagonal bars, large bar diameter and dense reinforcement space in each direction all have positive effect on increasing the deck's post-cracking torsional rigidity. The proposed equations can reliably predict the pre-cracking torsional strength and rigidity of GFRP-RC decks by considering the concrete compressive strength and geometric properties of the decks.

1.5. Summary

This research develops new knowledge to help address the limited understanding on the torsional behaviour of GFRP-reinforced concrete (GFRP-RC) pontoon decks, particularly those with an edge cutout. Utilizing both experimental and analytical approaches, including large-scale specimen tests and finite element method (FEM), the study explores the effect of various design parameters such as concrete compressive strength, cutout presence and geometry, and reinforcement configuration. The findings are documented in three technical journal papers, forming the technical chapters of this thesis. The aim is to develop design equations for accurately predicting the torsional behaviour of GFRP-RC pontoon decks. The insights and data obtained will significantly contribute to the future development of design specifications for GFRP reinforcements to future proof marine infrastructure.

CHAPTER 2: LITERATURE REVIEW

2.1. Introduction

The study of torsional behaviour in reinforced concrete (RC) structures, a pivotal component in structural engineering, involves analysing distinct phases: pre-crack, post-crack, and failure behaviour. This review chapter delves into these stages, aiming to identify key factors influencing torsional responses and to explore both traditional analytical theories and the application of Finite Element Method (FEM) in the context of RC structures. A significant focus is placed on the torsional behaviour of Glass Fibre - reinforced Polymer (GFRP) reinforced concrete structures. GFRP reinforcements, known for their non-corrosive properties and unique elastic characteristics, exhibit torsional responses that differ markedly from traditional steel reinforcements, especially due to the absence of yielding. This divergence highlights the necessity for in-depth research and the development of tailored design criteria for GFRP-RC structures.

As introduced in the first chapter, this thesis addresses the challenge of torsional damage in GFRP-RC pontoon decks, which are particularly susceptible to torsional stresses from wave actions in marine environments. The insights gained from this chapter are instrumental in identifying and bridging knowledge gaps in the field. Addressing these gaps is crucial for enhancing the field and ensuring the effective and safe design of GFRP-RC decks across a spectrum of engineering applications.

2.2. Torsional behaviour of reinforced concrete structures

The overall behaviour of RC structure consists of three distinct phases: pre-crack, post-crack and steel yielding (Lopes et al. 2014). Pre-crack refers to the status of RC structure when the first concrete crack has not been exhibited. After the first crack and

before the failure, the structure behaviour is in the post-crack phase. As the strain increases in the reinforcement, traditional reinforcement will yield, but, for GFRP reinforced concrete structure, yield of reinforcement will not happen because of GFRP material's elasticity. The last phrase will be determined by the failure that occurs to either concrete or GFRP reinforcement.

2.2.1. Pre-crack behaviour of reinforced concrete structure under torsion

Before the first crack, reinforced concrete structures could be considered as elastic material which response linearly to torsional force. Many researchers found a linear response before the first crack under torsional force in various reinforced concrete structures such as circular hollow column, square slab, circular concrete-filled FRP tubes, and reinforced L-shape beams, regardless of their reinforcement material and configuration (Deifalla et al. 2014; Anumolu et al. 2016; Nguyen & Pham 2017; St. Onge & Fam 2021). For example, six reinforced concrete beams with the same dimensions of 400 mm deep and 200 mm wide, and with three types of reinforcement configurations including rectangular spiral GFRP stirrup, regular GFRP stirrup and no transverse reinforcement were investigated for torsional behaviour in a study reported by Hadhood et al. (2020). The torque and twist curves for the six beams presented almost identical initial stiffness with a linear response before the first crack. In another study, the torsion behaviour of five 250 mm wide and 600 mm deep reinforced concrete beams were investigated to evaluate the effect of type and spacing of reinforcements (Mohamed et al. 2015). Experimental results indicated all the beams exhibited similar linear torque-twist behaviour before the occurrence of the first crack. The high initial stiffness of reinforced concrete members as reflected by the low twist angles in the pre-crack phrase is mainly provided by the concrete. This observation is supported by an experimental study implemented by comparing the torque and twist

behaviour between steel reinforced beams and plain concrete beams as shown in Figure 2.1 (Okay & Engin 2012). The torque-twist curve initiated from (0, 0) and linearly extend to (T_{cr}, ϕ_{cr}) which refer to cracking torque and the cracking twist respectively. T_u, and ϕ_u refer to the maximum torque achieved and the corresponding twist respectively. T_u, & ϕ_u refer to the final torque when reinforcement failure reached and the corresponding twist, respectively.

According to the theory of elasticity , the maximum shear stress occurs at the centre of the long face of the rectangular section subjected to pure torsion (Hsu, T. T. 1968). The cracking happens when the shear stress exceeds the concrete's tensile stress. Accordingly, the initial cracking strength depends on the concrete compressive strength and member's dimension.

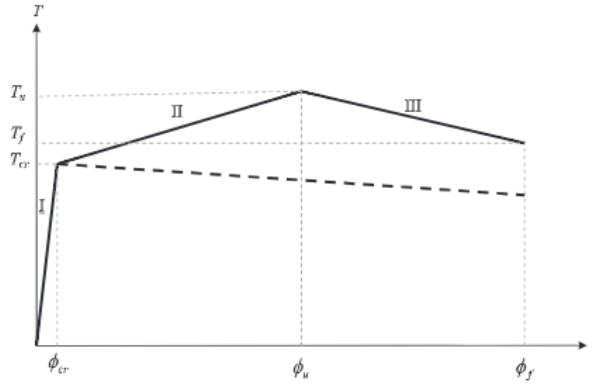

Figure 2.1. Proposed torsional behaviour model for reinforced concrete beams with/without steel (Okay & Engin 2012)

2.2.2. Post-cracking behaviour of reinforced concrete under torsion

The torsional behaviour of reinforced concrete transfers from linear to nonlinear after cracking. The structure repeatedly suffers a sudden increase of twists while the torque does not change too much. This can be explained that the concrete is losing its torsional resistance as the concrete is cracking. The widening cracks lead to larger deformation while no more loadings are resisted by the whole structure. The torsional

resistance now exists in the concrete core and torsion reinforcement (Bernardo & Lopes 2008). In concrete beams, this torsional behaviour is reflected in the torque-twist curve with a segment of horizontal line (Bernardo & Teixeira 2018). On the other hand, the segment of torque – twist curve which is presented by a jagged curve and gentle slope is caused by the development of more and wider cracks happening intermittently after the first concrete crack (Okay & Engin 2012; Jeng et al. 2014; Chai et al. 2015; Xu et al. 2018; Ibrahim et al. 2020). These researchers further indicated that the concrete structures' torsion stiffness will last longer during and after the crack when strong reinforcements are embedded. However, they have also indicated that it is hard to predict the torsional behaviour of the reinforced concrete structures in this cracking period.

The post-crack torsional behaviour of reinforced concrete structures remains linear after the cracking period. Concrete confinement provided by the stirrups and the longitudinal reinforcement both contribute to the torsional stiffness in this phrase. The influence of concrete in this phrase is too small and can be neglected in the analysis. The torsional resistance is mainly owing to the reinforcement whose elasticity will decide whether the reinforced concrete structure behaves linearly or non-linearly after crack. To illustrate, torque-twist curves in Figure 2.2 show that the linear post-crack torsional behaviour indicated a constant torsional stiffness in GFRP reinforced concrete beams (Mohamed & Benmokrane 2016). Many researchers related the post-crack torsional stiffness to the reinforcement's tensile strength and configurations (Deifalla et al. 2014; Anumolu et al. 2016; Nguyen & Pham 2017; St. Onge & Fam 2021).

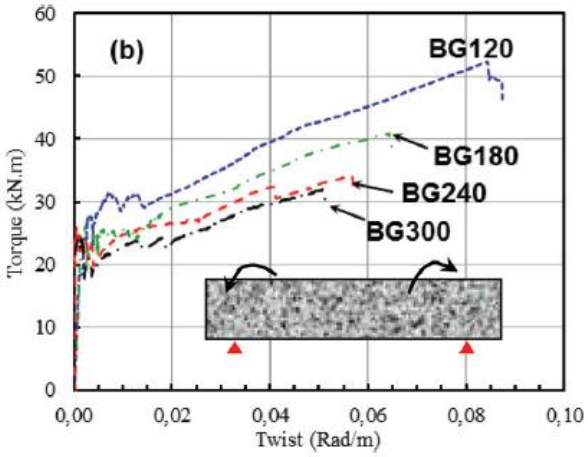

Figure 2.2. Torque - twist curves for concrete beams with variable reinforcement space (Mohamed & Benmokrane 2016)

2.2.3. Failure of reinforced concrete under torsion

The failure of reinforced concrete under torsion can occur either in the concrete or the reinforcement. Chen et al. (2018) evaluated the failure behaviour of steel reinforced concrete columns subject to combined bending – torsion cyclic loading. Other than the horizontal flat tensile cracks, a typical torsion failure was observed due to the appearance of 45 - degree diagonal cracks that distributed over the structure's whole surface. When the structures approach failure, these diagonal cracks can lead to concrete crushing (Ameli et al. 2007) or a wide crack width to separate the member into two independent bodies (Mohamed et al. 2015). The torsional failure of concrete beams with a higher amount of reinforcements is due to concrete crushing followed by the failure of reinforcement (Ju et al. 2020) while the concrete beams with a low amount of reinforcement failed when two independently rotating segments are developed (Joh et al. 2019). These studies shows that several parameters affect the torsional behaviour of GFRP reinforced concrete structures. The experimental test setup employed to investigate the torsional behaviour of reinforced concrete structures is explored and presented in Appendix A.

2.3. Design parameters affecting torsional behaviour

The design parameters that dominate the torsional behaviour of reinforced concrete structures vary throughout the three phases. Geometric parameters of specimen's cross section and concrete strength are highly concerned in pre-crack torsional behaviour of the reinforced concrete structure while reinforcement configuration and reinforcement property determine post-crack torsional behaviour. Failure mode in the third phase is influenced by the combined effect of geometric parameters, concrete strength and reinforcement configurations. More descriptions of the influence of these design parameters on the torsional behaviour of reinforced concrete structures is provided in the succeeding sections.

2.3.1. Influence of concrete strength

Concrete strength, typically measured by its compressive capacity, plays a pivotal role in determining the torsional performance of RC elements. In the pre-cracking phase, higher concrete strength generally results in increased initial stiffness and torsional resistance. This is because the material's inherent ability to withstand stress without cracking is directly linked to its compressive strength. Structures made from high-strength concrete exhibit greater resistance to the formation of initial cracks under torsional loads. Research indicates that beams made from higher strength concrete show lower twist angles in the pre-crack phase, suggesting a direct correlation between concrete strength and initial torsional rigidity (Rahal 2013; Mostafa et al. 2023). Upon the onset of cracking, the role of concrete strength becomes even more pronounced. While the transition from pre-cracking to post-cracking behaviour introduces complexity, the higher strength concrete continues to provide substantial resistance against torsional deformation. The higher the compressive strength, the more the concrete can contribute to the overall torsional stiffness of the structure, even

after initial cracking. This contribution is particularly crucial in the post-cracking phase where the torsional resistance is not solely dependent on the reinforcement but is also significantly influenced by the surrounding concrete matrix (Fang & Shiau 2004). Moreover, concrete strength influences the ultimate torsional capacity of RC structures. Beams with higher strength concrete tend to exhibit greater ultimate torsional strength. This is attributed to the material's enhanced capacity to withstand higher stresses and delay the progression of failure mechanisms, such as diagonal cracking and concrete crushing. Generally, the strength of concrete is a key determinant in the torsional behaviour of RC structures. It affects the initial stiffness, crack resistance, post-crack behaviour, and ultimate torsional capacity, underscoring the importance of considering concrete strength in the design and analysis of RC structures subjected to torsional loads.

2.3.2. Influence of reinforcement configuration

The configuration of reinforcement in RC structures significantly influences their torsional behaviour, particularly in the post-crack stage. Reinforcement configuration encompasses the type, placement, amount, and orientation of steel or FRP bars within the concrete matrix. In the pre-crack phase, the configuration of reinforcement has a limited impact on torsional behaviour as the concrete's intact structure primarily resists torsional forces. However, once cracking occurs, the reinforcement's role becomes pivotal. The distribution and orientation of reinforcement, especially transverse stirrups, and longitudinal bars, greatly affect the structure's capacity to resist further twisting and crack widening. Closely spaced stirrups and adequately arranged longitudinal reinforcement enhance the torsional stiffness and strength post-cracking by effectively confining the concrete and bridging the cracks (Kim et al. 2020; Lei et al. 2023). Moreover, the type of reinforcement material influences the torsional

response. For instance, GFRP bars, behave differently compared to steel reinforcement under torsional loads due to their lower modulus of elasticity and lack of yielding behaviour (Mohamed & Benmokrane 2015). The density of reinforcement (reinforcement ratio) also plays a crucial role. A higher reinforcement ratio usually increases the torsional capacity and rigidity of the structure but may lead to more brittle failure modes. Furthermore, the geometric arrangement of reinforcement, such as the use of closed-loop stirrups versus open stirrups, impacts the effectiveness of torsional resistance (Mohamed et al. 2015).

In summary, reinforcement configuration is a critical factor in the torsional performance of RC structures. It determines how well the structure can respond to torsional forces, especially after cracking, influencing both the stiffness and ultimate strength under torsional loads. Proper design, considering the type, placement, and amount of reinforcement, is essential for ensuring the desired torsional behaviour of RC structures.

2.3.3. Influence of bar diameter

The diameter of GFRP bars significantly influences the cracking pattern and overall structural performance of reinforced concrete structures. According to (El-Nemr et al. 2013; 2018), sand-coated GFRP bars, favoured for their strong bond performance due to a uniform sand particle surface, induce multiple cracks along the GFRP-RC beam's length but maintain narrower widths. This distribution of narrow cracks is advantageous for structural integrity, as it evenly disperses stress, thus enhancing the structure’s durability and reducing the likelihood of sudden failure. In contrast, smaller diameters of GFRP bars are prone to wider cracks. This finding, identified in the study of El-Nemr et al. (2013), indicates a potential vulnerability in structural performance, especially under flexural stress. However, Maranan et al. (2015) observed that the

flexural performance of beams was not significantly impacted by the diameter of GFRP bars, provided the elastic modulus remained constant. This suggests that while bar diameter influences crack width, other factors like material elasticity play a crucial role in flexural behaviour. El-Nemr et al. (2018) proposed a solution to the issue of wider cracks associated with smaller bar diameters: denser reinforcement. By increasing the density of the reinforcement, the adverse effects of smaller bar diameters can be mitigated, leading to a more robust and reliable structural performance in GFRP-reinforced concrete structures. This approach underscores the importance of not just the material properties, but also the reinforcement layout and density in designing efficient and durable reinforced concrete structures.

2.3.4. Influence of opening in concrete members

The opening in concrete structures can reduce structural stiffness and strength. The amount of reduction increases as the size of the opening is getting larger (Anil et al. 2014; Khajehdehi & Panahshahi 2016; Popescu et al. 2017; Yousef et al. 2019). A longer distance from the opening to the loading point weakens the stiffness reduction effect of the surface opening (Genikomsou & Polak 2017). A number of researchers have used FRP composites to strengthen concrete slabs with openings. Pachalla and Prakash (2017) showed that GFRP reinforcement can effectively increase the ultimate flexural and shear strength of hollow slabs with inner opening. Similarly, bonding carbon FRP (CFRP) components around the edges of the cut out in two way slabs' have increased the capacity up to 121% (Floruţ et al. 2014).

Investigation on the effect of opening on torsion is limited for steel RC beam structures. Hollow beams, considered as opening in the concrete core, was reported to have similar levels of initial torsion stiffness to solid reinforced beam (Kim et al. 2020). These authors have also indicated that the hollow beam had higher torsional stiffness and

peak torsional strength after the first torsional crack. Moreover, RC beams with inner opening in wide face showed initial torsional stiffness decreased corresponding to longer opening but the post crack stiffness was independent of the opening (Mansur et al. 1983). This decrease in capacity and stiffness is due to the concentrated stress on the corner of the opening promoting the first crack. The proposed diagonal reinforcements around the corner are anticipated to control the crack propagation and width for concrete structures under torsion.

2.2.5. Influence of rotational direction

The direction of rotation plays a subtle yet important role in determining the torsional behaviour of RC structures. Research has shown that although the overall torsional strength and failure patterns of RC structures are largely consistent, the direction in which the structure is rotated can influence the initiation and progression of cracks. In cases where reinforcement is asymmetric or the structure has an irregular shape, the rotation direction can lead to different stress distributions, thus affecting where and how cracks develop (Hussein & Eid 2019). Understanding the effects of rotation direction is crucial in the accurate modelling and analysis of torsional behaviour, particularly in complex or asymmetric structures. It assists in predicting potential vulnerabilities and optimizing reinforcement design to ensure balanced stress distribution and improved structural integrity.

2.4. Theories to evaluate torsional behaviour

Numerous analytical theories and equations have historically been developed, targeting different structural scenarios such as homogenous members, plain concrete, and reinforced concrete structures. Specifically, the theories and equations for the torsional behaviour of reinforced concrete structures are often centred on beams with

stirrups, each possessing distinct advantages and drawbacks. The upcoming sections will delve into the evolution of these analytical concepts and equations, as revealed through an extensive review of the literature.

2.4.1. Torsion in homogeneous members

Navier (1826) has developed a theoretical equation shown in Eq. 1 to calculate the torque of a circular shaft fixed at one end. In this equation, the torque, *T*, is obtained from the equilibrium condition by equating the external moment to the internal moment. It is formulated as torsional rigidity times angle of twist per unit length of the shaft:

$$T = GI_P\theta = G\theta \int r^2 dA \qquad \text{(Eq. 2.1)}$$

where *G* is the modulus of rigidity; I_p is the polar moment of inertia; θ is the angle of twist per unit length of the shaft; *r* is the distance from analysed area to the centre of the cross section.

Table 1.1. St. Venant's coefficients for rectangular sections (Hsu 1984).

y/x	*k*	*β*	*α*
1.0	0.675	0.141	0.208
1.2	0.759	0.166	0.219
1.4	0.822	0.187	0.227
1.6	0.867	0.204	0.234
1.8	0.904	0.217	0.24
2.0	0.930	0.229	0.246
2.5	0.968	0.249	0.258
3.0	0.985	0.264	0.267
4.0	0.997	0.281	0.282
5.0	0.999	0.291	0.291
10.0	1.000	0.312	0.312
100.0	1.000	0.331	0.331
∞	1.000	0.333	0.333

Navier's equation assumed that the shape of a cross section remains unchanged after twisting and a plane section remains plane after twisting (i.e., no warping). However, laboratory experimental observations for torsional deformation of rectangular section indicated warping of cross section occurs after twisting (Hsu 1984). A new method to evaluate the torsion in noncircular cross sections was proposed by de Saint-Venant (1856). This method is based on a 'semi-inverse' method and applies an assumed displacement. The equation is also based on the theory of elasticity and is derived a simple equation for torque in rectangular cross section (Eq. 2.2):

$$T = \beta x^3 y G \theta \qquad \text{(Eq. 2.2)}$$

where *x* is the width of the member; *y* is the height of the member; the coefficient *β* is a function of *y/x* and is also tabulated in Table 1.1; similarly, *k* is a function of *y/x* and is also tabulated; From the values of *y/x* in Table 1.1, it is clearly seen that the coefficients are applicable for beam sections where the height is higher than the width of the member.

2.4.2. Torsion in plain concrete members

The St. Venant's method can be applied to predict the torsional strength of plain concrete members (de Saint-Venant 1856). In this approach, it is assumed that torsional failure of a plain concrete member occurs when the maximum principal tensile stress σ_{max} reached the tensile strength of concrete f'_t. The elastic failure torque in concrete, T_e was derived as Eq. 2.3:

$$T_e = \alpha x^2 y f'_t \qquad \text{(Eq. 2.3)}$$

where α is St. Venant's coefficient. The value of $\alpha = \beta/k$ is presented in table 1.

This calculation method is still within the elastic range of materials and was proved to underestimate the failure strength of a plain concrete beam in torsion. The actual test

strength is roughly 50% greater than that calculated by the method. (Young et al. 1922; Andersen 1937; Cowan 1951; Humphreys 1957; Zia 1961).

Nylander suggested that the extra strength may be contributed by plastic property of concrete (Nylander 1945) as the concrete may develop plasticity increasing its ultimate strength. For this reason, a plastic coefficient $\alpha_p = (0.5 - x/6y)$ was proposed to replace St. Venant's coefficient α. The plastic failure torque, T_p, can therefore be expressed:

$$T_p = \alpha_p x^2 y f_t' \qquad \text{(Eq. 2.4)}$$

The value of plastic coefficient is constantly 50% larger than the St. Venant's coefficient showing that it can roughly account for the extra strength of concrete.

The plastic theory, however, also has a few problems. The most important one is plasticity is not the actual behaviour of concrete. Besides, the theory cannot account for size effect. Tests indicated that for small torsional specimens, the calculated plastic torques are usually smaller than the test values, whereas the opposite is true for large specimens (Hsu 1984).

2.4.3. Skew Bending Theory for reinforced concrete

The skew bending concept was first proposed by Lessig (1959). More researchers (Collins et al. 1968; Hsu, T. T. C. 1968; Below et al. 1975) further developed the skew bending concept to apply this theory to reinforced concrete beams subjected to torsion and bending. Below are the assumptions in skew bending theory:

- Both the longitudinal steel and the stirrups yield at failure i.e., reinforced beam.
- The tensile strength of the concrete is neglected.
- The spacing of stirrups is constant within the failure zone
- No external loads are present within the failure zone

- The effect of steel near the compression zone is neglected.
- The area of the shear-compression zone is rectangular.

Based on the above assumptions, the failure plane of a reinforced concrete beam in torsion was proposed to occur by bending about an axis parallel to the wider face (section y) and at an inclination of 45 degrees to the longitudinal axis (see Figure 2.3. It can be seen in the Figure 2.3 that half of the failure plane is in tension while the other half is in compression due to bending. This approach deduced the below equation to calculate the minimal torque, T_c resisted by the beam:

$$T_c = \left(\frac{x^2 y}{3}\right) f_r \qquad \text{(Eq. 2.5)}$$

where *x* and *y* are the width and depth of the section respectively; f_r is the modulus of rupture of the concrete (Lessig 1959). Since the modulus of rupture is often not available for analysis and design in concrete structures, the compressive strength f'_c was adopted in the empirical equation for estimating f_r. Hence, the torque resisted by concrete is expressed as Eq. 2.6:

$$T_c = \left(\frac{2.4}{\sqrt{x}}\right) x^2 y \sqrt{f'_c} \qquad \text{(Eq. 2.6)}$$

The above equation is for torsion resistance from the concrete only. However, in reinforced concrete, more resistance is from the reinforcement including longitudinal steel bars and stirrups. The torsional moment T_s resisted by the reinforcement can be expressed as below:

$$\mathrm{T_s} = \sqrt{m}\frac{f_{ly}}{f_{sy}}\left(1 + 0.2\frac{y_1}{x_1}\right)\frac{(\mathrm{x_1 y_1 A_t f_{sy}})}{\mathrm{s}} \qquad \text{(Eq. 2.7)}$$

$$m = \frac{2\overline{A_l}s}{2A_t(x_1+y_1)} \qquad \text{(Eq. 2.8)}$$

where x_1 = centre-to-centre distance of the longer leg of stirrups; y_1 = centre-to-centre distance of the shorter leg of stirrups; f_{ly}= yield strength of longitudinal reinforcement; f_{sy}= yield strength of stirrups; s =spacing of stirrups; A_t= cross section area of one leg of stirrup; A_l = cross section area of one longitudinal reinforcement. Thus, $T_n = T_c + T_s$, where T_n is the nominal moment capacity of the section (Lessig 1959).

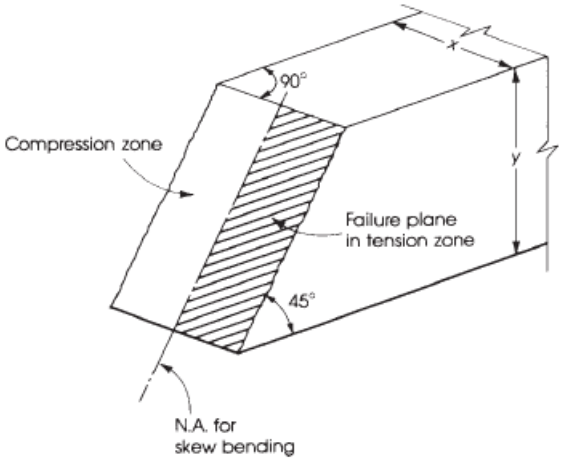

Figure 2.3. Skew bending failure plane (Hassoun & Al-Manaseer 2020)

2.4.4. Space Truss Analogy for reinforced concrete

Space truss analogy was first presented by Rausch (1929) to study the torsional behaviour of reinforced concrete structures. This method was further verified with extensive experimental works by (Lampert 1971; Lampert & Thürlimann 1972). In the space truss analogy, it is assumed that the torsional strength of a reinforced concrete rectangular section is derived from the reinforcement and the small amount of concrete surrounding the reinforcements. In this case, the reinforced concrete beam is simplified as a thin-walled rectangular concrete tube with longitudinal reinforcements and stirrups (see Figure 2.4). Analysis of torsional resistance in the tube is aided by treating it as a space truss where compression is resisted by the inclined concrete struts parallel to the spiral cracks, and the tensile resistance is provided by longitudinal bars and stirrups. Although this method underestimates the exact torsional strength of

the RC structure due to ignoring the tensile capacity of concrete, it is crucial for understanding and calculating the torsional capacity of the whole element (Hsu 1984).

The torsional resistance T_4 provided by the thin-wall tube could be presented as a sum of the contributions of the shears in each of the four walls. For the right-side wall, the torque due to shear is:

$$T_4 = \frac{V_4 x_0}{2} \quad \text{(Eq. 2.9)}$$

where V_4 is the shear force in the right-side wall; x_0 is the distance of the two most outside bottom longitudinal reinforcement bars.

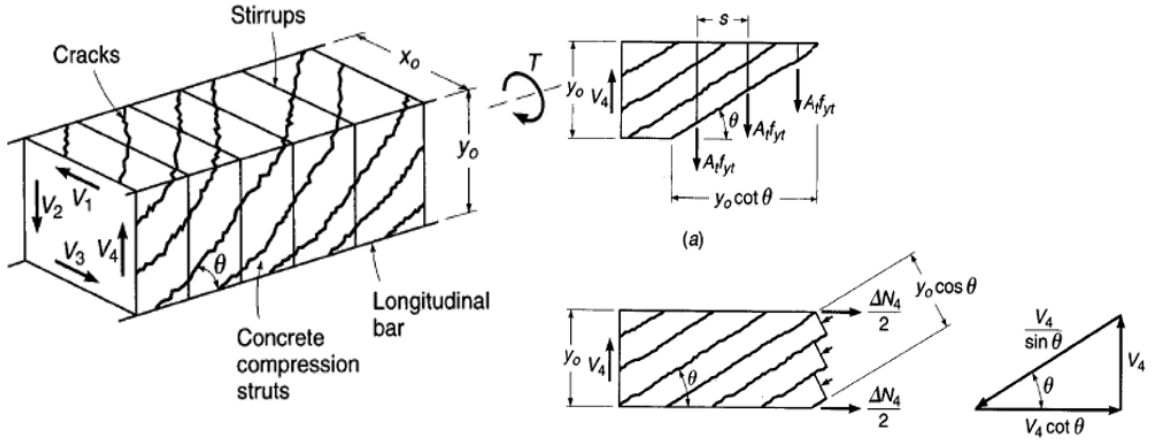

Figure 2.4. Space truss model of a reinforced concrete beam (Darwin et al. 2016)

The free body analysis of a small proportion of the right-side wall cut by the inclined cracks with an angle of θ shows that the shear is contributed by the legs of stirrups cut by the torsional crack. Shear is therefore calculated as:

$$V_4 = \frac{A_t f_{yt} y_0}{s} \cot\theta \quad \text{(Eq. 2.10)}$$

where A_t is the concrete area enclosed by stirrup; F_{yt} is the yield strength of reinforcement; y_0 is shown in Figure 2.4; θ is the inclined crack angle; s is the stirrup space.

It is easily shown that an identical expression is obtained for each horizontal and vertical wall. Thus, summing over all four sides, the nominal torsional capacity T_n of the section is:

$$T_n = \sum_{i=1}^{4} \frac{2A_t f_{yt} y_0 x_0}{s} \cot\theta \qquad \text{(Eq. 2.11)}$$

2.5. Finite Element Method for torsion study in reinforced concrete structures

The Finite Element Method (FEM) is a highly advanced computational technique extensively utilized in engineering for analysing complex structural behaviours by applying an array of algorithm to calculate approximate solutions (Sfikas et al. 2018). This approach breaks down complex structures into smaller, simpler parts called elements. These elements, interconnected at points called nodes, collectively form a mesh. The FEM calculates how each element behaves under specified conditions, combining these local responses to predict the behaviour of the entire structure. This method is particularly effective in analysing complex geometries and material behaviours, making it indispensable in engineering and physics.

In the realm of FEM software, ANSYS and ABAQUS are prominent. ANSYS is lauded for its user-friendly interface and wide application range, ideal for both linear and moderately non-linear analyses (Lee 2017). However, it might fall short in handling highly complex, non-linear problems. ABAQUS, on the other hand, excels in simulating complex non-linear behaviours, especially in materials like concrete (ABAQUS 2014). Its comprehensive features for modelling concrete cracking, crushing, and detailed non-linear material behaviour make it a preferred choice for analysing reinforced concrete structures. While it has a steeper learning curve compared to ANSYS, ABAQUS's capability to accurately simulate the inelastic behaviour and failure

mechanisms of concrete under various conditions is invaluable for researchers, explaining its widespread use in this domain. Hence, the study in this thesis prefers the FEM in ABQUS for torsional behaviour study of GFRP-RC pontoon decks.

In ABAQUS, several concrete damage models are available, each with its advantages and limitations (ABAQUS 2014). The most used models include the Concrete Damage Plasticity (CDP) model, the Brittle Cracking model, and the Smeared Cracking model.

- **Concrete Damage Plasticity (CDP) Model**: This model is favoured for its ability to simulate both compressive and tensile damage in concrete structures. It's particularly effective in representing post-cracking behaviour, making it ideal for studies involving complex loading conditions, such as cyclic loading or impact. However, it requires detailed input parameters, which can be challenging to obtain accurately.
- **Brittle Cracking Model**: This model is effective for simulating the cracking behaviour of concrete under tensile stress. It's simpler than the CDP model and requires fewer parameters. However, its application is limited as it cannot effectively represent post-cracking plastic deformation.
- **Smeared Cracking Model**: Useful for simulating crack propagation in concrete, this model spreads cracks over a wider area ('smearing' them), which can be advantageous for certain types of structural analysis. However, it may not be as accurate in predicting local crack behaviours and is less suitable for detailed crack analysis.

The Concrete Damage Plasticity (CDP) model is particularly suitable for studying the torsional behaviour of GFRP-RC pontoon decks due to its ability to accurately simulate both the compressive and tensile behaviour of concrete. This model effectively

captures the nonlinear response of concrete under complex loading conditions, such as torsion experienced by pontoon decks in marine environments. It can account for the gradual degradation of material properties, which is crucial in understanding the torsional response and potential failure mechanisms of such structures. The comprehensive nature of the CDP model allows for a more realistic and detailed analysis, making it a preferred choice for this specific application.

Some researchers have used FEM in the study of torsional behaviour of reinforced concrete structures. Although they are not carried out on the GFRP-RC decks, they provide guidance for applying FEM in the torsional behaviour of this structure. Broo et al. (2005) have implemented FEM to numerically analyse the torsional behaviour of prestressed hollow core units. The modelling procedure utilized torsional stiffness of the specimen and bond-slip relationship between strands and concrete obtained from practical experiment to manually define material characteristics. The numerical study successfully predicted the crack patterns and failure mechanism of hollow core unit with different thickness and void shapes. In another numerical study, Cao et al. (2020) analysed the behaviour of steel reinforced concrete columns under combined torsion. The authors highlighted the importance of formulating the constitutive relationship of reinforcement and concrete to reliably predict the torsional behaviour of concrete structures. Similar material characterization was done by Zhou et al. (2019) to model the behaviour of prestressed composite box girders with corrugated steel webs under pure torsion. ABAQUS has the flexibilities in customizing material's properties and constitutive models which are crucial for the accuracy of numerical modelling composite materials. For example, Raza et al. (2021) implemented finite element analysis about compressive behaviour of polypropylene macro synthetic fibre - reinforced concrete (MSFRC) columns with GFRP reinforcement in ABAQUS. They

manually defined elastic modules, Poisson's ratios, stress-strain relations (see Fig 2.5) as well as interface connection for the concrete and GFRP materials. On the other hand, Mondal and Prakash (2016) indicated that the bond-slip between bars and the concrete can be neglected as it will have an insignificant difference between the FEM simulation and experimentally observed behaviour of RC columns under torsion. In conclusion, FEM in ABAQUS is a powerful tool for torsional behaviour simulation of reinforced concrete structures, but not enough practices have been done to GFRP-RC pontoon decks.

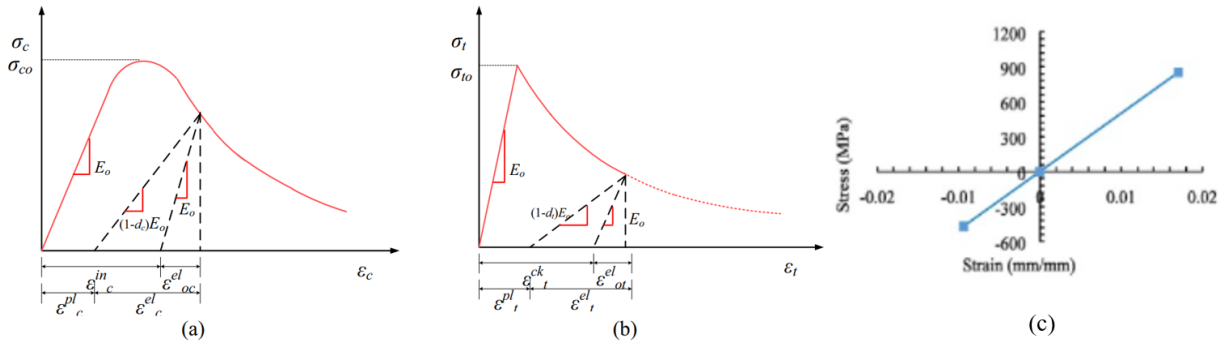

Figure 2.5. Stress- strain performance of MSFRC a) under compression, b) under tension; c) linear elastic performance of GFRP bar (Raza et al. 2021)

2.6. Research gap

The review of related literature highlighted the complex behaviour of reinforced concrete structures under torsional loads. While a few researchers have investigated the torsional behaviour of steel-reinforced concrete structures, investigations on GFRP-reinforced concrete structures are limited to beams. With the increasing interest in the use of GFRP bars for precast concrete decks in floating modules, a systematic understanding the torsional behaviour is required for their effective and safe design. Based on the review of literature, the following research gaps are identified.

- Torsional behaviour in steel reinforced concrete structures has been extensively studied, however, due to the different material property of GFRP

bar and the lack of data of torsional behaviour in decks, a thorough examination of GFRP-RC decks is required.

- Edge cut outs significantly reduced the strength and stiffness of reinforced concrete structures. The adverse effects in bending and shear strength in concrete structures with cut outs can be enhanced by strengthening with FRP composites in the corners of the cut out. However, the adverse effect of cutout and the enhancement provided by the FRP for the cutout have not been confirmed in the torsional behaviour of GFRP-RC decks.
- There are many design parameters related to the torsional behaviour of reinforced concrete structures. Concrete strength, reinforcement configuration, bar diameter and rotation direction have different influences on each stage of the RC structure's torsional response. However, their influence on the torsional behaviour of GFRP-RC decks with a cutout is still unexplored.
- There are limited understanding and insufficient design criteria to reliably predict the first crack torque, torsional stiffness and ultimate torsional strength for GFRP reinforced concrete pontoon deck without shear reinforcement. Similarly, torsion equations available are for beams and not for decks. It is important therefore to establish an equation that can reliably describe the overall behaviour of GFRP-reinforced concrete pontoon decks under torsion.

CHAPTER 3: PAPER 1 – TORSIONAL BEHAVIOUR OF GFRP-REINFORCED CONCRETE PONTOON DECKS WITH AND WITHOUT AN EDGE CUTOUT

3.1. Introduction

Chapter 2 highlighted that concrete structures in coastal environments, traditionally reinforced with steel, are susceptible to corrosion, leading to considerable safety risks and costly repairs. Fibre - reinforced polymer (FRP), especially glass fibre-reinforced polymer (GFRP), has gained prominence as an effective alternative. Offering high strength, lightweight, durability, and resistance to corrosion, GFRP holds significant potential for marine infrastructure. However, its mechanical properties differ markedly from steel, necessitating careful adaptation in structural applications.

The research on the torsional behaviour of GFRP-reinforced concrete, particularly in coastal structures like pontoons subjected to pure torsion from wave actions, is still in its emerging stages. This gap identified in Chapter 2 is notable in international design guidelines, where specific provisions for the torsional design of pontoon decks are lacking due to limited studies. The study in Chapter 3 contributes to bridging this knowledge gap by experimentally exploring the torsional behaviour of GFRP-reinforced concrete pontoon decks, focusing on factors like edge cutout, reinforcement distribution, and rotation direction. Five large-scale GFRP-reinforced concrete pontoon decks, both with and without cutout, were subjected to rigorous testing using a specially designed torsion test setup complemented by digital image correlation technique. Design equations either found from literature or established by the authors were verified with experimental data collected. The results and analysis are comprehensively presented in Chapter 3.

3.3. Links and implications

The study presented in Chapter 3 has shed light on the significant influence of edge cutout, reinforcement distribution, and rotation direction on the torsional behaviour of GFRP-RC pontoon decks. It was observed that edge cutout notably reduces the torsional capacity throughout the different phases of the decks' behaviour. While double-layer reinforcement distribution was found to enhance post-cracking torsional rigidity, it did not significantly impact pre-cracking behaviour and cracking torque. Furthermore, the rotation direction did not emerge as a critical factor influencing the deck’s torsional behaviour. The research also led to the development of equations for estimating cracking torque and post-cracking torsional rigidity.

Further research is needed to build upon these findings. Studies implemented and presented in Chapter 4 focus on devising and testing methods to optimize the design of edge cutout, particularly evaluating their effects on decks with both single-layer and double-layer mesh reinforcements. Additionally, to validate and refine the established equations, there is a need for more comprehensive data encompassing various reinforcement designs, which was evaluated in Chapter 5. This broader dataset will not only test the robustness of the existing predictive models but also enhance the reliability of their predictions. Such research endeavours will contribute significantly to the understanding and improvement of GFRP-RC pontoon decks, particularly in optimizing their design and performance in marine environments.

CHAPTER 4: PAPER 2 – TORSIONAL BEHAVIOUR OF GFRP-RC PONTOON DECKS WITH AN EDGE CUTOUT AND DIAGONAL REINFORCEMENTS

4.1. Introduction

Maritime structures such as pontoon decks frequently face torsional stress from uneven wave impacts, leading to concrete cracks and corrosion in traditional steel reinforcements. Chapter 3 introduces GFRP-RC pontoon decks as a solution to combat corrosion, showing their torsional performance is comparable to that of steel-reinforced decks. The chapter, however, identifies a reduction in performance due to cutout under torsional load, highlighting the need for better reinforcement strategies. Additionally, it points out the necessity for more experimental data to validate the established equations for torsional behaviour.

Expanding on these findings, Chapter 4 applies the pure torsion test to a broader range of GFRP-RC pontoon decks, exploring a variety of design parameters such as embedded diagonal reinforcement around the cutout, bar arrangement, and grid spacing. These design elements have been shown to potentially enhance the structural performance of GFRP-RC decks in other research, though their impact on torsional performance has not been extensively studied. This chapter analyses how these new design factors affect pre-cracking and post-cracking torsional rigidity, cracking torque, and failure mechanisms, thereby contributing to more effective torsional design strategies for GFRP-RC pontoon deck with an edge cutout. The collected data are further utilized to enhance the accuracy and reliability of the previously established predictive equations, ensuring a more precise assessment of torsional behaviour.

4.2. Submitted paper and under review

Structures

Torsional Behavior of GFRP-RC Pontoon Decks with an Edge Cutout and Diagonal Reinforcements

--Manuscript Draft--

Manuscript Number:	STRUCTURES-D-23-05265
Article Type:	Research Paper
Keywords:	Torsional behavior; GFRP reinforced concrete deck; edge cutout; bar arrangements; diagonal bars
Corresponding Author:	Omar Saleh AlAjarmeh, PhD University of Southern Queensland Toowoomba, AUSTRALIA
First Author:	Xian Yang
Order of Authors:	Xian Yang
	Allan Manalo
	Omar Saleh AlAjarmeh, PhD
	Brahim Benmokrane
	Zahra Gharineiat
	Shahrad Ebrahimzadeh
	Charles-Dean Sorbello
	Senarath Weerakoon
Abstract:	Although reinforced concrete (RC) pontoon decks are subjected to pure torsion caused by wave loading in marine environments, knowledge of their torsional behavior is limited. Moreover, edge cutouts—which represent pile location—negatively affects the structural performance of RC pontoon decks under torsion. This study experimentally investigated the torsional behavior of concrete pontoon decks reinforced with glass fiber-reinforced polymer (GFRP) bars. Large-scale pontoon decks with edge cutouts were tested and the effect of diagonal reinforcements, arrangement of bars, and reinforcement-grid space size was investigated. The generated experimental data demonstrated the enhancement in the pre-cracking torsional behavior provided by diagonal reinforcement in double-layered reinforcement. Meanwhile, a further improvement in the reinforcement design with a denser grid spacing of 100 mm in double-layer mesh exhibited 137% higher post-cracking torsional rigidity than that of the deck with a 250 mm grid spacing reinforcement. The former deck presented similar torsional behavior as the double-layered reinforced solid deck. The cracking torque and post-cracking torsional behavior of the pontoon decks can be accurately predicted with the introduced equations with consideration of the effective width related to the contribution of diagonal bars and considering the contribution of longitudinal GFRP bars, respectively.

Torsional Behavior of GFRP-RC Pontoon Decks with an Edge Cutout and Diagonal Reinforcements

Xian Yang,[a] Allan Manalo,[a,*] Omar Alajarmeh,[a] Brahim Benmokrane,[b] Zahra Gharineiat,[a] Shahrad Ebrahimzadeh,[a] Charles-Dean Sorbello,[c] and Senarath Weerakoon[c]

[a] *Centre for Future Materials (CFM), University of Southern Queensland, Toowoomba 4350, Australia*

[b] *University of Sherbrooke, Department of Civil Engineering, Sherbrooke, Quebec, Canada*

[c] *Boating Infrastructure Unit, Department of Transport and Main Roads, Brisbane City 4000, Australia*

Abstract

Although reinforced concrete (RC) pontoon decks are subjected to pure torsion caused by wave loading in marine environments, knowledge of their torsional behavior is limited. Moreover, edge cutouts—which represent pile location—negatively affects the structural performance of RC pontoon decks under torsion. This study experimentally investigated the torsional behavior of concrete pontoon decks reinforced with glass fiber-reinforced polymer (GFRP) bars. Large-scale pontoon decks with edge cutouts were tested and the effect of diagonal reinforcements, arrangement of bars, and reinforcement-grid space size was investigated. The generated experimental data demonstrated the enhancement in the pre-cracking torsional behavior provided by diagonal reinforcement in double-layered reinforcement. Meanwhile, a further improvement in the reinforcement design with a denser grid spacing of 100 mm in double-layer mesh exhibited 137% higher post-cracking torsional rigidity than that of the deck with a 250 mm grid spacing reinforcement. The former deck presented similar torsional behavior as the double-layered reinforced solid deck. The cracking torque and post-cracking torsional behavior of the pontoon decks can be accurately predicted with the introduced equations with consideration of the effective width related to the contribution of diagonal bars and considering the contribution of longitudinal GFRP bars, respectively.

Keywords: Torsional behavior; GFRP reinforced concrete deck; edge cutout; bar arrangements; diagonal bars.

*Corresponding author.

E-mail addresses: xian.yang@usq.edu.au (X. Yang), allan.manalo@usq.edu.au (A. Manalo), omar.alajarmeh@usq.edu.au (O. Alajarmeh), brahim.benmokrane@usherbrooke.ca (B. Benmokrane), zahra.gharineiat@usq.edu.au (Z. Gharineiat) sharhrad.ebrahimzadeh@usq.edu.au (S. Ebranhimzadeh), charles-dean.a.sorbello@msq.qld.gov.au (C.D. Sorbello), senarath.Z.Weerakoon@msq.qld.gov.au (S.Z. Weerakoon).

Introduction

In maritime infrastructures elements, such as pontoon decks, torsional loading is normally caused by wave loading and/or by wave impact acting unevenly on different sides of the deck. If the deck is not designed properly, the twists result in inclined torsional cracks in the deck at a very early age, which allows moisture to penetrate and causes steel reinforcement to corrode. Figure 1 presents the pontoon in wave action (from right side), torsional cracks and consequent reinforcement corrosion. Pursuing long-term endurance and reduced maintenance costs, engineers are now interested in reinforcing pontoon decks with glass fiber-reinforced polymer (GFRP) bars. While the behavior of concrete structures reinforced with GFRP bars in flexure [1-3], shear [4, 5], and compression [6, 7] have been widely investigated, the understanding of their behavior under torsion is limited. Moreover, due to the inadequate experimental databases [8], most FRP-RC codes or design guidelines [9-11] in the world do not contain the provisions governing torsional design. Indeed, the Canadian Standards Association (CSA S806) standard [9] only covers the torsional design of beams. As composite bars are now extensively used in concrete planks [3, 12] and suspended flooring systems [13, 14], there is a need to investigate their torsional behavior for effective and safe design.

Most of the reported works on torsional behavior have focused on steel-reinforced concrete beams. These studies have highlighted that the torsional strength and failure mechanism of RC structures under torsion are affected by concrete compressive strength, member geometry,

the concrete surface or embedded in the concrete around the cutout for enhancement and achieved significant improvement in structural performance. The enhancement measure of embedded diagonal GFRP bars were selected herein and the actual performance of it under torsion should be practically investigated.

Figure 1. Pontoon in wave action, torsional cracks and reinforcement corrosion.

This paper presents an experimental investigation of the torsional behavior of eight large-scale GFRP-RC pontoon decks. A design of diagonal reinforcement around the edge cutouts was proposed for enhancement. It was assessed together with other parameters: bar arrangement and grid space size on the failure mechanism, cracking torque, pre-cracking and post-cracking torsional rigidity, and post-cracking torsional strength. The applicability of ACI 318-14 (ACI 2014) provisions in predicting the cracking torque was evaluated by considering the effective width of the pontoon decks. Post-cracking torsional behavior was also predicted with a simple equation. The research findings and experimental datasets have contributed to a better understanding of the behavior of GFRP-RC pontoon decks subjected to torsion.

Experimental program

Materials

The pontoon decks tested in this study were reinforced with square-grid reinforcement mesh consisting of sand-coasted high-modulus Grade III (#3) GFRP bars [37] (see Figure.2 (a)),

depth-to-width ratio, concrete cover, and the relative amount of reinforcement in both directions [15-23]. Failure of beam under torsion manifest from brittle failure, ductile failure and clashing of concrete compressive struts depending on the amount of reinforcement. [20, 24]. Ibrahim et al. [18] found that the failure of the beams with thick concrete cover was controlled by concrete spalling and that the ultimate capacity of these beams was essentially equal to their initial crack. Some researchers experimentally compared the torsional behavior between steel reinforced beams and GFRP-RC beams[25, 26]. Though GFRP-reinforced beams match steel's cracking torque and torsional strength, they exhibit larger deflections and cracks due to GFRP's lower Young's modulus. Unlike ductile steel, GFRP's brittleness requires careful assessment in torsional actions for GFRP-RC structures. Yang et al. [27] experimentally investigated the torsional performance of designed GFRP-RC decks and concluded that the post-cracking torsional rigidity of the tested decks was comparable to steel-reinforced isotropic concrete slabs [28] and beams fully reinforced with GFRP bars [29]. Given compelling evidence showcasing the benefits of higher GFRP reinforcement ratios in enhancing structural performance of GFRP-RC planks [3, 4, 12], it becomes imperative to investigate strategies for achieving enhanced torsional performance in GFRP-RC decks by strategically arranging the reinforcements.

As an edge cutout is a compulsory design in pontoon decks for pile accommodation purpose [30], Yang et al. [27] assessed the torsional behavior of GFRP-RC pontoon decks with edge cutouts and determined the edge cutout led to 17% lower cracking torque and 50% lower post-cracking torsional rigidity than those of the double layer reinforced solid decks. That is because the cutout reduced the torsional constant J in the deck's midspan and cut off some longitudinal reinforcement bars, making them not contributing to the torsional resistance. Other researchers observed the similar findings related to the negative effect of openings on the structural performance of slabs and beams [31-36]. Furthermore, they used FRP materials attached on

with a nominal diameter of 10 mm. These bars were pultruded with unidirectional yarns of glass fibers impregnated with vinyl-ester resin, and their surface was sand-coated to enhance the bond strength with the surrounding concrete. These are the same GFRP bars used by Benmokrane et al. [38]; Table 1 provides their mechanical and physical properties. The concrete mix followed the provisions in MRTS70 [39] , and the cast concrete was class S50 strength grade to meet the durability requirement for classification C2 in marine environments. The average concrete strength fc obtained from the compression testing of concrete cylinders (see Figure 2 (b)) after 28 days is provided in Table 2 with the standard deviation in brackets. The pontoon design can benefit from deploying GFRP reinforcement by adapting the minimum 25 mm concrete cover for reinforcement protection, as suggested by Basaran and Kalkan [40], since this thickness has been found to not significantly affect the bond strength between the GFRP bars and concrete.

(a) Sand-coated GFRP bar (b) Compression test.

Figure 2.GFRP bar and concrete cylinder compression test.

Specimen details

Pontoon decks reinforced with double layer of GFRP bars—with and without edge cutouts—were first designed. Afterwards, test parameters, including bar arrangement, grid space, and diagonal reinforcement, were applied in the design of the other specimens, as listed in Table 2. Dimension of the decks and reinforcement details were drawn in Figure 3. As shown in Figure 3, the first set of diagonal bars (650 mm long) were tied to the longitudinal bars at a 45° incline to the longitudinal axis and 25 mm offset from the edge cutout. The second set diagonal bars

double layer of 100 mm square grid GFRP mesh and double diagonal reinforcement bars around the edge cutout in each layer of mesh. Decks G250L2CT, G150L1ST, and G250L2ST were set as references to evaluate the effect of diagonal bars, bar arrangement, and grid space, respectively.

Table 1. Physical and mechanical properties of the GFRP bars [27, 38]

Properties of #3 GFRP bar	Test method	Values
Nominal bar diameter (mm)	CSA S807 [9]	10
Nominal bar area (mm^2)	CSA S807 [9]	71
Ultimate tensile strength, f_u (MPa)	ASTM D7205/D7205M-21 [41]	1315
Modulus of elasticity, E_{GFRP} (GPa)	ASTM D7205/D7205M-21 [41]	62.5
Ultimate strain, ε_u (%)	ASTM D7205/D7205M-21 [41]	2.3
Shear modulus, G_{gfrp} (GPa)	[27]	1.37

Table 2. Test matrix

Identifier	Ave f_c' (MPa)	Grid space (mm)	Bar arrangement	Geometry	Diagonal reinforcement
G150L1DDT	76.8(6.4)	150	Single layer	Cutout	Double bars
G250L2DDT		250	Double layer	Cutout	Double bars
G100L2DDT		100	Double layer	Cutout	Double bars
G150L1DT		150	Single layer	Cutout	Single bar
G250L2DT		250	Double layer	Cutout	Single bar
G150L1ST		150	Single layer	Solid	N/A
G250L2ST		250	Double layer	Solid	N/A
G250L2CT		250	Double layer	Cutout	No

Test setup and instrumentation

The pure torsion test was conducted in the mechanical test laboratory of the Centre for Future Materials at the University of Southern Queensland. The applied test setup was adapted with modifications from the test setup used by Derkowski and Surma [42]. Figure 4 presents the photo of actual test setup in the laboratory. The specimen was totally fixed in the passive end by the passive support while the active end of the deck was free to spin around the pivot just below the deck. The center-to-center distance from active support to passive support was 2m. Torque was generated by applying a load perpendicular to the spread beam using a 500 kN electrohydraulic jack with a 500mm eccentricity. A spherical hinge connected the load cell

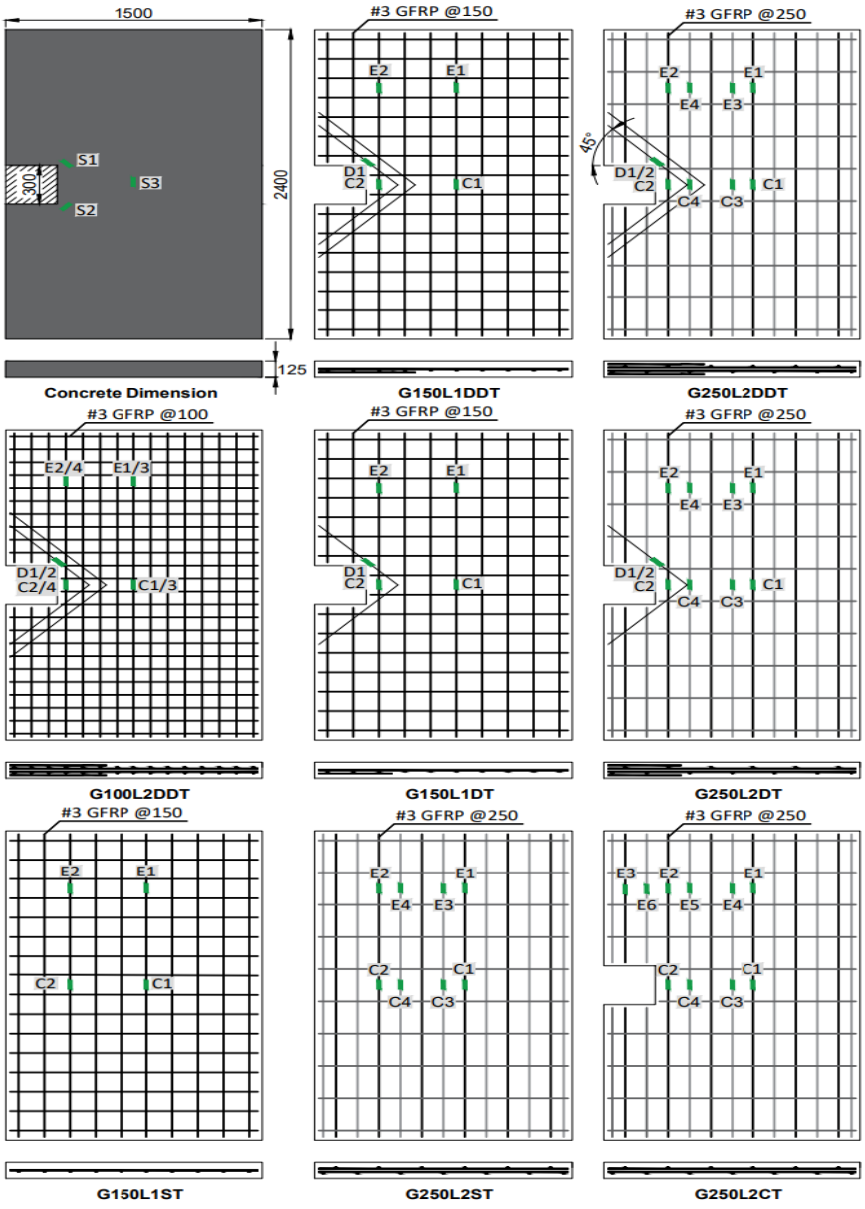

Figure 3. Design details of tested decks.

(850 mm long) were offset 100 mm from the first bars. The specimens were designated with a letter G—indicating sand-coated GFRP bars—followed by the reinforcement grid space in mm (150, 250, or 100); bar arrangement (L1 for single layered and L2 for double layered); geometry design/presence of diagonal reinforcement (S for solid, C for cutout without diagonal bars, D for cutout with single diagonal bars, DD for cutout with double diagonal bars); and T for torsion. For example, G100L2DDT is a deck with an edge cutout and is reinforced with a

with the loading foot, ensuring the load foot was constantly perpendicularly pressing the spread beam of active end. Displacement of the load point was recorded by the linear variable displacement transducer (LVDT) and a laser displacement sensor (LDS), as noted in Figure 4. The LDS data was latter used to verify the LVDT data. Strains in the longitudinal and diagonal bars, as well as concrete were measured with 6 mm long electrical resistance strain gauges at the locations marked green in Figure 3. During the test, a digital-image correlation (DIC) system was used to monitor deflection of the decks over the length of the loaded side by tracing the trajectories of the cross-marks drawn on the monitored surface in a 2D coordinate system. Only vertical deflections were collected for further analysis as the movement in other directions caused by concrete distortion were too small to be considered. Tests were stopped until cracks about 6 to 10 mm wide occurred in the concrete deck or until the deflection at the load point approached the maximum stroke of 85 mm.

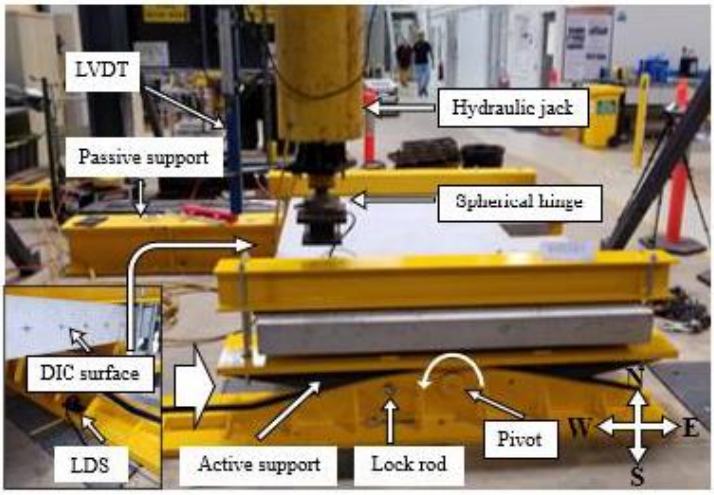

Figure 4. Details of setup

Results and observation

Crack propagation

Figure 5 shows the crack propagation in the GFRP-reinforced concrete deck along with the increase in torsional load and actual cracks at the edge cutout at the end of the test. The initial

cracks (highlighted in red) in the decks with edge cutouts—with the exception of G250L2DT—initiated from the corner of the edge cutout and crept to the passive end at an inclined angle with respect to the longitudinal axis, as shown in Figure 5 (a, b, c d, and h). Near the active end, the solid decks exhibited the first crack at the load of 64.7 kN for G150L1ST and 66.1 kN for G250L2ST, respectively, which were the highest among all the decks. In contrast, deck G250L2CT had the lowest cracking strength of 54.4 kN due to the narrow width at the mid-span, as was explained by Yang et al. [27]. Comparing to G250L2CT, the decks with diagonal reinforcement around the edge cutout (G150L1DDT, G250L2DDT, G100L2DDT, G150L1DT, and G250L2DT), however, all exhibited higher cracking. The cracking strength of G250L2DDT and G100L2DDT (64.5 and 61.8 kN, respectively) was close to that of the two solid decks. This result highlights the positive contribution of the diagonal reinforcement, which enhanced the concrete cracking resistance at the corners of the edge cutout. That is owing to the diagonal bars close to the concrete surface sharing the concentrated stress there. Enochsson et al. [31], who tested two-way welded steel-fabric reinforced concrete slabs under uniform loading also observed that external bonded carbon-FRP (CFRP) straps along the opening provided a maximum 70% increase in the cracking load.

After the initial cracks, new torsional cracks appeared near the edge of the deck at an inclined angle, and the existing cracks continued to widen. Similar cracking propagation was observed on the bottom surface of the deck, but in the opposite direction, mirrored about the transverse midline. Marti et al. [43] reported the similar observation in steel-reinforced concrete slabs under torsion, although the spacing of cracking in those slabs was much denser due to high amount of enclosed transverse reinforcement. The two solid decks tested herein both generated evenly distributed torsional cracks within the test region. In the decks with an edge cutout, cracks were attracted along the cutout, as indicated in many studies due to induced concentrated stress, which facilitated additional cracking [33, 34, 36]. Furthermore, the edge cutout exhibited

a wide, horizontal shear crack towards to the center of the deck (see Figure 5. a, b, c, d, e, and h). In these cases, the design of the diagonal reinforcement was expected to restrain the torsional and shear cracks in the area around the edge cutout.

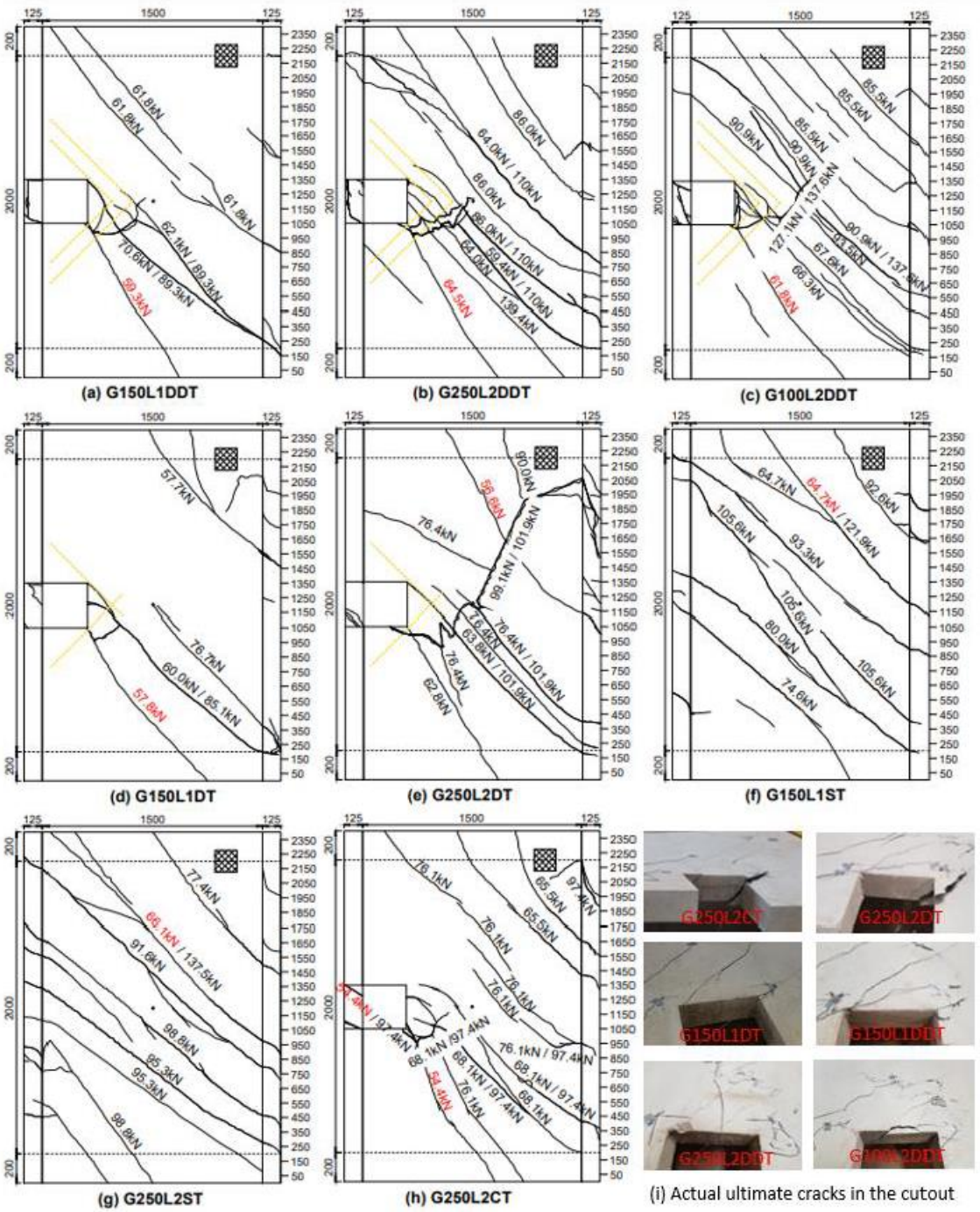

Figure 5. Crack propagation schematic diagram and actual photos.

Figure 6 provides video screen captures of the cracking propagation at applied torsional loads of 70, 90, and 110 kN in the eight tested decks extracted from documented videos. The loads were selected because all specimens achieved them within the post-cracking stage. Comparing G250L2DT to G250L2CT revealed that the single diagonal bar was able to restrain the shear crack at a load of 70 kN, which was just slightly higher than the concrete cracking strength. As the load increased to 90 kN, the shear cracks along the edge cutouts in the two decks achieved similar widths, which means that the cracking control provided by the single diagonal bar was quite limited in the post-cracking stage. In contrast, the double diagonal bars in deck G250L2DDT significantly benefited in restricting the width of the shear crack throughout the whole test (see Figure 6, c). A similar observation was made in the single-layered mesh-reinforced decks. G150L1DDT did not exhibit the wide torsional crack in the middle presented in G150L1DT. The better cracking control in double diagonal bar scenario could be explained by the greater number of diagonal bars increased contact surface between the diagonal bars and the concrete, which, in turn, impeded crack opening. It is noteworthy that, even though the single and double diagonal bars provided extra cracking restraint, the crack openings widened very fast after the first crack occurred. This could be due to the diagonal bars covering only a very small proportion of the deck and did not contribute to enhancing the deck's general torsional rigidity to resist twist deformation. The failure occurred to the decks with cutout, except G100L2DDT, for the same reason which was wide shear crack expending. A typical example of this failure mode is in G250L2CT, which was nearly separated by the horizontal shear crack induced by stress concentration in the corner of the cutout. The diagonal bars did not change the failure mode, but they delayed the crack widening. In the single-layered reinforced solid deck G150L1ST, failure occurred as the torsional crack width and deformation were large enough to be considered as serviceability loss. On the other hand, the most densely reinforced deck G100L2DDT, which had double diagonal reinforcement presented the smallest

shear crack in terms of width and length of all the decks. This result indicates that a design with a denser grid space (100mm), together with 10 mm diameter double diagonal bars, best restrained the growth and development of cracks around the edge cutout. That is because the denser reinforcement mesh provided high post-cracking torsional resistance and minimized the general twist deformation of the GFRP-reinforced deck. There is no sign of failure happened to the double-layered solid deck G250L2ST and the most densely reinforced deck G100L2DDT while only minor cracks were observed in the concrete surface and the torsional force was still gradually and steadily increasing under loading. It is important to note that, in these two cases, the tests needed to be terminated at around 85 mm deflection at the load point, which was the maximum stroke of the loading jack. Yang et al. [27] considered the solid decks exhibited similar crack propagation to that of RC beams reinforced with longitudinal GFRP bars and with 120mm spaced GFRP stirrups under torsion in which failure was slow and gradual [25]. Furthermore, the research explained that the double meshes protected the concrete core from serious splitting and provided extra torsional resistance. The decks with a cutout failed similarly to GFRP-RC beams with only longitudinal reinforcement: concrete splitting failure [29].

Deflection measurements along the length of decks

The deflection measurements recorded using the DIC along the length of the tested decks at the first cracking load, 70 kN, 90 kN, 110 kN and the maximum applied load are presented in Figure 7. A typical example of deformation in the monitored surface before and after load was demonstrated in Figure 7 (i) and (j). The nearly linear deflection curve at the first cracking load in each deck represented the linear elastic behavior of the concrete. After the first concrete crack occurred, the deflection significantly increased, even with only minor load changes. The shear cracks appeared on the monitored side surface, and the gradient (α) of the deflection curve along the length rapidly increased, indicating degradation of the local stiffness in the

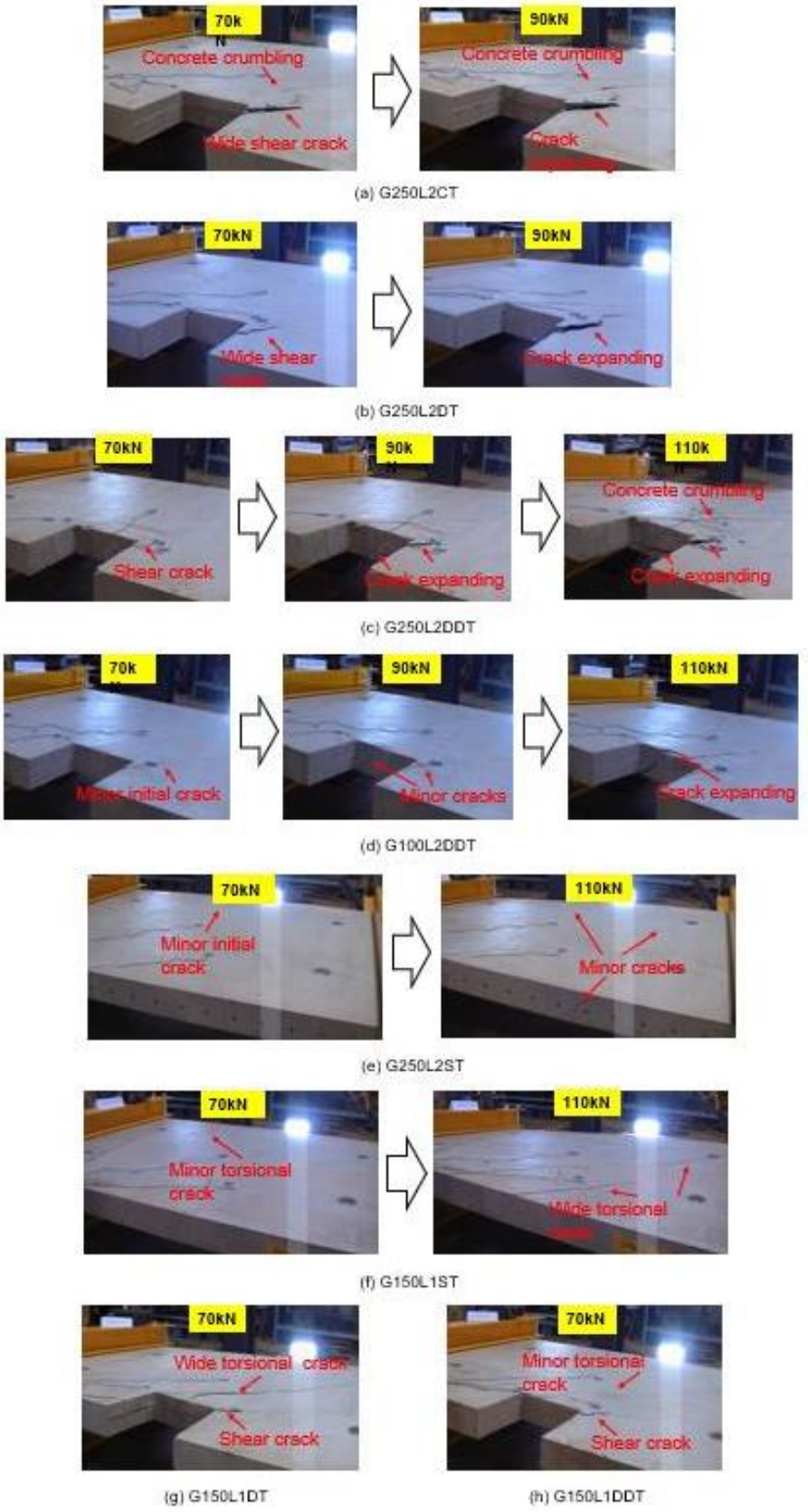

Figure 6. Comparison of cracks at 70, 90, and 110kN.

deck. To illustrate, it is obvious that there were gradient changes in G150L1DDT at 89.3 kN at 250 mm and 850 mm from the passive end, as shown in Figure 7 (a). These were the positions where shear cracks occurred, which could be confirmed by the crack propagation in Figure 7 (j). Ultimately, all the decks resulted in nonlinear profiles as the cracks made the decks discontinuous concrete media linked by the GFRP bars.

The deflection curves of reinforced concrete decks were used to determine the crack width by measuring the change in gradient $|\Delta\tan\alpha|$ between three adjacent points, as there was a positive correlation between this change and shear-crack width. The widest crack at 70kN in G150L1DDT occurred at 1550 mm from the passive end with $|\Delta\tan\alpha|$ of 0.025, while G150L1DT had a similar crack with a maximum $|\Delta\tan\alpha|$ of 0.026 at 1450 mm. Meanwhile, at the same applied load, the maximum $|\Delta\tan\alpha|$ of G250L2DDT was calculated to be 0.019 at 1950 mm and that of G250L2DT was about 0.013 at 1050 mm. Accordingly, double-layered decks with diagonal bars, G250L2DDT and G250L2DT, exhibited narrower shear cracks than their single-layered counterparts on the continuous side. Manalo et al. [3] made a similar observation in studying the flexural behavior of GFRP-reinforced boat-ramp planks which compared the cracking pattern in double-layered GFRP-bar reinforced concrete planks with single-layered reinforced ones. The narrower shear cracks observed in the double-layered decks can be attributed to several factors. Firstly, the double-layer reinforcement distributed in these decks offered greater post-cracking torsional resistance, resulting in less deformation under the same load. Secondly, the reinforcement bars were situated closer to the concrete surface in the double-layered decks, enabling them to respond earlier when cracks extended depth wise. At a higher load of 90 kN, G250L2DT exhibited a crack ($|\Delta\tan\alpha| = 0.030$ at 1050mm) similar to that in double diagonal bars reinforced G250L2DDT ($|\Delta\tan\alpha| = 0.032$ at 750 mm). These crack widths were nearly half of the cracks generated in G250L2CT, in which the maximum $|\Delta\tan\alpha|$ was 0.024 at 70 kN and 0.056 at 90 kN, both at 2050 mm. This means

that the diagonal bars on the discontinuous side not only limited crack expansion near the cutout but also affected crack growth on the continuous side.

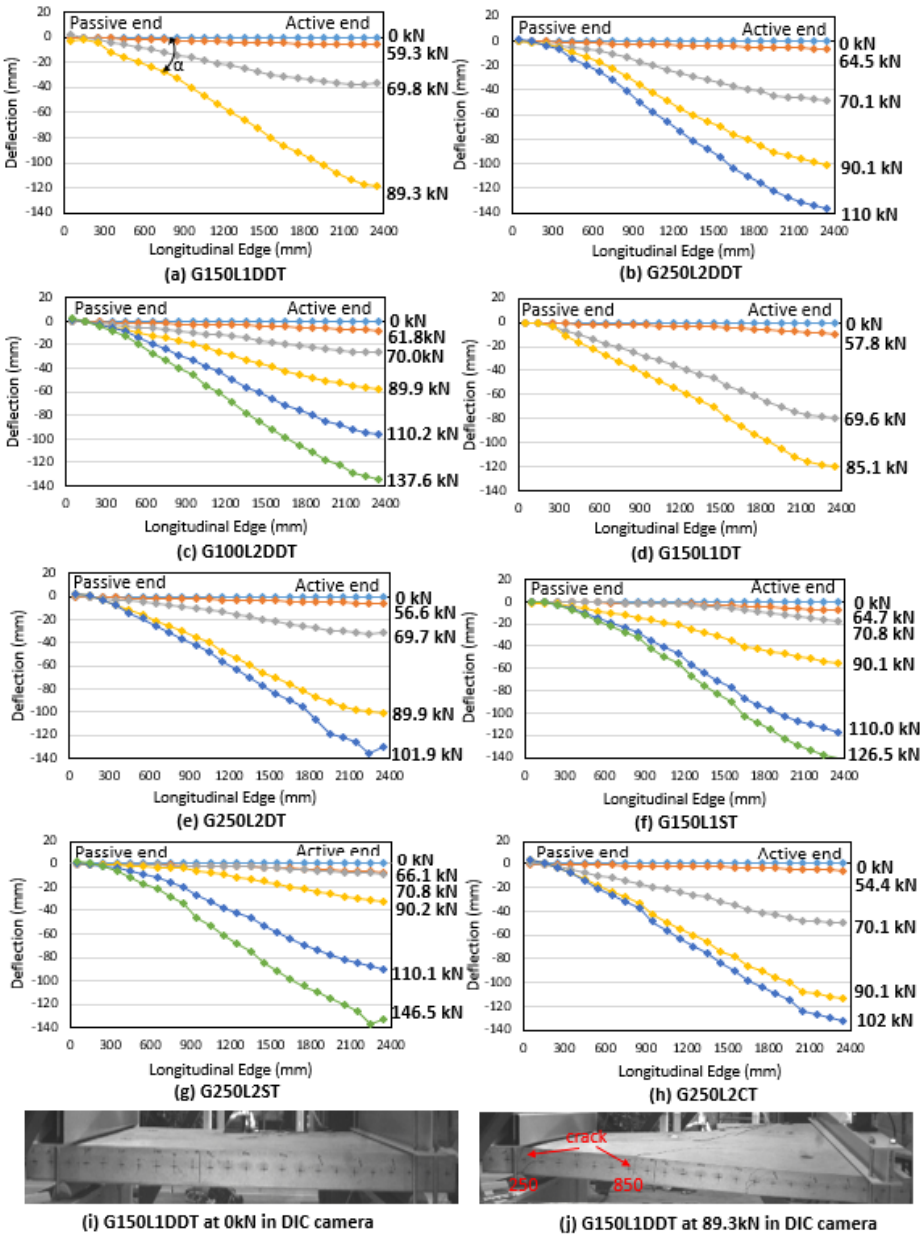

Figure 7. Deflection along the length measured using the DIC.

Crack widening in the single-layered reinforced solid deck G150L1ST achieved the maximum $|\Delta \tan \alpha|$ of 0.060 at a maximum load of 126.5 kN. Among all the tested decks, the most densely reinforced specimen (G100L2DDT) and the double-layered reinforced solid deck (G250L2ST) exhibited the narrowest shear cracks on the continuous side. At 70 kN, both G100L2DDT and

G250L2ST had a maximum |Δtan α| of 0.005, indicating that the dense reinforcement was effective in controlling cracks. Moreover, at 110 kN, G100L2DDT exhibited a crack width with |Δtan α| equal to 0.019 at 1350 mm, while G250L2ST exhibited a crack width with |Δtan α| equal to 0.041 at 850 mm. The crack on the continuous side in specimen G100L2DDT grew the slowest among all the tested decks, including the double-layered reinforced solid deck. Generally, with an effective design involving double-layered mesh, dense grid space, and double diagonal reinforcement bars, the decks with an edge cutout was able to achieve the crack control comparable to that of the solid decks. As wide shear cracks indicate the degradation of local stiffness along the length of the deck, the effective design can help attenuate the local stiffness degradation caused by concrete cracking.

Torque–twist response

Figure 8 shows the torque–twist response of the pontoon decks tested under pure torsion. The general torsional behavior curves of the GFRP-RC decks are similar to the GFRP-RC beams tested by Deifalla et al. [26], Mohamed and Benmokrane [29], Hadhood et al. [44]. The decks tested herein did not fail due to GFRP-bar rupture. The torsion test was stopped between 0.07 rad/m and 0.09 rad/m, as significantly wide cracks (around 6 to 10 mm in width) were observed within this range. The torsional behavior of the decks could be described as bilinear and were divided into two stages, pre-cracking and post-cracking, by the occurrence of the initial crack. The initial cracks of the tested decks occurred at very low twists, ranging from 0.0038 rad/m to 0.0072 rad/m, which were less than 1/10 of the maximum achieved twist. That was followed by a transition period in which the general torsional rigidity was continuously affected by concrete compression soften and tensile stiffen effect. The torque–twist response thereafter stabilized with a much reduced constant slope, representing the linear behavior of the GFRP bars. The torque–twist curves in Figure 8.b shows that G250L2ST, G250L2DT, G250L2DDT, and G100L2DDT achieved stabilization at an earlier level of twist (0.04 to 0.05

rad/m) than G150L1ST, G150L1DT, G150L1DDT, and G250L2CT. That is because the double-layered reinforcement provided stronger torsional resistance, and the diagonal bars restrained shear cracks to prevent further cracking in the concrete core between the double meshes.

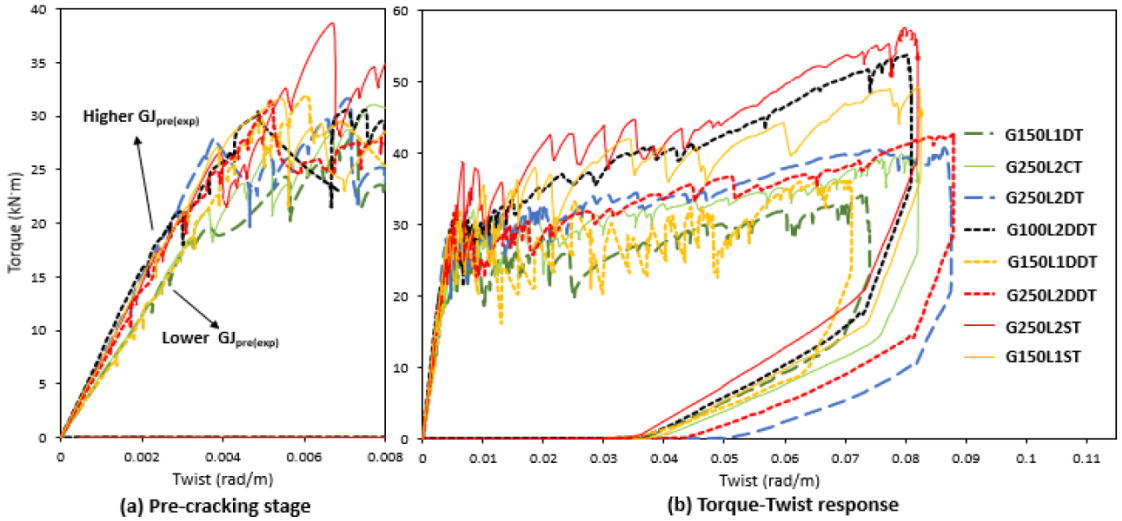

Figure 8. Torque–twist response

Table 3. Experimental results

Specimen	$T_{cr(exp)}$ (kN·m)	$T_{cr(pre)}$ (kN·m)	φ_{cr} (rad/m)	φ_{max} (rad/m)	$(GJ)_{cr(exp)}$ (kN·m²)	$(GJ)_{post(exp)}$ (kN·m²)	$(GJ)_{post(pre)}$ (kN·m)	$T_{\varphi=0.07(exp)}$ (kN·m)	$T_{\varphi=0.07(pre)}$ (kN·m)
G150L1DDT	29.26	31.30 (+7.0%)	0.0047	0.0750	5490	97	110 (+13.4%)	35.72	31.30
G250L2DDT	31.54	31.30 (-0.8%)	0.0051	0.0860	6339	130	153 (+17.7%)	38.05	31.30
G100L2DDT	30.41	31.30 (+2.8%)	0.0049	0.0803	7043	308	332 (+7.8%)	50.50	54.54
G150L1DT	28.27	31.30 (+10.7%)	0.0072	0.0734	5394	87	110 (+26.4%)	32.15	31.30
G250L2DT	27.96	31.30 (+11.9%)	0.0038	0.0752	7093	175	153 (-12.6%)	39.82	31.30
G150L1ST	31.56	31.30 (-0.8%)	0.0055	0.0823	6544	230	181 (-21.3%)	46.87	31.30
G250L2ST	32.59	31.30 (-4.0%)	0.0055	0.0800	6746	334	263 (-21.2%)	53.57	49.71
G250L2CT	26.76	24.57 (-8.2%)	0.0053	0.0796	5623	177	153 (-13.6%)	37.15	24.76

The fluctuation in the pre-cracking torque–twist curves (Figure 8. (a)) caused by the vibration movement of the test machine loading head was quite obvious when the applied torque was over 20 kN·m and approaching the cracking torque. Therefore, the experimental pre-cracking

torsional rigidity $(GJ)_{cr(exp)}$ was taken by regression equation for the initial part of the curves before 20 kN·m. The general slope of the curve between the first crack torque and maximum torque was used to estimate the experimental post-cracking torsional rigidity like that of the previous works.[27-29] The torsional rigidity decreased by about 95% to 98% after cracking occurred, indicating that most of the concrete was damaged at this point and would not be able to resist any applied torsion. The rigidity reduction after cracking was more significant when compared to that of the L-shaped GFRP-reinforced concrete beams tested by Deifalla et al. [26] (about 56% to 73% reduction). That is probably due to the different dimensions of the structure and enclosed stirrups in the beams. Table 3 presents all the test results and predictions which will be introduced latter. The post-cracking torque strength at φ=0.07 rad/m, —i.e., $T_{\phi=0.07}$ in each specimen—was selected as the two single-layered reinforced decks (G150L1DT and G150L1DDT) only reached this level when the test was stopped.

Torque–strain behavior

Strain data were registered by the strain gauges marked green in Figure 3. The strain gauge labels followed the rule as S for concrete surface, C for central reinforcement, E for edge reinforcement, and D for diagonal reinforcement. Unfortunately, some of gauges were damaged during concrete curing and did not record strains useful for analysis. The available strain data were analyzed and discussed as follows to better understand the mechanism of the tested GFRP-RC decks' behavior under torsion.

Torque–strain behavior on concrete

The torque–strain curves in Figure 9 reveal that both tension and compression occurred in the concrete's top surface during torsion. Initially, S1 and S2 recorded nearly equal levels of strain beside the cutout corner, with S1 in compression and S2 in tension (shown in Figure 9 a, b, c, & h). This suggests that the torque was distributed uniformly across the length of the deck. The linear torque–strain response of S1 and S2 at the beginning represents the linear elasticity of

the concrete. However, after reaching the cracking torque, the strain readings of S1 and S2 were either lost or became erratic due to the disturbance caused by the cracking and crumbling of concrete. Only S1 on G250L2DDT recorded the maximum compression strain of approximately -1273 $\mu\varepsilon$ until maximum torsional force. The strain in the center area was initially too small to be considered until the torque force approached the maximum. S3 recorded high compression stress under large torque force, indicating folding of the deck along a line across its centroid under excessive twist deformation. For instance, G250L2DT generated extensive compressive cracking in the middle traversing all the tensile cracks before the test ended. (Referring to Figure 5e).

The bars first reacted to strain varied in the eight tested decks. In the three decks without diagonal bars (G150L1ST, G250L2ST, and G250L2CT), the longitudinal bars closest to the location of the first crack were the first to react which was confirmed by the corresponding strain gauges E1, E4, and C2, located below each deck's first crack. This is because the stress in the concrete was released and transferred to the reinforcement bars through the cracks. In G250L2CT, the corners of the edge cutout induced stress concentration, which is evident by the lowest slopes in the S1 and S2 curves. In decks with diagonal bars, D1 strain gauge showed simultaneous response with S1 and S2, indicating that diagonal bars shared the concentrated stress with the concrete. S1 strains in G250L2DT, 250L2DDT and G100L2DDT were -64, -101, and -85 $\mu\varepsilon$ at 20 kN·m, while D1 strains were -30, -35, and -32 $\mu\varepsilon$ respectively. These values were much lower than -123 $\mu\varepsilon$ of S1 and 135 $\mu\varepsilon$ of S2 in G250L2CT under the same torque. Similarly, low values of strain recorded by S2 in the three decks (80, 92, and 90 $\mu\varepsilon$ at 20 kN·m, respectively) supported that the diagonal bar shared tensile concentrated stress in the other corner of the edge cutout where the first crack initiated. Therefore, diagonal bars in

double-layered decks delayed the first crack occurrence by sharing the concentrated stress induced by the sharp corner of the cutout.

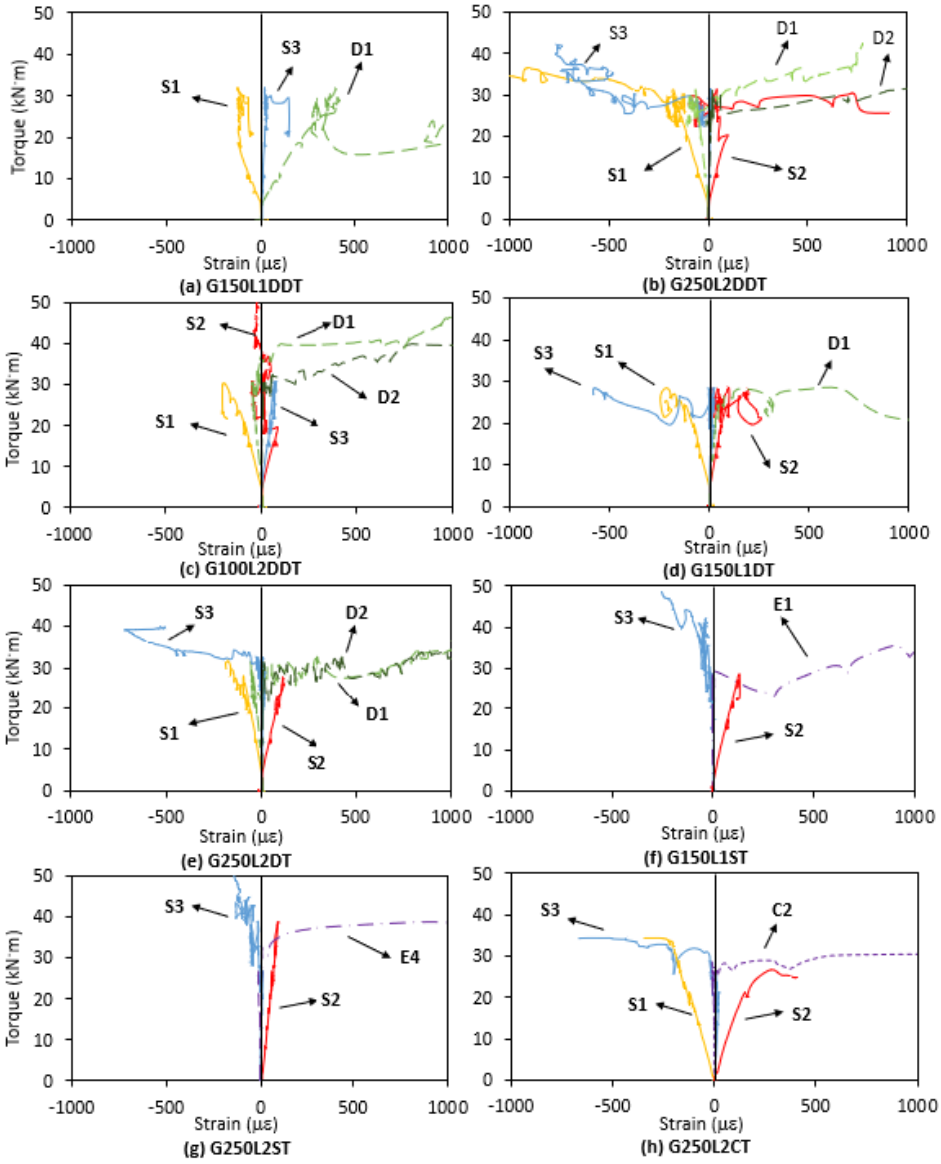

Figure 9. Strain on the concrete surface and the GFRP bars first to react.

Strain gauge D2 in double-layered decks had no strain before cracking, whereas D1 in single-layered decks showed slight tension. Figure 10 demonstrated the stress distribution pre-cracking in the deck's cross-section along the diagonal bar under S1, based on recorded strains. The neutral line (NL) in double-layered decks was lower than in single-layered decks, with 80% of concrete in compression versus less than 50%. The arrangement of reinforcement in

double-layered decks made better use of the concrete, making reinforcement more effective in resisting torsional forces in the pre-cracking stage.

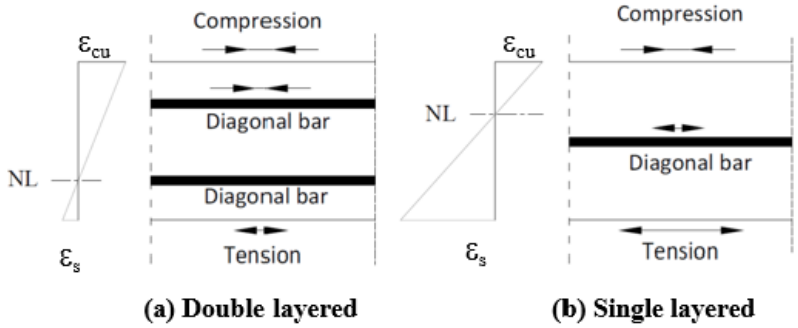

Figure 10. Cross section profile along diagonal bar under S1.

Torque–strain behavior in the longitudinal bars

The torque- strain behavior in the longitudinal bars in each tested decks was plot in Figure 11. Until the cracking torque was reached, there was no significant strain response in the bars, after which the strain increased rapidly, suggesting low post-cracking torsional resistance. The strain curves fluctuated during testing due to the effect of concrete softening and reinforcement stiffening, as well as loading head vibration. The loops at the end of the curves (C3 on G250L2DDT, Figure 11 (b)) resulted from damaged strain gauges. The GFRP bars did not exceed their ultimate strain by the end of the test, indicating no damage to the bars at maximum torque. According to CSA S806-12 [9], the maximum allowable stress in GFRP bars embedded in reinforced concrete beams under torsion should not exceed 0.4 F_u or 1200 MPa, which equates to a maximum allowable strain of 9600 $\mu\varepsilon$ herein. As shown in Figure 11, only C3 in G250L2DT and C2 in G250L2CT, where these strain gauges are attached on the longitudinal bars in the central area, recorded strains at the level of the maximum allowable strain soon after the cracking torque was reached (9392 and 12793 $\mu\varepsilon$, respectively). Other decks (G250L2DDT, G150L1DDT, and G150L1DT) with similar or weaker post-cracking torsional rigidity might be in the same situation although no direct data is evident because some strain gauges in the

central area were lost while the specimens were being fabricated and in handling. The high level of strain in the central area in these decks could be attributed to the concentrated stress induced by the edge cutout. In contrast, the stress distribution in the solid decks is relatively even as the strain readings in the central area and the end were almost same. The other impact of the edge cutout is that the recess cut off the longitudinal bars near the deck edge, making the bars discontinuous and not activated by the torsional force. This is confirmed by the zero-strain reading of E6 for specimen G250L2CT.

The strain data from G100L2DDT shows that the highest strain occurred at C3, the gauge in the middle of the bottom layer reinforcement mesh. To analyze the effect of diagonal bars and grid spacing, the maximum strains from G250L2DT, G250L2DDT, and G100L2DDT need to be compared. Strains at 33 kN·m were selected as all the strain curves were linear and stable at this level of torque. In G100L2DDT, C3 recorded a maximum strain of 2037 με, the lowest among the three decks while G250L2DDT and G250L2DT recorded C3 strains of 4824 and 5949 $\mu\varepsilon$, respectively. Using single diagonal bars resulted in 23.3% higher strain than using double diagonal bars in double-layered reinforced decks. G100L2DDT's C3 strain was only 42.2% of G250L2DDT's C3 strain due to its denser reinforcement providing higher post-cracking torsional rigidity, resulting in less deformation under the same level of torsional force. The strain data of C3 is not available in G250L2CT. However, an extremely high strain of 12812 $\mu\varepsilon$ was recorded by C2, which was on the top layer mesh and beside the cutout, at the maximum torque of around only 37 kN·m. This is significantly higher than the maximum strain in the central reinforcement mesh recorded by any other decks reinforced with double-layered reinforced decks with diagonal bars, which reveals that the diagonal bars in double layer mesh were effective in reducing the stress in the critical parts of the reinforcement mesh. The maximum strain achieved in double-layered reinforced solid deck G250L2ST was 5323 $\mu\varepsilon$ at 53.57 kN·m at E3, while that for the most densely reinforced deck with double diagonal bars

(G100L2DDT) was 6618 $\mu\varepsilon$ at 50.50 kN·m at C3. The expected ultimate torsional capacity in G100L2DDT would be still weaker than that in G250L2ST. In general, denser grid space and double diagonal bars in double-layer reinforcement arrangement helps reduce the critical stress induced by edge cutouts in the post-cracking torsional behavior.

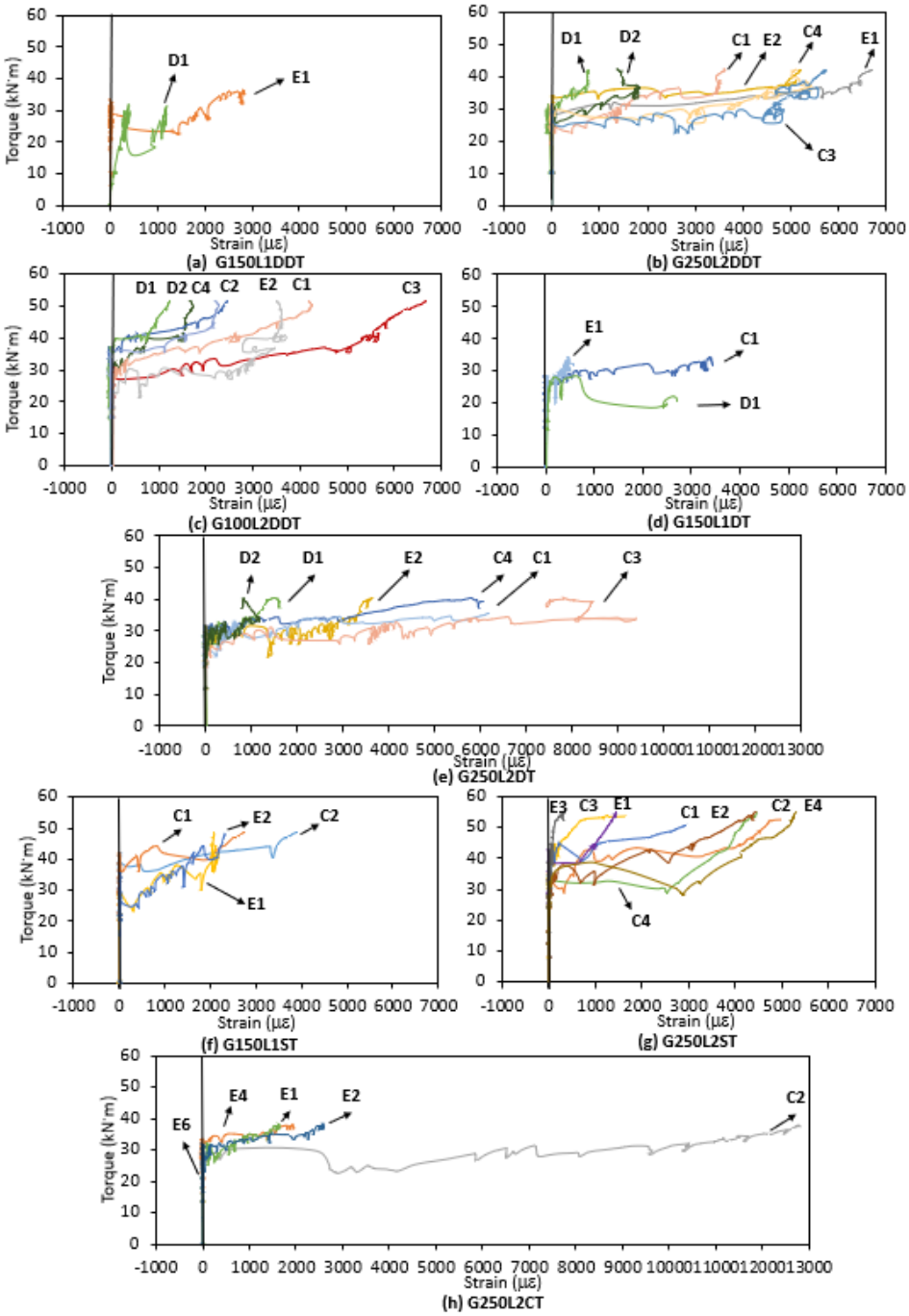

Figure 11. Torque–strain behavior in the longitudinal bars.

Discussion

Effect on initial cracking torque

The double-layered mesh combined with the diagonal bars increased the cracking torque despite the negative effect of edge cutout. The impact of bar arrangement on torsional cracking torque was negligible as shown in Table 3 that the three single-layered reinforced decks—G150L1DDT, G150L1DT, and G150L1ST—all generated similar levels of cracking torque compared to their double-layered reinforced counterparts with only 7.2%, -1.1%, and 3.2% difference. Hsu [16] stated that torsional cracking is primarily influenced by the structure's aspect ratio and material properties. Thus, the variation of up to 7.2% is likely due to the difference in concrete compressive strength. Additionally, the most densely reinforced deck with a 100 mm grid space (G100L2DDT) and G250L2DDT with a 250 mm grid space had similar cracking torques. Due to the edge cutout, G250L2CT1 resulted in a lower torsional cracking torque (26.76 kN·m) compared to G150L1ST or G250L2ST (18.0% or 21.8% lower, respectively). Note that the edge cutout reduced the cross-sectional area of the concrete by 20%. The employed diagonal bars improved the cracking torque performance by 9.3% in G150L1DDT, 17.9% in G250L2DDT, 13.7% in G100L2DDT, 5.6% in G150L1DT, and 4.5% in G250L2DT when compared to G250L2CT. This was attributed to the strain measurement and analysis that revealed the diagonal bars near the edge cutout corner effectively distributed the concentrated stress, thus delaying the onset of cracking. The double-layered reinforced decks with double diagonal bars (G250L2DDT and G100L2DDT) had a larger increase in the cracking torque (up to 17.9%), which was no surprise as the diagonal bars in the double-layered mesh were closer to the top and bottom concrete surface for an early response, and the double bars spread in the cracking direction had more contract surfaces with the concrete to share more stress than the single bars did.

Effect on pre-cracking torsional rigidities

Theoretical torsional rigidity GJ is mainly influenced by the torsional constant J, a function of cross section dimension, while G is the shear modulus of concrete. The presence of a cutout reduced $(GJ)_{pre(exp)}$ 18.2% lower, on average, as demonstrated by G150L1ST (6544 kN·m^2), G250L2ST (6746 kN·m^2), and G250L2CT (5623 kN·m^2). Similar to G250L2CT, the single-layered mesh reinforced decks with cutouts, G150L1DT and G150L1DDT, generated close $(GJ)_{post(exp)}$ values of 5394 and 5490 kN·m^2, respectively. On the other hand, the three double-layered reinforced decks with diagonal bars—G250L2DDT, G100L2DDT, and G250L2DT—had $(GJ)_{pre(exp)}$ values equal to or higher than the two solid decks (12.7%, 25.3% and 26.1%, respectively). The double-layered reinforcement arrangement plus diagonal bars improved pre-cracking torsional rigidity, mitigating the negative effect of the edge cutout. That is due to the vertically distributed diagonal bars in the double meshes, which enhanced the weakest points at the cutout corners. Since no other reinforcement bars reacted to strains before cracking, only the diagonal reinforcement beside the edge cutout was considered to contribute to the pre-cracking torsional rigidity. Thus, it was concluded that the arrangement and spacing of reinforcement bars, in the absence of diagonal bars, did not have a significant effect on pre-cracking torsional rigidity.

Effect on post-cracking torsional rigidities

GFRP reinforcement was found to be the main factor affecting post-cracking torsional rigidity of the pontoon decks. Diagonal bars did not have a clear impact on post-cracking torsional rigidity as $(GJ)_{post(exp)}$ in decks G250L2CT and G250L2DT were almost identical. Single-layered reinforced decks with single set and double sets of diagonal bars showed only a 10.3% difference in $(GJ)_{post(exp)}$, which was also close to a similar deck but without diagonal bars reported by Yang et al. [27]. The diagonal bars only helped bridge local shear cracks and did not contribute to the torsional rigidity after concrete cracking. Double-layered reinforced decks showed much higher $(GJ)_{post(exp)}$ compared to single-layered decks. G250L2DDT had a 33.6%

higher $(GJ)_{post(exp)}$ than G150L1DDT, and G250L2DT had double the $(GJ)_{post(exp)}$ of G150L1DT. The higher torsional rigidity in double-layered reinforced decks was due to the separated double-layered bar arrangement creating a higher J from GFRP mesh. The $(GJ)_{post(exp)}$ in G150L1DDT, G250L2DDT, G150L1DT, G250L2DT, and G250L2CT all generated at least 50% lower $(GJ)_{post(exp)}$ than their solid-geometry counterparts due the cut off discontinuous longitudinal bars. However, G100L2DDT had a $(GJ)_{post(exp)}$ only 7.7% lower than the strongest double-layered reinforced solid deck (G250L2ST), which implies that the dense reinforcement design allowed a deck with an edge cutout to achieve comparable post-cracking torsional rigidities as a double-layered reinforced solid deck. That is because G100L2DDT had 2.4 times the number of continuous longitudinal bars resisting the torsion force than the three double-layered reinforced decks with an edge cutout. In general, the double-layered bar arrangement and denser grid space provided up to 137% higher post-cracking torsional rigidities among double-layered reinforced decks, while the diagonal bars did not change the post-cracking torsional rigidity.

Effect on the post-cracking torsional strength

Large twist deformation for pontoon decks normally comes together with wide crack width, which should be avoided to maintain deck serviceability. So the post-cracking torsional strength at a limited twist of 0.07 rad/m, $T_{\varphi=0.07(exp)}$, is discussed herein. The increases in torsional strength resulting from the use of GFRP mesh were 22.1% in G150L1DDT, 20.6% in G250L2DDT, 66.0% in G100L2DDT, 13.8% in G150L1DT, 42.4% in G250L2DT, 48.5% in G150L1ST, 64.4% in G250L2ST, and 38.8% in G250L2CT, respectively, of the eight decks' cracking torques. The enhancement was obvious, especially in double-layered reinforced solid deck G250L2ST (53.57 kN·m) and the most densely reinforced deck G100L2DDT (50.5 kN·m). It is worth mentioning that G100L2DDT achieved $T_{\varphi=0.07(exp)}$ at least 26.8% higher than any other decks except G250L2ST. This can be attributed to the diagonal bars, which increased

the cracking torque weakened by the cutout, and the dense double-layered reinforcement mesh, which provided high post-cracking torsional rigidity. The decks with cutouts exhibited improved post-cracking torsional strength when reinforced with double-layered reinforcement arrangement, double diagonal bars, and a denser grid space. These enhancements resulted in a post-cracking torsional strength that was comparable to that of a double-layered reinforced solid deck. However, design engineers should consider the specific reinforcement details when evaluating the post-cracking torsional rigidity of GFRP-RC pontoon decks. The single layer reinforced decks G150L1DT, G150L1DDT, G150L1ST, and double layer reinforced decks G250L2CT, G250L2DT and G250L2DDT all failed due to cracking which was supported by crack propagation observation and the strain data analysis. Their actual post-cracking torsional strength is essentially the cracking torque. On the contrast, G100L2DDT and G250L2ST maintained narrow crack width and sound post-cracking torsional rigidity after cracking, so the post-cracking strength can be calculated based on the achieved twist angle, which is described latter in this study.

Prediction of cracking torque

The cracking torque equation introduced in ACI 318-14 [45] have been assessed as the most accurate prediction method for GFRP reinforced concrete beam and slabs tested in the previous studies [25, 27]. The ACI 318-14 method is based on a thin-wall, hollow-space truss analogy and is expressed as:

$$T_{cr} = 0.33\sqrt{f_c}\left(\frac{{A_{cp}}^2}{P_{cp}}\right) \quad (1)$$

where A_{cp} is the area enclosed by the outside perimeter of the concrete cross section; and P_{cp} is the outsider perimeter of the concrete cross section.

Table 3 tabulated the estimated cracking torque $T_{cr(pre)}$ with error in percentage. Note that the edge cutout without diagonal reinforcement was considered by reducing deck's effective width

in the mid length of the deck from 1.5m to 1.2 m as the cutout is 300 mm deep [27], and they resulted in 21.5% less predicted cracking torque. The reduction is close to the difference between $T_{cr(exp)}$ of G250L2CT and $T_{cr(exp)}$ of G250L2ST, which was 17.9%. In addition, the decks with diagonal bars were considered to have same effective width as the solid decks since the experimental results indicate that the diagonal bars could bridge the shear crack in edge cutouts, resulting in higher torsional cracks. The prediction cracking torque of the other seven decks had a standard deviation of 3.8 kN·m compared to the experimental results. In conclusion, the ACI318-14 equation—when considering the effect of edge cutout and diagonal bars—provided good estimates of the tested decks' cracking torque.

Prediction for post-cracking torsional strength

Yang et al. [27] proposed a simple method to predict the post-cracking behavior of the GFRP-RC decks by considering pure torsion happened to the longitudinal bars. This method is formulated as:

$$T_{\varphi} = T_{cr} + (GJ)_{post} \times \varphi \tag{2}$$

$$(GJ)_{post} = \sum_{i=1}^{n} G_{gfrp} I_i = G_{gfrp} \sum_{i=1}^{n} I_i \tag{3}$$

where G_{gfrp} is the shear modulus of GFRP bars; φ is the achieved twist after cracking; I_i is each longitudinal bar's polar moment of inertia around the longitudinal axis going through the deck's cross section centroid; and n is the total number of longitudinal bars.

Table 3 listed the calculated results of the post-cracking torsional rigidity with error in percentage and torsional strength at 0.070 rad/m twist $T_{\varphi=0.07(exp)}$. In general, the $GJ_{post(pre)}$ is in the same magnitude level of the experimental post-cracking torsional rigidity. As G250L2ST and G100L2DDT had the strongest post-cracking torsional rigidity and did not present any signs of failure until the test was stopped due to reaching the maximum loading stroke, Eq. 2 is suitable for predicting $T_{\varphi=0.07\,(pre)}$ of G250L2ST and G100L2DDT with a difference between

the predicted and experimental results of less than 8%. In contrast, the other six decks experienced failure controlled by wide cracks that occurred following the initial torsional crack, so the post-cracking torsional rigidity is essentially the predicted cracking torque.

Conclusion

The report presents the main experimental outcomes of pure torsion tests conducted on GFRP-RC pontoon decks with an edge cutout. The study investigated different GFRP bar arrangements, diagonal bars, and grid space. The test results were analyzed, and the following conclusions were drawn based on the analysis:

- The edge cutout induced concentrated stress leading to the decks failing just after the initial crack due to wide cracks or concrete crumbling. The double-layered reinforcement with diagonal bars and dense grid space, however, significantly enhanced the torsional capacity of the deck, which did not fail until the test was stopped due to reaching the maximum load stroke.
- The diagonal bars enhanced the pre-cracking torsional behavior while their influence on the torsional performance after cracking was negligible. Both single and double set of diagonal bars can improve the cracking performance by up to17.9%, but only when they were applied together with double layer reinforcement arrangement, the pre-cracking torsional rigidity can be enhanced by 26%. That is contributed by that the diagonal bars close to the concrete surface bridged the crack openings and constrained the shear cracks from expanding.
- The double-layered reinforced decks strengthened the post-cracking torsional rigidity by up to 100% when compared with decks reinforced with only single layer. That is because the double-layered reinforcement arrangement created a vertical distance from each bar to the cross-section centroid and resulted in a higher torsional constant J.

- Dense grid space improved the post-cracking torsional behavior and cracking control. This can be attributed to the larger number of continuous longitudinal bars that provided additional torsion resistance and kept the torsional crack from expanding.
- The densely reinforced deck with double diagonal bars achieved similar torsional performance as the double-layered reinforced solid deck did within the tested twist deformation. The expected ultimate torsional capacity of G100L2DDT was, however, lower than that the solid deck as the edge cutout induced a high level of concentrated stress that was not fully handled by the diagonal bar and denser reinforcement.
- The ACI 318-14 equation yielded an accurate prediction of deck cracking torque with a standard deviation of only 12% when considering the diagonal bars can eliminate the influence from edge cutout. Meanwhile, a method to predict post-cracking behaviour including post-cracking torsional rigidity and failure by considering the reinforcement details was introduced based on the test results.

Further research is required to investigate the effect of other parameters in the torsional design of GFRP-RC planks. Considering the time cost and safety risk in the physical experiment, numerical modeling like FEA in Abaqus is a good option. Moreover, theoretical method to predict the ultimate torsional capacity for the GFRP-RC planks without enclosed shear reinforcement warrants further exploration as it can be a guide for practical design.

Acknowledgments

The authors express their gratitude to the following organizations for their financial support: the Queensland Department of Transport and Main Roads (DTMR), the Advance Queensland Industry Research Fellowship Program (AQIRF 119-2019RD2), and the Natural Science and Engineering Research Council (NSERC) of Canada. The authors also thank Sustainable Alliance Pty Ltd (Inconmat) for providing the GFRP reinforcement, and Jetty Specialist for

fabricating the precast-concrete pontoon decks. Special thanks go to the technicians and students at the University of Southern Queensland for their assistance during plank manufacturing and testing.

References

1. Maranan, Manalo, Benmokrane, Karunasena, and Mendis, *Evaluation of the flexural strength and serviceability of geopolymer concrete beams reinforced with glass-fibre-reinforced polymer (GFRP) bars.* Engineering Structures, 2015. **101**: p. 529-541.
2. Adam, Said, Mahmoud, and Shanour, *Analytical and experimental flexural behavior of concrete beams reinforced with glass fiber reinforced polymers bars.* Construction and building materials, 2015. **84**: p. 354-366.
3. Manalo, Alajarmeh, Cooper, Sorbello, Weerakoon, and Benmokrane. *Manufacturing and structural performance of glass-fiber-reinforced precast-concrete boat ramp planks*. in *Structures*. 2020. Elsevier.
4. Nguyen-Minh and Rovňák, *Punching shear resistance of interior GFRP reinforced slab-column connections.* Journal of Composites for Construction, 2013. **17**(1): p. 2-13.
5. Choi, Choi, Feo, Jang, and Yun, *In-plane shear behavior of insulated precast concrete sandwich panels reinforced with corrugated GFRP shear connectors.* Composites Part B: Engineering, 2015. **79**: p. 419-429.
6. Alajarmeh, Manalo, Benmokrane, Ferdous, Mohammed, Abousnina, Elchalakani, and Edoo, *Behavior of circular concrete columns reinforced with hollow composite sections and GFRP bars.* Marine Structures, 2020. **72**: p. 102785.
7. Maranan, Manalo, Benmokrane, Karunasena, and Mendis, *Behavior of concentrically loaded geopolymer-concrete circular columns reinforced longitudinally and transversely with GFRP bars.* Engineering Structures, 2016. **117**: p. 422-436.
8. Razaqpur, Bencardino, Rizzuti, and Spadea, *FRP reinforced/prestressed concrete members: A torsional design model.* Composites Part B: Engineering, 2015. **79**: p. 144-155.
9. CSA, *Design and construction of building structures with fibre-reinforced polymers.* Canadian Standards Association, CAN/CSA-S806-12, 2012.
10. ACI, *Guide for the Design and Construction of Structural Concrete Reinforced with Fiber-Reinforced Polymer (FRP) Bar, (440. 1R-15)* American Concrete Institute, 2015.
11. Association, *GB 50608-2010 Technical Code for Infrastructure Application of FRP Composites*. 2010, China Planning Press: Beijing, Chian.
12. Wiater and Siwowski, *Serviceability and ultimate behaviour of GFRP reinforced lightweight concrete slabs: experimental test versus code prediction.* Composite Structures, 2020. **239**: p. 112020.
13. Hollaway, *The evolution of and the way forward for advanced polymer composites in the civil infrastructure.* Construction and Building Materials, 2003. **17**(6-7): p. 365-378.
14. Lv, Lu, and Liu. *Vibration serviceability of suspended floor: Full-scale experimental study and assessment*. in *Structures*. 2021. Elsevier.
15. Hsu, *Torsion of Structural Concrete - A summary on Pure Tension.* PCA Development Department Bulletin, 1968. **18**: p. 165-178.
16. Hsu, *Torsion of structural concrete-behavior of reinforced concrete rectangular members.* Special Publication, 1968. **18**: p. 261-306.
17. Hsu, *Torsion of reinforced concrete*. 1984.

18. Ibrahim, Gebreyouhannes, Muhdin, and Gebre, *Effect of concrete cover on the pure torsional behavior of reinforced concrete beams.* Engineering Structures, 2020. **216**: p. 110790.
19. Chiu, Fang, Young, and Shiau, *Behavior of reinforced concrete beams with minimum torsional reinforcement.* Engineering Structures, 2007. **29**(9): p. 2193-2205.
20. Ju, Lee, Kim, and Kim. *Maximum torsional reinforcement ratio of reinforced concrete beams*. in *Structures*. 2020. Elsevier.
21. Rahal, *Torsional strength of normal and high strength reinforced concrete beams.* Engineering Structures, 2013. **56**: p. 2206-2216.
22. Kim, Kim, Lee, Kim, Lee, and Kim, *Pure torsional behavior of RC beams in relation to the amount of torsional reinforcement and cross-sectional properties.* Construction and Building Materials, 2020. **260**: p. 119801.
23. Lopes and Bernardo, *Twist behavior of high-strength concrete hollow beams–formation of plastic hinges along the length.* Engineering Structures, 2009. **31**(1): p. 138-149.
24. Joh, Kwahk, Lee, Yang, and Kim, *Torsional behavior of high-strength concrete beams with minimum reinforcement ratio.* Advances in Civil Engineering, 2019. **2019**.
25. Mohamed and Benmokrane, *Reinforced concrete beams with and without FRP web reinforcement under pure torsion.* Journal of Bridge Engineering, 2016. **21**(3): p. 04015070.
26. Deifalla, Hamed, Saleh, and Ali, *Exploring GFRP bars as reinforcement for rectangular and L-shaped beams subjected to significant torsion: An experimental study.* Engineering structures, 2014. **59**: p. 776-786.
27. Yang, Alajarmeh, Manalo, Benmokrane, Gharineiat, Ebrahimzadeh, Sorbello, and Weerakoon, *Torsional behavior of GFRP-reinforced concrete pontoon decks with and without an edge cutout.* Marine Structures, 2023. **88**: p. 103345.
28. Lopes, Lopes, and do Carmo, *Stiffness of reinforced concrete slabs subjected to torsion.* Materials and structures, 2014. **47**(1): p. 227-238.
29. Mohamed and Benmokrane, *Torsion behavior of concrete beams reinforced with glass fiber-reinforced polymer bars and stirrups.* ACI Structural Journal, 2015. **112**(5): p. 543.
30. DTMR. *Design Criteria for Floating Walkways and Pontoons*. Queensland Department of Transport and Main Roads 2015; Available from: https://www.tmr.qld.gov.au/business-industry/Technical-standards-publications/Design-criteria-Marine.
31. Enochsson, Lundqvist, Täljsten, Rusinowski, and Olofsson, *CFRP strengthened openings in two-way concrete slabs–An experimental and numerical study.* Construction and Building Materials, 2007. **21**(4): p. 810-826.
32. Anil, Kaya, and Arslan, *Strengthening of one way RC slab with opening using CFRP strips.* Construction and Building Materials, 2013. **48**: p. 883-893.
33. Floruţ, Sas, Popescu, and Stoian, *Tests on reinforced concrete slabs with cut-out openings strengthened with fibre-reinforced polymers.* Composites Part B: Engineering, 2014. **66**: p. 484-493.
34. Hussein, Jabir, and Al-Gasham, *Retrofitting of reinforced concrete flat slabs with cut-out edge opening.* Case Studies in Construction Materials, 2021. **14**: p. e00537.
35. Arabasi and El-Maaddawy, *Reinforcing of discontinuity regions in concrete deep beams with GFRP composite bars.* Composites Part C: Open Access, 2020. **3**: p. 100064.
36. Smith and Kim, *Strengthening of one-way spanning RC slabs with cutouts using FRP composites.* Construction and Building materials, 2009. **23**(4): p. 1578-1590.
37. CSA, *Specification for fibre reinforced polymers.* Canadian Standards Association, CAN/CSA-S806-10, 2010.
38. Benmokrane, Manalo, Bouhet, Mohamed, and Robert, *Effects of diameter on the durability of glass fiber–reinforced polymer bars conditioned in alkaline solution.* Journal of Composites for Construction, 2017. **21**(5): p. 04017040.
39. DTMR, *Transport and Main Roads Specifications MRTS70 Concrete.* Transport and Main Roads Specifications 2018.

40. Basaran and Kalkan, *Investigation on variables affecting bond strength between FRP reinforcing bar and concrete by modified hinged beam tests.* Composite Structures, 2020. **242**: p. 112185.
41. ASTM, *Standard test method for tensile properties of fiber reinforced polymer matrix composite bars.* ASTM D7205-11, 2011.
42. Derkowski and Surma, *Torsion of precast hollow core slabs.* Czasopismo Techniczne, 2015.
43. Marti, Leesti, and Khalifa, *Torsion tests on reinforced concrete slab elements.* Journal of Structural Engineering, 1987. **113**(5): p. 994-1010.
44. Hadhood, Gouda, Agamy, Mohamed, and Sherif, *Torsion in concrete beams reinforced with GFRP spirals.* Engineering Structures, 2020. **206**: p. 110174.
45. ACI, *Building code requirements for structural concrete.* ACI 318-14 and commentary 2014.

4.3. Links and implications

Chapter 4 presents an experimental analysis on the impact of diagonal bars, bar arrangement, and reinforcement grid spacing on the torsional behaviour of GFRP-RC pontoon decks. The study revealed that integrating two sets of diagonal bars with double-layer mesh significantly improves the pre-cracking torsional behaviour. Additionally, it was found that decks with dense reinforcement grids notably enhance post-cracking torsional rigidity. This combination of diagonal bars, double-layer mesh, and dense grid spacing effectively aligns the performance of GFRP-RC decks with double-layer reinforced solid decks across all torsional response stages. The experiments also affirm the accuracy of the ACI 318-19 equation for predicting cracking torque, particularly when accounting for the diagonal bars' ability to mitigate the cutout's reduction effects and validate the methodology for estimating post-cracking torsional rigidity.

Despite these insights, the experimental approach proved costly in terms of time and resources and was constrained by lab conditions. To overcome these limitations, employing Finite Element Methods (FEM) such as ABAQUS could provide detailed customization in loading schemes, boundary conditions, and material properties. The research presented in the next chapter (Chapter 5) expands to include a broader range of design parameters like concrete strength, cutout geometry, and reinforcement strategies, ensuring these factors are adequately incorporated into the predictive equations. This approach will enable a more comprehensive understanding of the torsional behaviour of GFRP-RC pontoon decks with cutout, leading to improved design and construction guidelines for practical engineers.

CHAPTER 5: PAPER 3 – TORSIONAL BEHAVIOUR IN GFRP-RC PONTOON DECKS WITH EDGE CUTOUT - STUDY OF CRITICAL DESIGN PARAMETERS

5.1. Introduction

Chapters 3 and 4 implemented extensive experimental methods to analyse the torsional behaviour of GFRP-RC pontoon decks with an edge cutout, evaluating the effects of cutout, diagonal bar, bar arrangement, rotation direction, and reinforcement grid space. While these chapters provided a general understanding of the novel design's torsional performance, the critical design parameters for resisting torsional loading remained unclear due to limitations in experimental resources and time. To address this, Chapter 5 employed Finite Element Method (FEM) using ABAQUS software, facilitating an intensive parametric study with satisfactory accuracy and reliability. This approach involved developing 27 FE models using the Concrete Damage Plasticity (CDP) model which can be easily deviated from concrete compressive strength. These models were calibrated against experimental data to accurately reflect the decks' detailed torsional behaviour, including torque-twist response, stress distribution, and crack propagation. The study extended to parameters previously examined in other GFRP-RC structures, like concrete compressive strength, cutout geometry, cutout reinforcement distribution, bar diameter, and reinforcement spacing, but not specifically in the context of torsional behaviour of GFRP-RC decks with cutout. Chapter 5 also established and validated equations for cracking torque and pre-cracking torsional rigidity, enhancing the understanding of critical design aspects for GFRP-RC pontoon decks. The chapter comprehensively documents the modelling methodology and presents the results.

1.2. Submitted paper and under review

Engineering Structures

Torsional behavior in GFRP-RC pontoon decks with edge cutout - Study of critical design parameters

--Manuscript Draft--

Manuscript Number:	ENGSTRUCT-D-24-00096
Article Type:	VSI: Marine Concrete Structures
Section/Category:	Oceania, Mainland China, Taiwan, Hong Kong, Macau, Singapore, Japan, Korea
Keywords:	Torsion; GFRP-RC; deck; FEM; CDP; cutout; reinforcement configuration
Corresponding Author:	Omar AlAjarmeh, PhD University of Southern Queensland Toowoomba, Queensland AUSTRALIA
First Author:	Xian Yang
Order of Authors:	Xian Yang
	Omar AlAjarmeh, PhD
	Allan Manalo
	Brahim Benmokrane
	Zahra Gharineiat
	Shahrad Ebrahimzadeh
	Charles-Dean Sorbello
	Senarath Weerakoon
Manuscript Region of Origin:	Asia Pacific
Abstract:	Reinforced concrete (RC) pontoon decks are susceptible to torsional cracking especially at the cutout locations because of the twisting caused by the wave actions. However, understanding the torsional behavior of RC pontoon decks is limited. This study implemented an intensive finite element (FE) analysis to evaluate the effects of critical design parameters on the torsional behavior of concrete decks reinforced with glass fiber reinforced polymer (GFRP) bars. The FE models were validated with the experiment test results of three large scale decks, i.e. solid, with edge cutout and without diagonal bars, and with edge cutout and reinforced with diagonal bars. Parametric investigations covering concrete compressive strength (32, 50, and 70 MPa), cutout geometry (chamfer, fillet, and half round shape) and reinforcement configuration including cutout reinforcement distribution, (two, four and six sets of diagonal bars), reinforcement bar diameter (10mm, 12mm and 16mm) and reinforcement spacing (100mm, 200mm, 250mm and 350mm). The results showed significant sensitivity of the concrete compressive strength in the pre-cracking torsional behavior and the reinforcement configurations contributing positively to the post-cracking torsional rigidity and crack propagations. However, the cutout geometry did not present obvious effect on the deck's pre-cracking torsional behavior and only slightly changed the crack propagation. Prediction equations for estimating the initial torsional rigidity, general pre-cracking torsional rigidity and cracking torque were established and had good correlations with the FEM results.
Suggested Reviewers:	Yazan Almomani, PhD Associate Professor of Structural Engineering, University of Petra yazan.almomani@uop.edu.jo This research is within the suggested reviewer's expertise
	Ghassan Almasabha, PhD Assistant Professor, The Hashemite University ghassans@hu.edu.jo This research is within the suggested reviewer's expertise
Opposed Reviewers:	

Torsional behavior in GFRP-RC pontoon decks with edge cutout - Study of critical design parameters

Xian Yang,[a] Omar Alajarmeh,[a,*] Allan Manalo,[a] Brahim Benmokrane,[b] Zahra Gharineiat,[a] Shahrad Ebrahimzadeh,[a] Charles-Dean Sorbello,[c] and Senarath Weerakoon[c]

[a] *Centre for Future Materials (CFM), University of Southern Queensland, Toowoomba 4350, Australia*
[b] *University of Sherbrooke, Department of Civil Engineering, Sherbrooke, Quebec, Canada*
[c] *Boating Infrastructure Unit, Department of Transport and Main Roads, Brisbane City 4000, Australia*

Abstract

Reinforced concrete (RC) pontoon decks are susceptible to torsional cracking especially at the cutout locations because of the twisting caused by the wave actions. However, understanding the torsional behavior of RC pontoon decks is limited. This study implemented an intensive finite element (FE) analysis to evaluate the effects of critical design parameters on the torsional behavior of concrete decks reinforced with glass fiber reinforced polymer (GFRP) bars. The FE models were validated with the experiment test results of three large scale decks, i.e. solid, with edge cutout and without diagonal bars, and with edge cutout and reinforced with diagonal bars. Parametric investigations covering concrete compressive strength (32, 50, and 70 MPa), cutout geometry (chamfer, fillet, and half round shape) and reinforcement configuration including cutout reinforcement distribution, (two, four and six sets of diagonal bars), reinforcement bar diameter (10mm, 12mm and 16mm) and reinforcement spacing (100mm, 200mm, 250mm and 350mm). The results showed significant sensitivity of the concrete compressive strength in the pre-cracking torsional behavior and the reinforcement configurations contributing positively to the post-cracking torsional rigidity and crack propagations. However, the cutout geometry did not present obvious effect on the deck's pre-cracking torsional behavior and only slightly changed the crack propagation. Prediction equations for estimating the initial torsional rigidity, general pre-cracking torsional rigidity and cracking torque were established and had good correlations with the FEM results.

Keywords: Torsion; GFRP-RC; deck; FEM; CDP; cutout; reinforcement configuration.

*Corresponding author.

E-mail addresses: xian.yang@unisq.edu.au (X. Yang), omar.alajarmeh@unisq.edu.au (O. Alajarmeh), allan.manalo@unisq.edu.au (A. Manalo), brahim.benmokrane@usherbrooke.ca (B. Benmokrane), zahra.gharineiat@unisq.edu.au (Z. Gharineiat) sharhrad.ebrahimzadeh@unisq.edu.au (S. Ebranhimzadeh), charles-dean.a.sorbello@msq.qld.gov.au (C.D. Sorbello), senarath.Z.Weerakoon@msq.qld.gov.au (S.Z. Weerakoon).

1. Introduction

Maritime pontoon decks, especially those with edge cutouts, experiences torsional cracking from wave impacts [1]. Glass fiber-reinforced polymer (GFRP) bars are now becoming an effective reinforcement for reinforced concrete (RC) pontoon decks because of their non-corrosive performance, eliminating the corrosion problem in this critical infrastructure. However, understanding the torsional behavior of GFRP-RC decks is limited, even as torsion's relevance extends from maritime projects to other civil engineering applications like bridges and floor systems under uneven loading conditions and harsh environment. Because of the shortage of relevant data, existing design guidelines inadequately address torsional aspects of GFRP-RC decks [2-4]. Additionally, strategies to strengthen the cutout of these decks under torsional loads remain a challenge even though deck openings are prevalent. Reviewing the current database, several researchers have conducted experimental investigation on the torsional behavior of reinforced concrete structures. The torsional rigidity, cracking strength, and failure mechanism of them, whether reinforced with conventional steel or novel alternative materials like GFRP, hinges on several parameters including, but not limited to concrete compressive strength, member geometry, and reinforcement configuration [5-13]. Meanwhile, the opening in slabs is supposed to be enhanced by applying embedded reinforcement bars [14-17]. Unfortunately, the structural performance of these approaches have not been evaluated under torsion. Yang et al. [1] have provided experimental evidence on how the reinforcement distribution and the edge cutout affect the torsion in GFRP-RC decks. Yet, the roles of concrete compressive strength, geometry of the edge cutout, reinforcement configuration in the deck and the embedded reinforcement in the cutout are not investigated. A detailed study on the impact of these critical design parameters is therefore warranted to understand in more detail the torsional performance of GFRP-RC decks.

Research into the torsional behavior of reinforced structures is scarce. Experimental method was carried out in the study of torsion in GFRP-RC box girders [18], concrete filled circular FRP Tube [19] and GFRP-RC L shape beam [20], which all require elaborated and specialized setup and test procedures, far more complex than those for standard structural performance assessments. On the other hand, the exploration of RC structures under torsion through finite element method (FEM) using commercial computational simulation technique such as ABAQUS [21] will allow for detailed study of material characteristics, loading conditions and boundary control without involving those complex test setup and procedures. For instance, Cao et al. [22] numerically investigated on how load and reinforcement ratios, along with concrete strength, affect the torsional performance of steel reinforced concrete columns and calibrated with the experimental data. The following parametric study showed that the higher concrete compressive strength can improve the torsional stiffness and strength, while the reinforcement ratio markedly impacts the column's torsional capacity. Several studies have adopted the same hybrid approach of experimental and numerical analyses to explore the torsional behavior of reinforced concrete beams strengthened with FRP composites [19, 23-26]. These studies primarily focused on beams strengthened externally with FRP sheets or strips. Other FEM studies also investigated the behavior of GFRP-RC decks under impact [27, 28] and bending [29]. The existing research demonstrated the benefit of FE simulation in providing new knowledge in the behavior of GFRP-RC structures. Moreover, the results of these studies offer substantial guidance for developing a non-linear finite element model of GFRP-RC decks under torsional loading, serving as a foundation for an extensive parametric analysis.

This study presents results of intensive finite element analyses, adopting the concrete damage plasticity (CDP) formulations with some modifications, to understand the torsional behavior of GFRP-RC decks with an edge cutout and evaluate the effect of critical design parameters in the overall torsional behavior. The accuracy of the model was validated from the experimental

results from three physically tested large-scale GFRP-RC decks. Subsequently, a comprehensive parametric investigation was undertaken by varying the concrete compressive strength $f'c$, cutout geometry and reinforcement configurations, including reinforcement spacing, bar diameter and cutout reinforcement distribution. Simplified design equations that can reliably predict the GFRP-RC deck's torsional behavior were proposed. The outcome of this research can help broaden the knowledge on the torsional responses of GFRP-RC structures. Moreover, this work can pave way for the evolution of resilient infrastructure to endure the challenges of rapidly changing climate.

2. Details of specimens for pure torsion experiment

Three large-scale GFRP-reinforced decks were physically tested under pure torsion. Each deck has an overall dimension of 1500 mm (width) by 2400 mm (length) by 125mm (thickness). Two of the decks have an edge cutout of 300 mm x 300 mm square in the middle of the longer edge. The reinforcement mesh of the decks consists of Grade III (#3) GFRP bars with mechanical properties listed in Table 1. The reinforcement details and instrumentation of the three decks are shown in Figure 1. The specimen G250L2ST refers to the solid deck reinforced longitudinally and transversely with GFRP bars spaced at 250mm on centres and in double layers. Specimen G250L2CT is similar to G250L2ST except that it has a 300 mm x 300 mm edge cutout while specimen G250L2DDT is reinforced with two sets of diagonal bars around the edge cutout. The double diagonal bars are intended to restrain the stress concentration induced at the corner of the edge cutout. The decks were designed for pontoons employed within the Queensland (Australia) coastal line, the concrete compressive strength is aimed to be at least grade S50 to satisfy the durability requirements in marine environment as suggested in the DTMR [30]. The test of concrete cylinders yielded an average concrete compressive strength f'_c of around 70MPa. The deck specimens were tested by using the pure torsion setup introduced in Yang et al. [1]. As shown in Figure 2, the deck was placed on a passive support

and an active support spaced 2m on center. The passive support is totally bolted on one end of the deck to the strong concrete floor while the active support is allowed the other end of the deck to rotate freely (with no translation). The surface contacting with the support was protected by a 5 mm thick rubber mat to prevent pre-mature failure of the concrete surface. The torque-twist response and the cracking propagation observed from the experimental results are reported in next section and compared with the FE results.

Table 1. Properties of used GFRP bars

Properties of #3 GFRP bar	Test method	Values
Designated bar diameter (mm)	CSA S807 [3]	10
Nominal bar area (mm^2)	CSA S807 [3]	71
Ultimate tensile strength, f_u (MPa)	ASTM D7205/D7205M-06 [31]	1315
Modulus of elasticity, E_{GFRP} (GPa)	ASTM D7205/D7205M-06 [31]	62.5
Ultimate strain, ε_u (%)	ASTM D7205/D7205M-06 [31]	2.3
Shear modulus, G_{gfrp} (GPa)	[1]	1.37

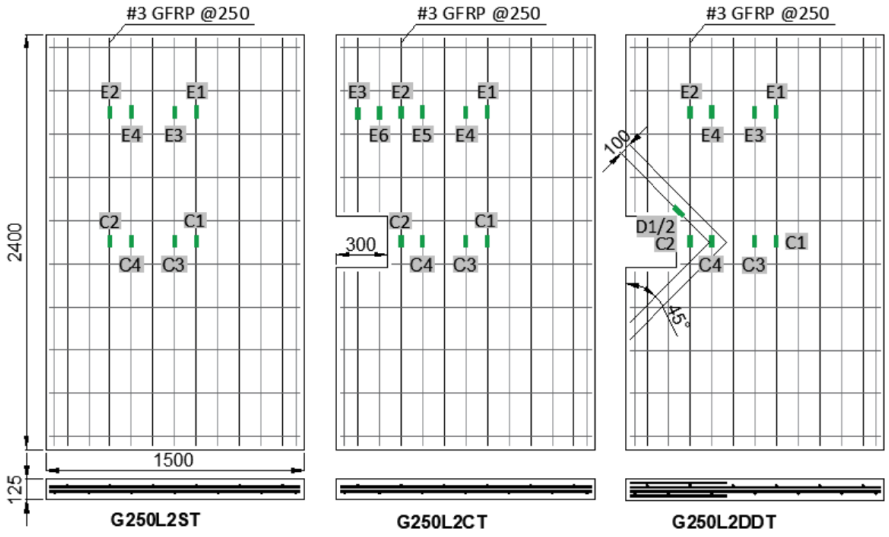

Figure 1. Design details and instrumentation of physically tested GFRP-RC decks.

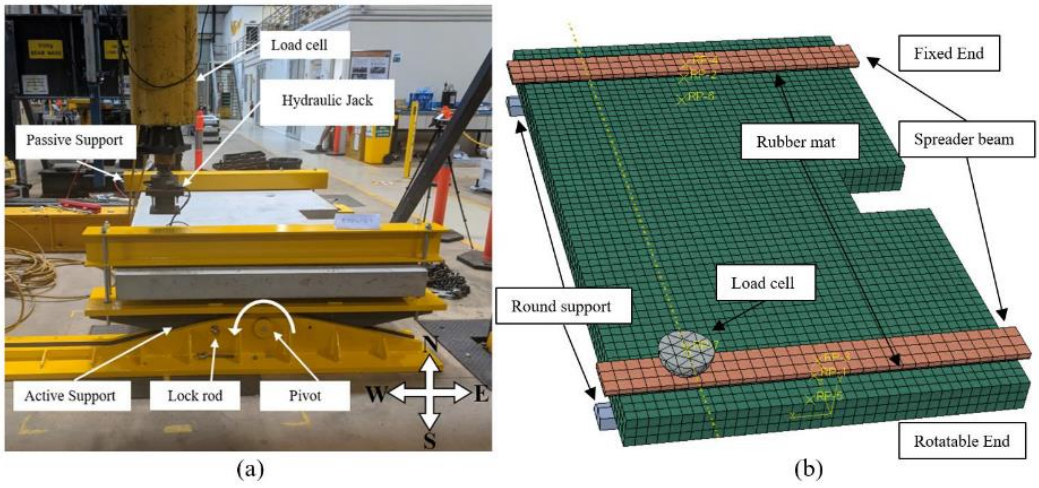

Figure 2. Torsion test and simulation: (a) Test setup [1] and (b) FEM in ABAQUS

3. FEA model in ABAQUS

The GFRP-RC pontoon decks were numerically modelled using the commercial Finite Element Method (FEM) software package ABAQUS [21] to validate the results of the experiment. The objective is to use the validated model for the investigation and evaluation of the effect of critical design parameters including concrete compressive strength, geometry of the cutouts and reinforcement configuration both within the deck and cutouts on the torsional behavior of the pontoon decks. A three-dimensional nonlinear finite element model was developed in dynamic explicit analysis to simulate the behavior of the three large-scale decks, G250L2ST, G250L2CT and G250L2DDT. The reliability of the developed model was validated by comparing the generated numerical results with the experimental data obtained from the laboratory test. Afterwards, the simulation is extended to testing decks with the various parameters for exploring more in depth the torsional behavior of the GFRP-RC pontoon decks with cutout.

3.1 Material model and assumptions

3.1.1 Concrete

The constitutive model of concrete is important in the FEM of RC structures as it dominates the behavior of concrete both in compression and tension. In the FE analyses of the torsional behavior of the GFRP-RC pontoon decks, the Softened Membrane Model (SMM) presented by Jeng and Hsu [32] and which was originally developed for shear [33] was widely used. The model applied a soften coefficient in the concrete's compression behavior to present the attenuation of principal compression stress resolved from shear stress, so the presented concrete strength is lower throughout the compression behavior curve. This approach was employed by Ganganagoudar et al. [25] in a strain controlled algorithm for the torsional analysis of FRP strengthened reinforced concrete beams using MATLAB. The calculated torque-twist curve in MATLAB algorithm with SSM was compared with that generated by FEM with concrete damage plasticity (CDP) in ABAQUS, and the same level of accuracy in presenting the torsional response was concluded. Considering the CDP model is much better known to the engineer's community and the convenience of material characteristic customization in ABAQUS, the CDP model is chosen for the numerical simulation herein.

The CDP is the built-in concrete damage model in ABAQUS that characterizes the concrete's uniaxial compressive and tensile behavior with damaged plasticity. This model is highly suitable for the analysis of RC structures subjected to monotonic or cyclic dynamic loading under low confining pressure as also implemented by other researchers [34]. Hsu and Hsu [35] adapted the compressive model by assuming the initial yielding of the concrete at $0.5\,f'c$ while the descending portion ends until $0.3\,f'c$. The compressive model is described by the following equations:

$$f_c = \left(\frac{n\beta(\varepsilon_c/\varepsilon_0)}{n\beta-1+(\varepsilon_c/\varepsilon_0)^{n\beta}}\right) f_c' \quad (1)$$

where f_c is the compressive stress in general; ε_c is the total strain; ε_0 is the cracking strain; n and β are the material parameters.

The value of n is 1 in the ascending portion while for the descending portion, n=1 if 0< $f'c \leq$62 MPa; n=2, if 62MPa < $f'c \leq$76MPa; and n=3 if 76 MPa < $f'c \leq$90 MPa. This assumption means that the higher compressive strength of the concrete is, the more brittle the behavior is, which is presented by the steeper descending portion in the compressive model after the cracking strain. Nevertheless, Yang et al. [1] has pointed out that double layers of GFRP mesh in the deck can help maintain the concrete core's integrity, resulting in less brittle post-cracking behavior. Consequently, it is proposed that the compressive model for concrete should adopt n=1 for 70MPa strength concrete to accurately reflect this scenario.

The parameter β is expressed by equation 2 and cracking strain ε_0 is given by equation 3.

$$\beta = \frac{1}{1-[f_c'/(\varepsilon_0 E_0)]} \tag{2}$$

$$\varepsilon_0 = 1.2908 \times 10^{-5} f_c' + 2.114 \times 10^{-3} \tag{3}$$

The initial elastic modulus, E_0 can be calculated by:

$$E_0 = 1.1243 \times 10^2 f_c' + 2.2636 \times 10^4 \tag{4}$$

A typical tension stiffening model is approximately linear elastic up to the maximum tensile strength f_{t0}. After the peak point, the tensile strain ε_t decreases gradually until zero. It should be mentioned that, to avoid the convergence issue in ABAQUS, the descending proportion of the applied tensile model ends at selected 0.9 damage parameter. The exponential model [36], proposed for RC girders under cyclic torsion and torsion combined with shear, is used in this study to consider the tension stiffening effect after concrete cracking. The following equation describes the descending proportion of the tension stiffening model.

$$f_t = f_{t0} e^{350(\varepsilon_{t0} - \varepsilon_t)} \tag{5}$$

where f_t is the tensile stress in general; f_{t0} is the tensile strength; ε_{t0} is the cracking tensile strain; and ε_t is the yielded tensile strain.

The tensile strength formulation is normally expressed as a constant multiply to the square root of $f'c$. However, there is a considerable variation in the value of the constant across reported literature because of the different loading types and specimen sizes in the measurement. The constant 0.3 is therefore used herein, which is within the range suggested by the existing concrete design standards [37-39].

$$f_{t0} = 0.3\sqrt{f_c'} \tag{6}$$

The calculated compressive and tensile models for 32, 50 and 70MPa concrete are depicted in Figure 3.

The other required input CDP parameters, including damage parameters for compression and tension, cracking strain as well as inelastic strain was calculated by following the ABAQUS manual [21]. Default values for the compressive stiffness recovery factor w_c and tensile stiffness recovery factor w_t are used, i.e. w_c=1 and w_t=0. The former means the concrete gain full recovered compressive stiffness with no damage when the stress was from tension to compression. However, the latter refers to negligibly small or even no tensile stiffness recovery after cracking [40]. In addition, a value of 0.2 is used as Poisson's ratio of concrete. The applied values of the failure ratios were tabulated in Table 2.

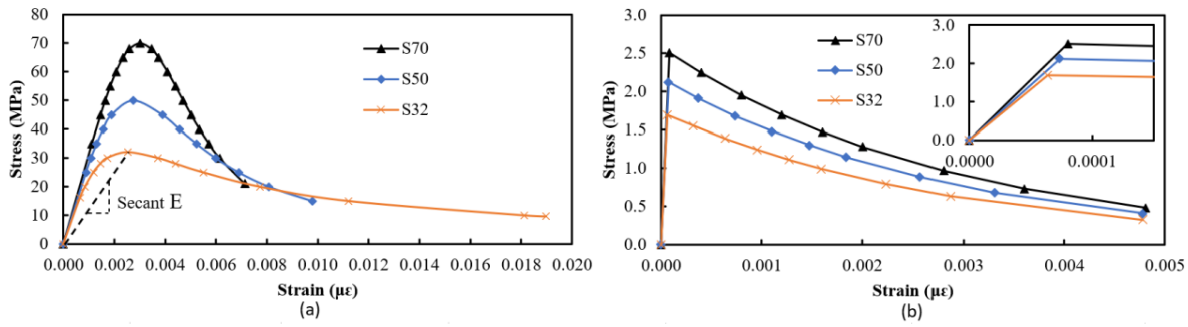

Figure 3. Concrete constitutive model of S70, S50 and S32 concrete: (a) Compressive model and (b) Tensile model.

Table 2. Applied values of the failure ratios

Dilation angle	Eccentricity	Biaxial to uniaxial compressive strength ratio fb0/fc0	K	Viscosity Parameter
36°	0.1	1.16	0.6667	0

3.1.2. GFRP bars, rubber and steel

The GFRP bars were modelled in the ABAQUS model as an isotropic linear elastic material up to failure. The rubber material was assumed to be isotropic and elastic, with a Young's modulus of 3 MPa and a Poisson's ratio of 0.49. Although 0.4999 Poisson's ratio for natural rubber is suggested by some researchers [41], 0.49 was assumed because high decimal digits of that value in ABAQUS dramatically increased the computational time. The steel components in the model were treated as rigid bodies, assuming no deformations or elasticity.

3.2 Interaction

The concrete-GFRP reinforcement interaction is created as embedded region with perfect bond. Similar approach was implemented by Mondal and Prakash [34] when they numerically investigated the effect of bond slip model on the torsional behavior of steel reinforced concrete bridge columns. This approach significantly reduced the computational time and improved the accuracy of the prediction. A coupling constraint was established to synchronize the motion of the round support and the spreader beam at each end. This is same to the actual setup where the beam and support are fully bolted together.

3.3 Load and boundary conditions

The FE modeling incorporated the key components of the physical test setup, such as the round supports, spreader beams, load cell and rubber mat as shown in Figure 2 (b) to accurately simulate the physical pure torsion test. The load cell was simplified with a 400 mm diameter hemispherical rigid body where the boundary conditions were applied to the reference point.

The support and spreader beam at the fixed end were constrained in all directions, while the rotatable end was allowed to rotate freely along the Z-axis. Consequently, the deck was fixed at one end, and the other end was free to rotate along the Z-axis. The torsion was simulated by applying a smoothly increasing displacement downwards in the active end until 70mm at the reference point of the load cell. This modeling approach accurately replicated the level of displacement applied during the experimental tests.

3.4 Dynamic explicit scheme

The explicit integration scheme, used in time marching algorithms, is well-suited for highly nonlinear problems where a static problem can be treated as dynamic. This scheme is stable and less prone to convergence issues compared to the implicit method [25]. In the study, a time period analysis was conducted as was also implemented by Cao et al. [22] and Mondal and Prakash [34]. It was observed that the FE results remained constant when the time exceeded 2 seconds. This is because the load increment was gradual, resulting in negligible inertial forces. Therefore, the explicit integration scheme is effective in accurately capturing the behavior of the system in this study.

3.5 Meshing

The element type used for modeling the concrete in the deck was defined as 3D 8-node linear brick elements (C3D8R) with three translational degrees of freedom at each node. Reduced integration was applied to minimize the stiffness matrix's sensitivity to shear locking. Hourglass control was automatically implemented by ABAQUS based on the element type to eliminate spurious modes. This concrete element type has been widely used by previous researchers [22, 25, 27, 29, 34] and has been verified to be able to accurately follow the constitutive law of integration. The rubber material and GFRP reinforcement bar were modeled using the same element type (C3D8R) as the concrete. It should be noticed that the widely

utilized 2-node linear 3D truss element (T3D2R) for GFRP bars in previous studies [23, 29] cannot provide torsional resistance in the model as torsion is a 3D behavior involving both shear and flexure in all directions. Therefore, 3D deformable solid element (C3D8R) for GFRP bars in torsional simulation is required.

Element deletion is an approximate approach to simulate the formation of cracks for simplicity and a powerful tool to get rid of distorted elements that prevents the simulation from converging [42]. This approach was applied in the model and the generated results with and without element deletion are shown in Figure 4 (a). The post-cracking part in the torque-twist curve of the model with element deletion is slightly lower than that in the other model without element deletion. It is to be noted that element deletion can cause disconnection in the nodes surrounding the deleted element and the effect is small since the element already achieved the maximum damage value.

The mesh size of the model is crucial for results accuracy and computational efficiency. Figure 4 (b) presented the result of mesh sensitivity analysis conducted to determine the optimal mesh size that strikes a balance between result accuracy and computational efficiency. As the mesh size is reducing from 60 mm to 30 mm, the torque- twist curves are closer to the experimental curve, and the value of the cracking torque is almost constant. However, the computational time was increasing dramatically along with the reduced mesh size. Hence, mesh size of 40 mm was implemented in the models.

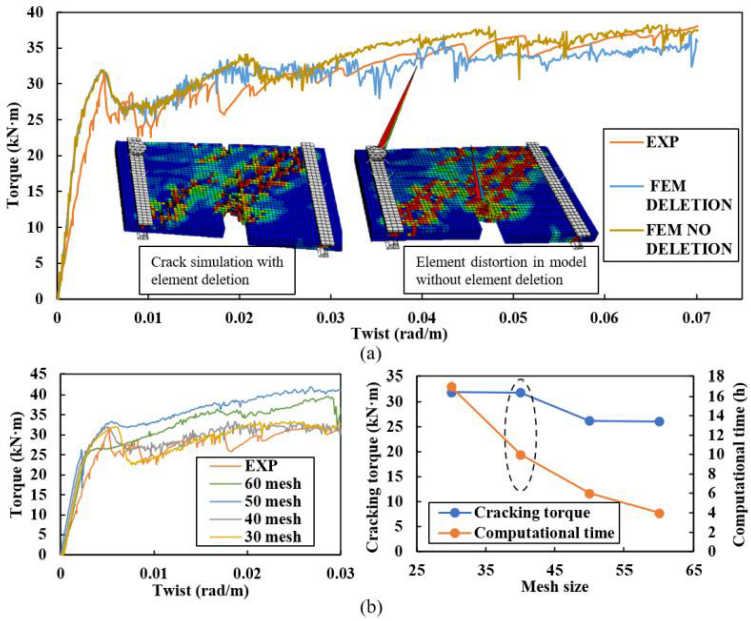

Figure 4. Meshing of model G250L2DDT: (a) Element distortion eliminated by element deletion and (b) Mesh sensitivity study.

4. FEA model results and comparison with the experiments

4.1 Torque-twist response

Figure 5 presents the over-all torque-twist response of the experimental results and FEM results for specimens G250L2ST, G250L2CT and G250L2DDT. In general, there is a reasonable match between the FEM generated curves and the experimental curves. It is worth mentioning that some discrepancies at the post-cracking behavior in G250L2ST between FEM and experiment can be due to the applied compressive model for concrete. Cao et al. [19] suggested a longer lasting confined effect in the descending portion of the compressive model so the concrete core can continue to resist the applied torque. Despite this variation, the model can accurately predict the whole experimental behavior for decks G250L2CT and G250L2DDT, and up to 0.05 rad/m twist in deck G250L2ST.

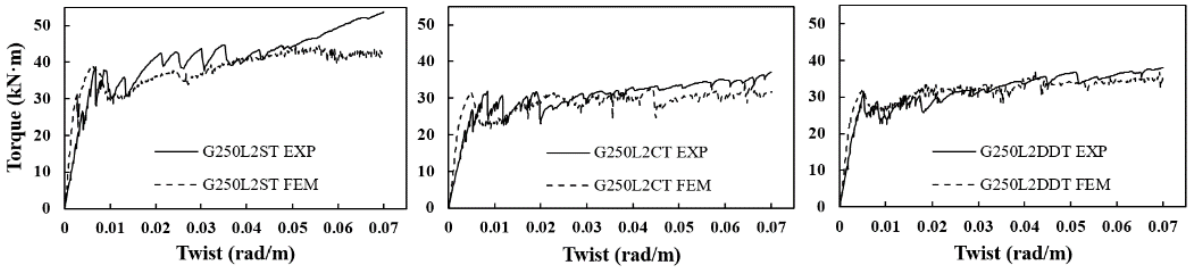

Figure 5. Comparison of torque-twist response between experiment and FEM

4.2 Crack propagation

The crack propagation in the FEM models is demonstrated with tension damage variable (DAMAGET) distribution. This variable ranges between zero and one where the former means no damage and the latter refers to a complete damage. In this model, the deletion of element happens when the maximum 0.9 damage variable defined in the CDP model was achieved. As shown in Figure 6, the distribution of element deletion due to tensile damage in the three models were very close to the observed crack propagation in the physical tests. The edge cutout led to concentrated cracks while the solid deck has evenly distributed torsional cracks. Furthermore, the application of the diagonal bars did not change the failure mode but the severity of damage around the cutout was lesser than the model without diagonal bars. Due to the cutout reinforcement, the torsional cracks happened in larger areas of the deck. Additionally, the bottom cracks of the decks were mirroring the cracks on the top. The formation of the first cracks in FEM were in line with the second exhibited cracks in the physical test. The first cracks in the model initiated from the further edge of the fixed end while they were observed to start from the corner of the edge cutout in the experiment. The initiation of first crack in the model is triggered by concrete stress concentration induced by the round support on bottom. A detailed observation of stress distribution as shown in Figure 7 proved that the stress around the cutout and at the further edge of the fixed end were in similarly high level. The cracks initiated in the area where least longitudinal reinforcement was applied. Beyond that, there are other minor differences between the model and the physical decks. First,

the FEM deck did not involve the embedded lift up hooks and holes where those hooks located (see Figure 6) and they affected the consistency of stiffness in the concrete surface in real case. Second, the interaction between supports, beams, rubbers, load cell and the concrete deck was complicated and cannot achieve exact recurrence. Hence, slight difference in the crack propagation is expected. In general, the FEM is presenting correct crack propagation of GFRP-RC decks under torsional load with acceptable difference with the real cases.

4.3 Stress distribution

Figure 7 demonstrates the absolute principal stress distribution on the concrete's top surfaces of the three FE models just before cracking happened. Both tension and compression exist in the concrete under torsion. The maximum compressive stress happened in edge of the bottom surface contacting with the end of the round support, but this value is negligible comparing to the concrete's compressive strength. The maximum tensile stress was distributed beside the central area in about 45-degree inclination. This is different from the elastic membrane theory that the maximum stress of a rectangular element under torsion should be in the center of the wide surface. The reason for this can be attributed to the supports and spreader beam disturbed the stress distribution and caused concentrated stress at the edge of the decks. The corresponding maximum strain is calculated to be 104 με, which is similar to the cracking strain recorded in the test by strain gauges attached to the concrete on the corner of the edge cutout with 45° inclination [1]. The existence of edge cutout significantly attracted the stress concentration and the corners of the edge cutout experienced high level of stress. Furthermore, the regions of highly concentrated stress around the cutout corner slightly became smaller with the application of diagonal bars in G250L2DDT model while the general stress distribution did not change much. These are all consistent with the experimental observations reported in Yang et al. [1] for the torque-strain response of concrete in GFRP-RC pontoon decks.

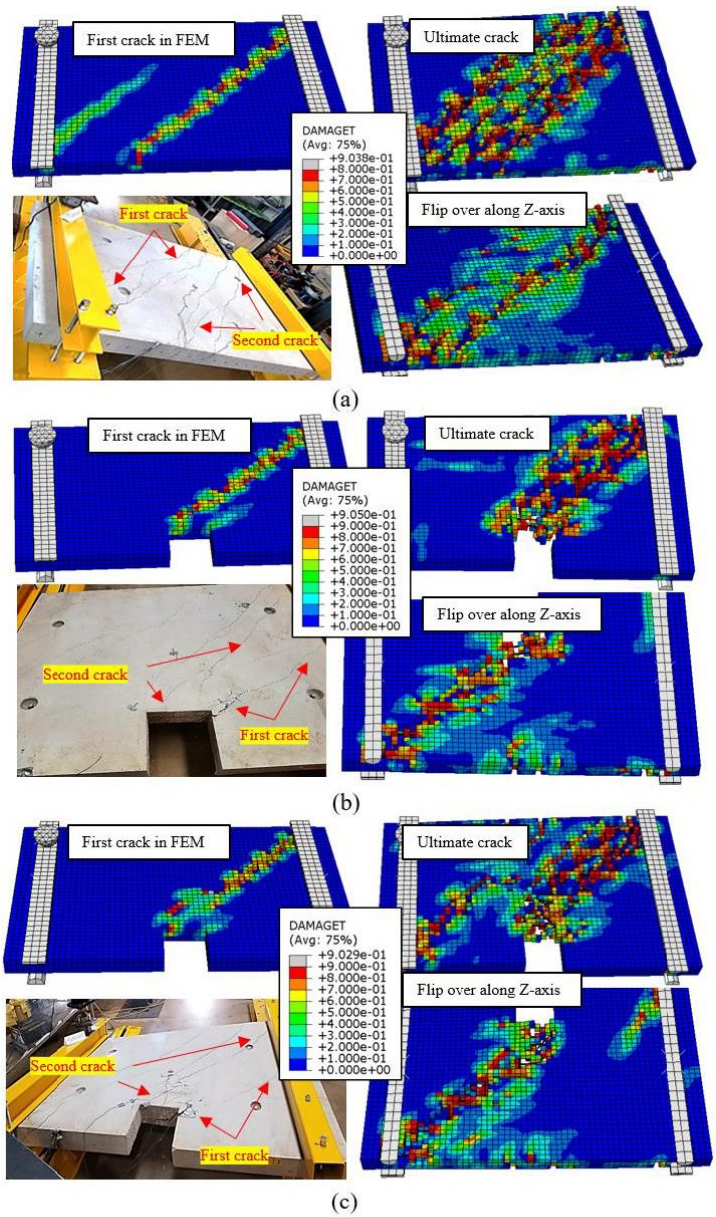

Figure 6. Crack propagation in FEM and test: (a) G250L2ST; (b) G250L2CT; (c) G250L2DDT.

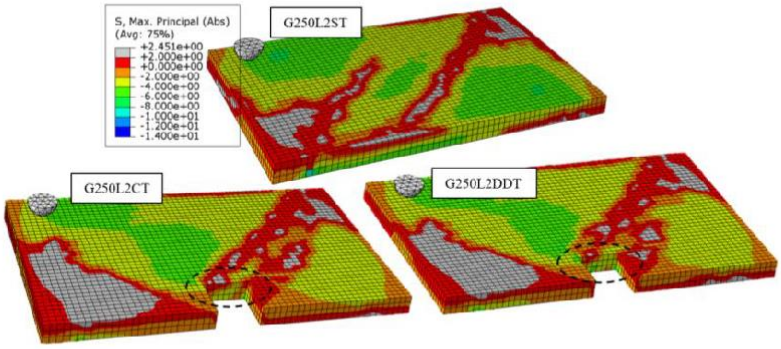

Figure 7. Stress distribution in concrete before cracking.

Figure 8 illustrates the distribution of absolute principal stress in the reinforcement at pre-cracking and post-cracking stages, under respective identical twists, for the three decks. The GFRP reinforcements experienced high stress levels concurrent with the formation of torsional cracks in the concrete. Figure 9 presents the experimental torque-twist response of the three physically tested decks, as recorded by strain gauges shown in Figure 1. Some findings in experimental torque-twist response can be reflected in the stress distribution contour in the reinforcement. Notably, strain gauges of E2, C2, E4, and C4 in the physical deck returned a close level of strain values which indicated a consistent stress distribution in the reinforcement mesh. This can be clearly visualized in the right side of Figure 8 in G250L2ST wherein the FEM stress distribution contour show high level of stress in a number of reinforcing bars along the diagonal line of the mesh. Moreover, strain gauge C2 in the physical G250L2CT deck revealed the longitudinal bar beside the cutout experiencing high level of stress. This can be evidenced by the noted maximum stress in the right-side stress distribution contour of G250L2CT and G250L2DDT shown in the FEM results. Additionally, the low level of strain recorded by D1 in the physical G250L2DDT specimen before cracking means that the diagonal bar helped mitigate initial cracking at the corner of the edge cutout. This is reflected by the noted maximum stress in the diagonal bar of G250L2DDT FEM before cracking. It is also noticed that the diagonal bars did not contribute to reducing the maximum stress in the reinforcement after cracking. The maximum stress in the reinforcement of G250L2DDT FEM was as high as that of G250L2CT FEM. Interestingly, the FEM stress distribution contour revealed significant stress in the transverse bars, an aspect not measured during the physical tests. The FEM showed that stress in certain deck areas on the transverse bars could be similar to that in the longitudinal bars, indicating the need for similar amounts of transverse and longitudinal reinforcement in the deck under torsion. Generally, the FEM models are closely

reflecting the stress response recorded in the test and provide more detailed information of stress distribution.

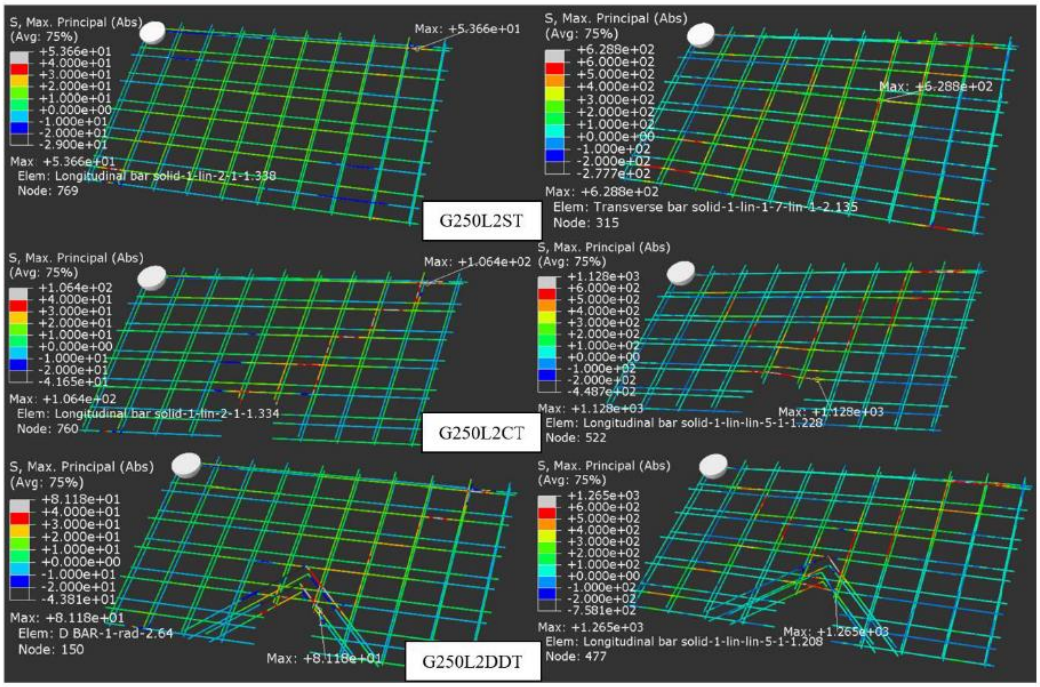

Figure 8. Stress distribution in the reinforcement: Before cracking (left); Maximum twist (right).

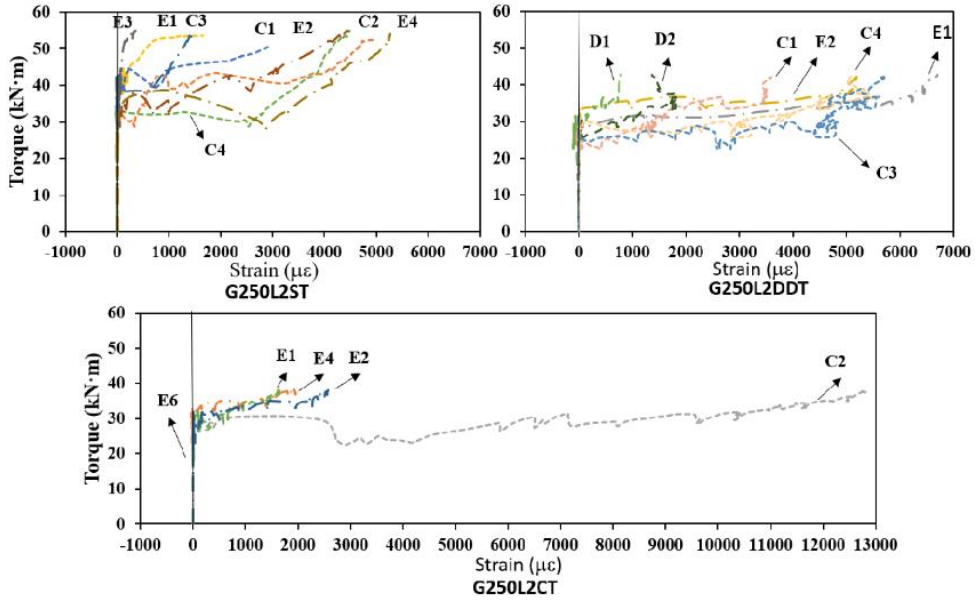

Figure 9. Experimental torque-strain response recorded by strain gauges.

5. Parametric study of the torsional behavior of GFRP-RC decks

Parametric study was carried out using the validated FEM for further understanding of the effect of various design parameters on the deck's torsional behavior. The three validated models were extended to a total of 27 models with variational parameters as specified in Table 3. There are three types of numerical models, including solid deck (S), decks with cutout (C), and decks with cutout reinforced by diagonal bars (D). Published works on torsional behavior of GFRP-RC structures suggested a number of design parameters affecting the torsional behavior. These includes concrete compressive strength $f'c$ (32, 50, 70MPa), geometry of cutout (chamfer, fillet and half round), cutout reinforcement distribution (two sets, four sets and six sets of diagonal bars), reinforcement spacing (100 mm, 200 mm, 250 mm and 350 mm on centers), and reinforcement bar diameter (10mm, 12mm and 16mm). As the design criteria requires grade S50 for pontoon [43], the parametric was based on the models built with a concrete compressive strength of 50 MPa. Pontoon decks that have a cutout with and without two sets of diagonal bars were taken as references in the following comparison. The generated numerical results are tabulated in Table 4 and the overall torsional behavior are discussed in the succeeding sections.

Table 3. Design table for parametric study

No.	Type	$f'c$ (MPa)	Cutout	Diagonal bar	Reinforcement		
					L	T	Diameter (mm)
1	**S**	70	NA	NA	13(0.54%)/@250	20(0.52%)/@250	10
2		70	Square	NA	13(0.54%)/@250	20(0.52%)/@250	10
3		50	Square	NA	13(0.54%)/@250	20(0.52%)/@250	10
4		32	Square	NA	13(0.54%)/@250	20(0.52%)/@250	10
5		50	Chamfer 40	NA	13(0.54%)/@250	20(0.52%)/@250	10
6	**C**	50	Chamfer 80	NA	13(0.54%)/@250	20(0.52%)/@250	10
7		50	Chamfer 120	NA	13(0.54%)/@250	20(0.52%)/@250	10
8		50	Fillet 40	NA	13(0.54%)/@250	20(0.52%)/@250	10
9		50	Fillet 80	NA	13(0.54%)/@250	20(0.52%)/@250	10
10		50	Fillet 120	NA	13(0.54%)/@250	20(0.52%)/@250	10
11		50	Half round	NA	13(0.54%)/@250	20(0.52%)/@250	10

12		70	Square	2 SETS	13(0.54%)/@250	20(0.52%)/@250	10
13		50	Square	2 SETS	13(0.54%)/@250	20(0.52%)/@250	10
14		32	Square	2 SETS	13(0.54%)/@250	20(0.52%)/@250	10
15		50	Square	4 SETS	13(0.54%)/@250	20(0.52%)/@250	10
16		50	Square	6 SETS	13(0.54%)/@250	20(0.52%)/@250	10
17		50	Square	2 SETS	13(0.79%)/@250	20(0.75%)/@250	12
18		50	Square	2 SETS	13(1.39%)/@250	20(1.34%)/@250	16
19	**D**	50	Square	2 SETS	30(1.26%)/@100	20(0.52%)/@250	10
20		50	Square	2 SETS	16(0.67%)/@200	20(0.52%)/@250	10
21		50	Square	2 SETS	8(0.42%)/@350	20(0.52%)/@250	10
22		50	Square	2 SETS	13(0.54%)/@250	48(1.26%)/@100	10
23		50	Square	2 SETS	13(0.54%)/@250	24(0.63%)/@200	10
24		50	Square	2 SETS	13(0.54%)/@250	14(0.37%)/@350	10
25		50	Square	2 SETS	30(1.26%)/@100	48(1.26%)/@100	10
26		50	Square	2 SETS	16(0.67%)/@200	24(0.63%)/@200	10
27		50	Square	2 SETS	8(0.42%)/@350	14(0.37%)/@350	10

Table 4. FEM and calculated results.

No.	FEM						Calculation					
	$(GJ)_{ini}$ (kN·m²)	φ_{cr} (rad/m)	T_{cr} (kN·m)	$(GJ)_{pre}$ (kN·m²)	$T_{0.07\varphi}$ (kN·m)	$(GJ)_{post}$ (kN·m²)	$(GJ)_{ini}$ (kN·m²)		$(GJ)_{pre}$ (kN·m²)		T_{cr} (kN·m)	
1	14120	0.003324	31.29	9414	42.15	163	12082	0.86	8944	0.95	29.87	0.95
2	10039	0.004810	31.16	6478	31.72	9	9532	0.95	7056	1.09	29.87	0.96
3	9320	0.004624	27.09	5859	31.56	68	8776	0.94	5511	0.94	25.24	0.93
4	8679	0.004503	21.46	4767	30.13	132	8095	0.93	3852	0.81	20.19	0.94
5	9357	0.004563	26.76	5865	32.47	87	8776	0.94	5511	0.94	25.24	0.94
6	9478	0.004686	27.16	5796	32.61	83	8776	0.93	5511	0.95	25.24	0.93
7	9557	0.004686	27.32	5830	29.41	32	8776	0.92	5511	0.95	25.24	0.92
8	9329	0.004685	26.61	5680	32.56	91	8776	0.94	5511	0.97	25.24	0.95
9	9421	0.004685	27.11	5786	27.91	12	8776	0.93	5511	0.95	25.24	0.93
10	9463	0.004810	26.91	5594	31.92	77	8776	0.93	5511	0.99	25.24	0.94
11	9518	0.004685	27.30	5828	32.54	81	8776	0.92	5511	0.95	25.24	0.92
12	9992	0.004937	31.89	6459	36.22	67	9532	0.95	7056	1.09	29.87	0.94
13	9323	0.005066	27.58	5445	36.32	134	8776	0.94	5511	1.01	25.24	0.92
14	8830	0.005066	22.59	4459	35.33	196	8095	0.92	3852	0.86	20.19	0.89
15	9419	0.005066	27.96	5519	43.07	232	8776	0.93	5511	1.00	25.24	0.90
16	9419	0.005066	28.49	5624	56.66	433	8776	0.93	5511	0.98	25.24	0.89
17	9422	0.005001	28.21	5641	42.30	218	8776	0.93	5511	0.98	25.24	0.89
18	9612	0.005001	28.94	5786	56.00	417	8776	0.91	5511	0.95	25.24	0.87
19	9451	0.005462	29.56	5413	52.71	358	8776	0.93	5511	1.02	25.24	0.85
20	9531	0.004686	27.55	5879	38.71	171	8776	0.92	5511	0.94	25.24	0.92
21	9453	0.004748	27.31	5752	35.59	127	8776	0.93	5511	0.96	25.24	0.92
22	9411	0.004748	28.09	5917	56.31	426	8776	0.93	5511	0.93	25.24	0.90
23	9327	0.004937	27.74	5619	44.67	260	8776	0.94	5511	0.98	25.24	0.91
24	9466	0.004502	26.94	5983	38.73	180	8776	0.93	5511	0.92	25.24	0.94

25	9559	0.005196	30.08	5789	74.90	691	8776	0.92	5511	0.95	25.24	0.84
26	9344	0.005066	28.03	5534	43.27	234	8776	0.94	5511	1.00	25.24	0.90
27	9434	0.004502	27.34	6073	28.57	19	8776	0.93	5511	0.91	25.24	0.92

5.1 Effect of concrete compressive strength *f'c*

Concrete compressive strengths of 32 MPa, 50 MPa and 70 MPa were applied to models G250L2CT and G250L2DDT. The generated torque-twist curves for these decks are demonstrated in Figure 10. Models of G250L2CT and G250L2DDT are showing the same trend. The concrete compressive strength has notable effect throughout the analyses. Firstly, the cracking torque of the pontoon decks significantly increased along with the increasing concrete compressive strength. The cracking torque of the decks with 70MPa concrete strength is 43% higher than that of the decks with 32MPa concrete strength as listed in Table 4. The normalized cracking toque to concrete strength ratios of the six decks are listed in Table 5. The results revealed that the lower concrete compressive strength presented a greater efficiency in resisting torsional cracks than the higher concrete strength. These findings can be explained by the same reason that the first torsional crack was controlled by the concrete tensile strength which has a direct co-relation with the square root of concrete compressive strength as shown in Equation 6. Secondly, the higher concrete strength is, the stronger torsional rigidity in the pre-cracking stage was exhibited. Due to the elastoplastic characteristic of concrete, the pre-cracking torsional behavior of the models was linear first and then it became non-linear when approaching the cracking torque. The difference between the models with variable concrete strength in the linear portion of the curve was minor as shown by magnifying the results, as shown in Figure 10. The initial torsional rigidity $(GJ)_{ini}$, calculated with the slope of the linear portion, presents the strongest torsional resistance of a deck. Owing to the compressive softening effect of the concrete after 0.5 *f'c* yield stress (see Figure 3 (a)), the concrete was more ductile in lower than higher strength concrete, resulting in significantly reduced torsional

rigidity before cracking. In Table 4, a general pre-cracking torsional rigidity $(GJ)_{pre}$ is calculated by dividing the cracking torque to the corresponding twist. The values of the six models are reflecting a positive effect of increased concrete compressive strength on the pre-cracking torsional rigidity. For instance, when the concrete strength in G250L2CT and G250L2DT increased from 32MPa to 50MPa, the $(GJ)_{pre}$ increased by 23%. However, the post-cracking torsional rigidity decreased as the concrete compressive strength increases and the post-cracking behavior were more stable in the decks with the lowest 32MPa concrete compressive strength. The latter can be explained by that the constitutive model of 32 MPa concrete in tension and compression to have a lesser gradient than 50MPa and 70MPa concrete's constitutive models. It is expected therefore that the decks using 32 MPa concrete will experience less deviations in the torsional resistance after cracking. The former is because the applied concrete compressive models with high concrete compressive strength ends at low strain which means the high strength concrete were to be fully damaged earlier than the low strength concrete under compressive deformation. Therefore, the decks with higher strength of concrete rely on torsional resistance from reinforcements soon after cracking while there is still residual torsional resistance from the concrete contributing to the general post-cracking torsional rigidity in the decks with lower strength concrete. This is also supported by the experimental findings reported by Yang et al. [1] that double meshes prevented excessive cracks in the concrete core between meshes, so the concrete can still contribute to the post-cracking torsional resistance. Eventually, the post-cracking torsional rigidity is supposed to be fully dependent on the reinforcement after the concrete is completely damaged. In conclusion, higher concrete compressive strength results in greater torsional rigidity in the pre-cracking stage and stronger cracking torque.

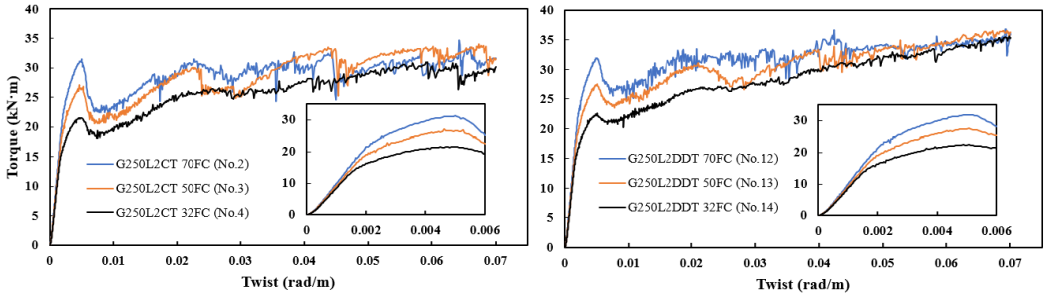

Figure 10. Effect of concrete strength on the torsional behaviour of GFRP-RC decks with an edge cutout and with diagonal bars

Table 5. Normalized cracking torque to concrete strength ratio.

SPECIMEN	G250L2CT			G250L2DDT		
	70 MPa	50 MPa	32 MPa	70 MPa	50 MPa	32 MPa
T_{cr}/f'_c	0.39	0.53	0.85	0.40	0.58	0.95

5.2 Effect of cutout geometry

Evaluation of the cutout geometry was carried out using the FE models for deck G250L2CT with 50MPa concrete compressive strength. Three sizes of chamfers, fillets and a half round shape as listed in Table 3 were applied to the square cutout, and the generated torque-twist curves of the seven FE models simulated are plotted in Figure 11. The figure shows all decks exhibited nearly identical torsional behavior before 0.01 rad/m twist, but the rest part of the torque-twist curve for the decks are different in the deviation, which means the post-cracking crack propagations slightly varied. Table 4 lists the values of T_{cr}, $(GJ)_{pre}$ and $(GJ)_{post}$ of the seven simulated decks with variable cutout geometry (No.5-11). The values are very close to those of the deck with square cutout (No.3), and the maximum variations in T_{cr} and $(GJ)_{pre}$ between them are 5% and 2%, respectively. Figure 12 shows that the geometric shape of the cutout has no obvious effect on the stress distribution in the concrete. The maximum stress always occurred to the node in the edge of top surface in the cutout regardless of the cutout shape. Afterwards, the maximum stress in concrete suddenly shifted to the further edge of the fixed end and the first crack initiated there. This is exactly same as the first crack formation in

the model with square cutout. The cutout geometry does not have a significant effect on the pre-cracking torsional behavior of the tested decks. In terms of post-cracking behavior, the residual post-cracking torsional rigidity of the tested models are only 0.5%-1.6% of the uncracked stage, which means that the decks already failed after cracking. The crack propagation is also similar to that of deck G250L2CT with 70MPa as shown in Figure 6. Generally, the results showed that the cutout geometry did not have influence on the pre-cracking torsional behavior, and it just slightly changed the crack propagation.

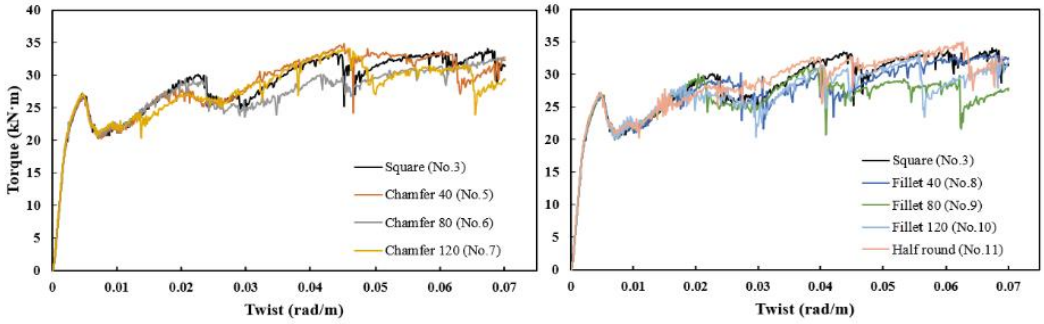

Figure 11. Effect of cutout geometry on the torsional behaviour of GFRP-RC decks

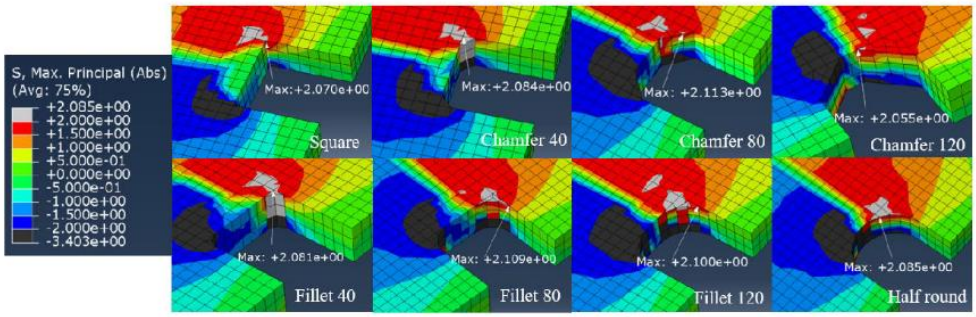

Figure 12. Maximum stress in the cutout with geometric shapes

5.3 Effect of cutout reinforcement distribution

The diagonal bars embedded 25mm offset the cutout corner can enhance the cutout and improve the torsional resistance of the decks as demonstrated from the experimental works. In the parametric study, decks with two sets, four sets and six sets of diagonal bars were simulated. The generated torque-twist curves were compared with the model without diagonal bars as shown in Figure 13. There was no discrepancy observed in the elastic range. However, the

cracking torque and post-cracking torsional rigidity increase as more diagonal bars were applied at the corners of the edge cutout. Comparing with the deck without diagonal bars (No.3), the decks with two sets (No.13), four sets (No.15) and six sets (No.16) diagonal bars delayed the formation of the first crack, and the cracking torque was improved by 2%, 3% and 5%, respectively. The small enhancement effect of the diagonal bars on the cracking torque can be primarily due to that the first crack forming from the further edge of the concrete in the fixed end where concentrated stress was induced by the round support rather than from the cutout corner. However, the increase in the post-cracking torsional rigidity is significant, especially in the deck with six diagonal bars. This deck exhibited a 433 kN·m^2 $(GJ)_{post}$ or 6.4 times that of the deck without diagonal bars. This result suggests that the application of more number and longer length of diagonal bars can enhance the torsional resistance in central area of the deck. This approach can also prevent the formation of torsional cracks perpendicular to the diagonal bar distribution as shown in Figure 14. It should be mentioned that the provision of two sets of diagonal bars did not change much the torsional behavior of the deck compares to that of the deck without diagonal bars. This is because the two sets diagonal bars are short and can only influence the stress distribution in a limited area around the cutout. Consequently, the application of at least four diagonal bars can delay the formation of the first crack and can significantly improve the post-cracking behavior.

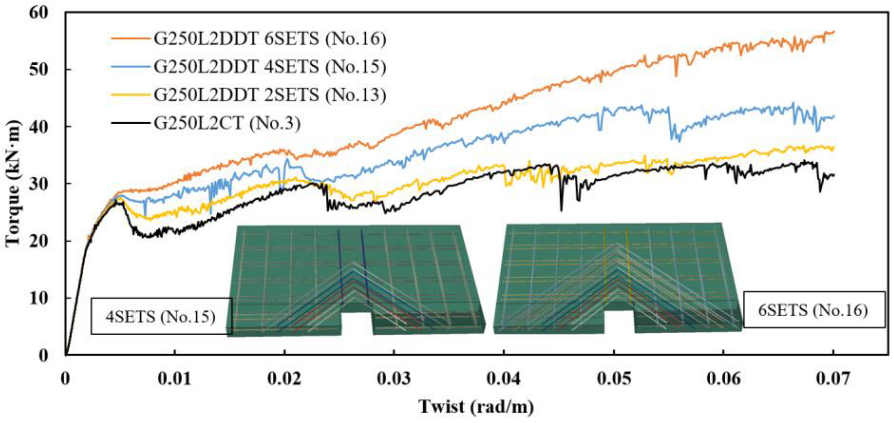

Figure 13. Effect of cutout reinforcement

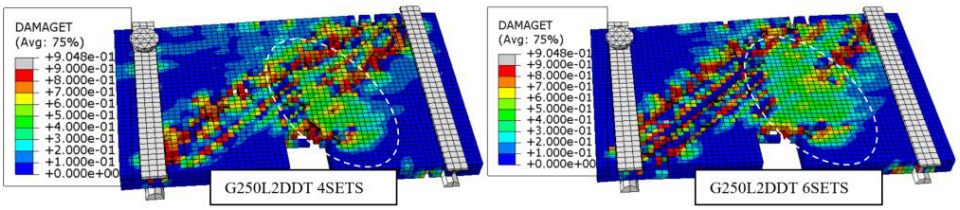

Figure 14. The diagonal bars prevented torsional cracks perpendicular to the bar distribution in the deck models with 4sets and 6sets diagonal bars.

5.4 Effect of bar diameter

The effect of bar diameter was evaluated by replacing the 10 mm diameter bars in model No.13 with 12mm and 16mm bars, respectively, and keeping the reinforcement configuration, diagonal bar, and bar properties same. Figure 15 compares the torque-twist response between the decks reinforced with 10 mm, 12 mm and 16 mm diameter bars. As shown in the figure, the notable influence by changing the bar diameter begins from the first peak, where the cracking torque was increased by 2% for 12 mm diameter bars and 5% for 16 mm diameter bars. This increase in the cracking torque can be attributed to the larger contact surface between the bigger diameter bars and the concrete than smaller diameter bars. This composite action resulted in higher bonding strength and better crack control. For the same reason, the exhibited cracks in the decks with larger diameter bars were minor under the same level of twist as shown in Figure 15. Furthermore, the post-cracking torsional rigidity of these decks are 1.6 times and 3.1 times, respectively, higher than that of deck reinforced with 10 mm diameter bar. That is because the torsional constant J of the decks after cracking is mainly contributed by the reinforcement bars [1]. With increasing bar diameter, the J is increasing because of the larger cross-sectional area of the bars. It is noticed that the $(GJ)_{post}$ of decks with 12mm diameter bar and 16mm diameter are similar to those of decks with four sets and six sets diagonal bars, respectively, but the later ones exhibited wider cracks after cracking. Larger diameter bars provide strong torsional resistance throughout the whole deck while diagonal bars only protect local area covered by the diagonal bars. Consequently, the larger bar diameter slightly increases

the cracking torque and has a more obvious positive effect on the post-cracking torsional rigidity than smaller diameter bars.

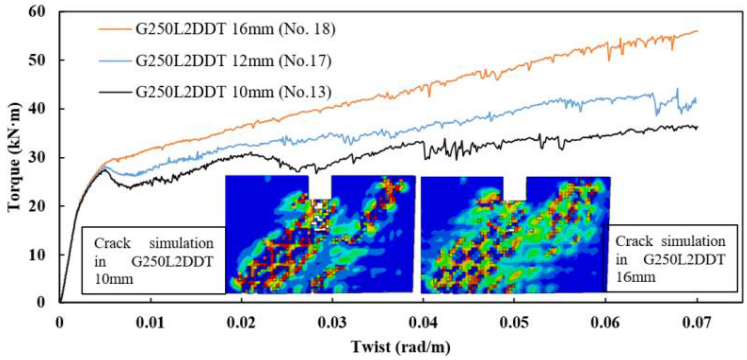

Figure 15. Crack simulation in the decks with 10 and 16 mm reinforcement bar at 0.07 rad/m twist

5.5 Effect of reinforcement spacing

The last nine models specified in Table 3 are for the decks with different spacing of transverse and longitudinal reinforcements. Decks reinforced with 10 mm diameter GFRP bars and spaced at 100 mm, 200 mm, 250 mm, and 350 mm on centers in each direction were evaluated. The generated torque-twist curves of the nine models were compared with that of model No.13 as shown in Figure 16. In general, the changes of reinforcement spacing did not visually affect the decks' pre-cracking behavior in the elastic range while the denser the reinforcement was, the higher post-cracking torsional rigidity was generated. Moreover, the collected results in Table 4 show that providing denser spacing of reinforcement in each direction can slightly increase the cracking torque. The most obvious can be seen in the deck with 100 mm bar spacing. Models No.19, No.22 and No.25 had a cracking torque of 7%, 4% and 9%, respectively higher than that of model No.13. The $(GJ)_{post}$ of them is 358, 426, 691kN·m^2, which is 2.7, 3.2 and 5.1 times higher that of the model of No.13, respectively, or 7%, 7% and 12% of their respective $(GJ)_{pre}$. This behavior can be explained by large numbers of GFRP reinforcement bars providing high post-cracking torsional rigidity and strong cracking control.

This is a clear improvement in the cracking torque and post-cracking torsional behavior attributed by the densely spaced reinforcement.

The right side of Figure 16 compared the torque-twist responses of decks with unequal reinforcement spacing in transverse and longitudinal directions. The main influence caused by the unequal reinforcement space is in the post-cracking behavior. Models No.19, No.20 and No.21 fixed the transverse reinforcement space at 250 mm, while the longitudinal reinforcement ratio are 233%, 124% and 78% higher than model No.13. The corresponding post-cracking torsional rigidity of the former three decks are 266%, 127% and 94%, respectively, of the $(GJ)_{post}$ of the latter one. Similarly, models No. 22, No.23 and No.24 reversed the reinforcement spacing in the two directions with fixed 250 mm reinforcement space in longitudinal direction. While the percentage of reinforcement ratio variation remained same, the $(GJ)_{post}$ of these three decks are 317%, 194% and 134%, respectively, of the $(GJ)_{post}$ in model No.13. The changes of $(GJ)_{post}$ due to variation in transverse reinforcement ratio are generally higher than the variation in the longitudinal reinforcement ratio variation, implying that the deck's transverse reinforcement is of lesser as importance than longitudinal reinforcement in resisting torsional force. Furthermore, the crack propagation in Figure 17 shows that the torsional crack tended to extend in the direction with less reinforcement ratio as there are longitudinal cracks in the model No.22 and transverse cracks in the model No.19. Equal reinforcement spacing in two directions resulted in inclined torsional cracks in model No.25. In conclusion, transverse and longitudinal reinforcement contribute equally to the deck's post-cracking behavior in $(GJ)_{post}$ and crack propagation.

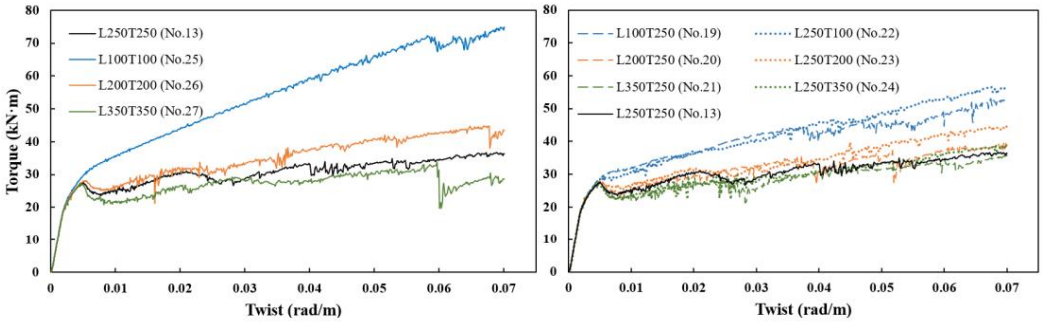

Figure 16. Effect of reinforcement spacing

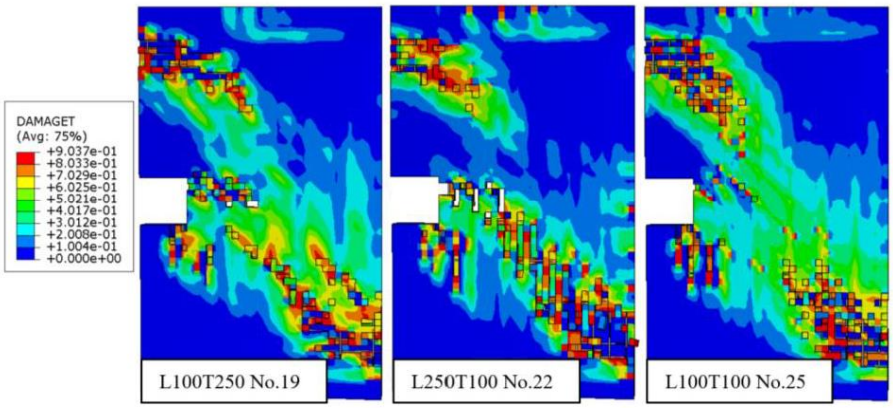

Figure 17. Cracking propagation in decks with unequal reinforcement spacing in longitudinal and transverse directions

6. Theoretical analysis equations

The parametric study revealed that the pre-cracking torsional behavior of the GFRP-RC deck is mainly dependent on the concrete. This is consistent with the findings in previous studies which related the pre-cracking torsional behavior of reinforced concrete structures to the concrete property and structure's dimension [5, 6]. The torsional rigidity of an elastic member is defined as GJ, shear modulus times torsional constant. For elastic material, G can be expressed with elastic modulus and Poisson's ratio by Equation 7.

$$G = (0.5E/(1+v)) \tag{7}$$

Furthermore, the torsional constant J of a rectangular cross section objective can be roughly calculated by the following equation [44]:

$$J = \frac{y}{2} \times \left(\frac{x}{2}\right)^3 \times \left(\frac{16}{3} - 3.36 \times \frac{x}{y} \times (1 - x^4/(12 \times y^4))\right) \quad (8)$$

where y is the length of the long side; and x is the length of the short side.

As the initial torsional behavior of the GFRP-RC decks was presenting the concrete's elastic characteristic, the initial torsional rigidity $(GJ)_{ini}$ can be calculated by combining the equation 7 and 8 as following:

$$(GJ)_{ini} = (0.5E_0/(1+v)) \times \left(\frac{y}{2} \times \left(\frac{x}{2}\right)^3 \times \left(\frac{16}{3} - 3.36 \times \frac{x}{y} \times (1 - x^4/(12 \times y^4))\right)\right) \quad (9)$$

where E_0 is the elastic modulus of concrete; ν is Poisson's ratio of concrete, and 0.2 value is used; x is the thickness of the deck; y is the width of the deck, and it is adjusted by reducing the depth of cutout in the decks with cutout.

The calculated $(GJ)_{ini}$ is listed in Table 4 with the comparison with the FEM results (Cal/FEM) next to it. The prediction equation generally underestimated the initial torsional rigidity as the Cal/FEM values are all lower than 1.0. The maximum disparity happened to model No.1, the solid deck, with Cal/FEM value of 0.86, while the rest Cal/FEM values are all between 0.91 and 0.95. The difference is probably due to the variation of Poisson's ratio for different grades of concrete ignored in the simulation. However, the equation is still accurate in predicting the initial torsional rigidity of the decks.

The initial torsional rigidity only presents the decks' torsional resistance in the concrete's elastic range, while the general pre-cracking torsional rigidity is more practical for engineers to evaluate the deck's general ability to resist torsion before cracking. The nonlinear portion of the deck's pre-cracking torsional behavior is related to the elastoplastic range of the concrete compressive model. It is assumed that the softened elastic modulus of concrete at torsional cracking equals to the secant elastic modulus (Secant E) at compressive cracking, which can

be calculated by the maximum stress divided by the corresponding strain in the concrete compressive model (see Figure 3). The general pre-cracking torsional rigidity $(GJ)_{pre}$ can be obtained by substituting the Secant E to the elastic modulus in equation 9. The results are listed in Table 4 with the corresponding Cal/FEM ratio. The Cal/FEM values range from 0.81 to 1.09 with the lowest correlations were for models No.4 and No.14, which were built with 32MPa concrete. This can be also explained by the Poisson's ratio effect as well. Generally, considering the softened elastic modulus E equals to Secant E in equation 9 can provide a good prediction for the general torsional rigidity of the decks at the pre-cracking stage.

Yang et al. [1] have introduced the following equation 10 from ACI 318-14 [39] for prediction of cracking torque in GFRP-RC decks and validated the accuracy in predicting T_{cr} for decks with and without cutout by considering the cutout reducing the deck's width in the midspan cross section. However, the reduction effect on T_{cr} due to the cutout was not obviously reflected in the simulated models as Table 4 shows the No.1 model, solid deck's T_{cr} was nearly equal to the decks with an edge cutout (No.2 and No.12). This is attributed to the deck's first cracking formation difference between the modelling and the physic test as explained before. Although the general pre-cracking torsional rigidity in the models and physical decks are similar, there is stiffness difference in some local areas of the deck due to the factors other than the decks themselves, i.e. embedded hooks and components interaction. Since the cutout reduction effect on T_{cr} was not observed in the FEM, equation 10 is established to calculate the first torsional cracking of the decks.

$$T_{cr} = 0.33\sqrt{f'_c}\left(\frac{{A_{cp}}^2}{P_{cp}}\right) = 0.33\sqrt{f'_c}\left(\frac{x^2y^2}{2(x+y)}\right) \quad (10)$$

where A_{cp} is the area enclosed by the outside perimeter of the concrete cross section; and P_{cp} is the outsider perimeter of the concrete cross section; y is width of deck's cross section; x is the height of the deck's cross section.

The calculated T_{cr} with the Cal/FEM ratio are reported in Table 4. The results showed good correlation but slightly underestimated the cracking torque of the decks with strong reinforcement design, including larger bar diameter, more sets of diagonal bars and dense reinforcement space. As noted, the first torsional crack is governed by the compressive strength of the concrete and the geometry of the deck but does not involve any parameters related to the internal GFRP reinforcements. The Cal/FEM ratio values range from 0.84 to 0.96. The lowest Cal/FEM ratio is in the model with 100 x 100 mm reinforcement or No.25. Generally, the equation well predicted the cracking torque.

7. Conclusion

This paper presented a detailed finite element (FE) analyses of the torsional behavior of GFRP-RC deck investigating the effects of critical design parameters such as the concrete compressive strength, cutout geometry, cutout reinforcement distribution, bar diameter and reinforcement spacing. The FE model was validated with the experimental results of large scale GFRP-RC decks. Based on all the generated results, the following conclusion can be drawn:

- The pre-cracking torsional behavior of the GFRP-RC deck is significantly affected by the levels of concrete compressive strength with the GFRP bars affected to some degree the cracking torque. The higher concrete compressive strength leads to stronger $(GJ)_{ini}$, $(GJ)_{pre}$ and T_{cr}.
- The cutout geometry has no effect of the pre-cracking torsional behavior. The cracking of the decks with chamfer, fillet and half round shape cutouts all initiated in the edge of top surface in the cutout and shifted to the further edge of the fixed end.
- The GFRP reinforcement i.e. diagonal bar, large bar diameter and dense reinforcement spacing has only a minor effect on the first cracking torque but has a significant contribution in the post-cracking behaviour. More than four sets diagonal bars, large

bar diameter and dense reinforcement space in each direction all have positive effect on increasing the deck's $(GJ)_{post}$. Moreover, cracks are narrowed in the decks with large bar diameter and dense reinforcement space after cracking.

- The proposed equations can reliably predict the pre-cracking torsional strength and rigidity of GFRP-RC decks by considering the concrete compressive strength and geometric properties of the decks.

The results of the FE simulations are validated with the actual torsional behaviour of GFRP-RC decks. Other important design parameters such as the dimension and location of the cutout is proposed for future study to further improve the model's accuracy in reflecting the cutout reduction effect on the cracking torque, and to understand in more detail the torsional capacity of the GFRP-RC decks.

8. Acknowledgments

The authors gratefully acknowledge the financial support provided by the Queensland Department of Transport and Main Roads (DTMR), the Advance Queensland Industry Research Fellowship Program (AQIRF 119-2019RD2), and the Natural Science and Engineering Research Council (NSERC) of Canada. We extend our appreciation to Sustainable Alliance Pty Ltd (Inconmat) for supplying the GFRP reinforcement and to Jetty Specialist for their craftsmanship in producing the precast-concrete pontoon decks. We are also thankful to the dedicated technicians and students at the University of Southern Queensland for their invaluable support during the plank production and evaluation process.

9. References

1. Yang, X., O. Alajarmeh, A. Manalo, B. Benmokrane, Z. Gharineiat, S. Ebrahimzadeh, C.-D. Sorbello, and S. Weerakoon, *Torsional behavior of GFRP-reinforced concrete pontoon decks with and without an edge cutout.* Marine Structures, 2023. **88**: p. 103345.
2. ACI, *Guide for the Design and Construction of Structural Concrete Reinforced with Fiber-Reinforced Polymer (FRP) Bar, (440. 1R-15)* American Concrete Institute, 2015.
3. CSA, *Design and construction of building structures with fibre-reinforced polymers.* Canadian Standards Association, CAN/CSA-S806-12, 2012.
4. Razaqpur, A., F. Bencardino, L. Rizzuti, and G. Spadea, *FRP reinforced/prestressed concrete members: A torsional design model.* Composites Part B: Engineering, 2015. **79**: p. 144-155.
5. Hsu, T.T., *Torsion of structural concrete-behavior of reinforced concrete rectangular members.* Special Publication, 1968. **18**: p. 261-306.
6. Hsu, T.T.C., *Torsion of reinforced concrete*. 1984.
7. Chiu, H.-J., I.-K. Fang, W.-T. Young, and J.-K. Shiau, *Behavior of reinforced concrete beams with minimum torsional reinforcement.* Engineering Structures, 2007. **29**(9): p. 2193-2205.
8. Lopes, A.V., S.M. Lopes, and R.N. do Carmo, *Stiffness of reinforced concrete slabs subjected to torsion.* Materials and structures, 2014. **47**(1): p. 227-238.
9. Rahal, K.N., *Torsional strength of normal and high strength reinforced concrete beams.* Engineering Structures, 2013. **56**: p. 2206-2216.
10. Ju, H., D. Lee, J.R. Kim, and K.S. Kim. *Maximum torsional reinforcement ratio of reinforced concrete beams*. in *Structures*. 2020. Elsevier.
11. Kim, M.-J., H.-G. Kim, Y.-J. Lee, D.-H. Kim, J.-Y. Lee, and K.-H. Kim, *Pure torsional behavior of RC beams in relation to the amount of torsional reinforcement and cross-sectional properties.* Construction and Building Materials, 2020. **260**: p. 119801.
12. Hadhood, A., M.G. Gouda, M.H. Agamy, H.M. Mohamed, and A. Sherif, *Torsion in concrete beams reinforced with GFRP spirals.* Engineering Structures, 2020. **206**: p. 110174.
13. Mohamed, H.M. and B. Benmokrane, *Reinforced concrete beams with and without FRP web reinforcement under pure torsion.* Journal of Bridge Engineering, 2016. **21**(3): p. 04015070.
14. Floruț, S.-C., G. Sas, C. Popescu, and V. Stoian, *Tests on reinforced concrete slabs with cut-out openings strengthened with fibre-reinforced polymers.* Composites Part B: Engineering, 2014. **66**: p. 484-493.
15. Enochsson, O., J. Lundqvist, B. Täljsten, P. Rusinowski, and T. Olofsson, *CFRP strengthened openings in two-way concrete slabs–An experimental and numerical study.* Construction and Building Materials, 2007. **21**(4): p. 810-826.
16. Hussein, M.J., H.A. Jabir, and T.S. Al-Gasham, *Retrofitting of reinforced concrete flat slabs with cut-out edge opening.* Case Studies in Construction Materials, 2021. **14**: p. e00537.
17. Mahlis, M., A.E. Shoeib, S. Abd Elnaby, and A. Sherif. *The effect of cutting openings on the behavior of two-way solid loaded slabs*. in *Structures*. 2018. Elsevier.
18. Mostafa, I.T., S. Mousa, H.M. Mohamed, and B. Benmokrane, *Behavior of high-strength concrete (HSC) box girders reinforced with GFRP bars, ties, and spirals under torsion.* Engineering Structures, 2023. **294**: p. 116726.
19. St. Onge, J. and A. Fam, *Torsional Behavior of Circular Concrete-Filled FRP Tubes.* Journal of Composites for Construction, 2021. **25**(3): p. 04021013.
20. Deifalla, A., M. Hamed, A. Saleh, and T. Ali, *Exploring GFRP bars as reinforcement for rectangular and L-shaped beams subjected to significant torsion: An experimental study.* Engineering structures, 2014. **59**: p. 776-786.
21. ABAQUS, H., *ABAQUS standard user's manual, version 6.14.* Providence, RI, USA: Dassault Systèmes, 2014.
22. Cao, X., L. Wu, and Z. Li, *Behaviour of steel-reinforced concrete columns under combined torsion based on ABAQUS FEA.* Engineering Structures, 2020. **209**: p. 109980.

23. ELWakkad, N.Y., K.M. Heiza, and W. Mansour, *Experimental study and finite element modelling of the torsional behavior of self-compacting reinforced concrete (SCRC) beams strengthened by GFRP.* Case Studies in Construction Materials, 2023. **18**: p. e02123.
24. Lei, Y., L. Jin, D. Li, H. Zhu, and X. Du, *Comparison of torsional damage and size effects of BFRP- and steel-reinforced concrete beams with different stirrup ratios.* Engineering Structures, 2023. **285**: p. 116042.
25. Ganganagoudar, A., T.G. Mondal, and S.S. Prakash, *Analytical and finite element studies on behavior of FRP strengthened RC beams under torsion.* Composite Structures, 2016. **153**: p. 876-885.
26. Hii, A.K. and R. Al-Mahaidi, *An experimental and numerical investigation on torsional strengthening of solid and box-section RC beams using CFRP laminates.* Composite structures, 2006. **75**(1-4): p. 213-221.
27. Jin, L., J. Bai, R. Zhang, L. Li, and X. Du, *Effect of elevated temperature on thelow-velocity impact performances of reinforced concrete slabs.* International Journal of Impact Engineering, 2021. **149**: p. 103797.
28. Sadraie, H., A. Khaloo, and H. Soltani, *Dynamic performance of concrete slabs reinforced with steel and GFRP bars under impact loading.* Engineering Structures, 2019. **191**: p. 62-81.
29. Karim, R. and B. Shafei, *Performance of fiber-reinforced concrete link slabs with embedded steel and GFRP rebars.* Engineering Structures, 2021. **229**: p. 111590.
30. DTMR, *Transport and Main Roads Specifications MRTS70 Concrete.* Transport and Main Roads Specifications 2018.
31. ASTM, *Standard test method for tensile properties of fiber reinforced polymer matrix composite bars.* ASTM D7205-11, 2011.
32. Jeng, C.-H. and T.T. Hsu, *A softened membrane model for torsion in reinforced concrete members.* Engineering Structures, 2009. **31**(9): p. 1944-1954.
33. Belarbi, A. and T.T. Hsu, *Constitutive laws of concrete in tension and reinforcing bars stiffened by concrete.* Structural Journal, 1994. **91**(4): p. 465-474.
34. Mondal, T.G. and S.S. Prakash, *Nonlinear finite-element analysis of RC bridge columns under torsion with and without axial compression.* Journal of Bridge Engineering, 2016. **21**(2): p. 04015037.
35. Hsu, L. and C.-T. Hsu, *Complete stress—strain behaviour of high-strength concrete under compression.* Magazine of concrete research, 1994. **46**(169): p. 301-312.
36. Greene Jr, G.G., *Behavior of reinforced concrete girders under cyclic torsion and torsion combined with shear: Experimental investigation and analytical models*. 2006: University of Missouri-Rolla.
37. Hsu, T.T.C., *Torsion of Structural Concrete - A summary on Pure Tension.* PCA Development Department Bulletin, 1968. **18**: p. 165-178.
38. Standards, A., *Concrete structures AS 3600:2018.* Standards Australia, 2018.
39. ACI, *Building code requirements for structural concrete.* ACI 318-14 and commentary 2014.
40. Rahnavard, R., A. Hassanipour, and A. Mounesi, *Numerical study on important parameters of composite steel-concrete shear walls.* Journal of Constructional Steel Research, 2016. **121**: p. 441-456.
41. Mott, P. and C. Roland, *Limits to Poisson's ratio in isotropic materials.* Physical review B, 2009. **80**(13): p. 132104.
42. Alomar, Z., C. Cappellini, and F. Concli, *An Element Deletion Algorithm for an Open-Source Finite Element Software*, in *Design, Simulation, Manufacturing: The Innovation Exchange*. 2022, Springer. p. 137-144.
43. DTMR. *Design Criteria for Floating Walkways and Pontoons*. Queensland Department of Transport and Main Roads 2015; Available from: https://www.tmr.qld.gov.au/business-industry/Technical-standards-publications/Design-criteria-Marine.

44. Warren, C.Y. and G.B. Richard, *ROARK'S FORMULAS FOR STRESS AND STRAIN*. 2000: MCGRAW-HILL.

5.3. Links and implications

Study in Chapter 5 conducted a comprehensive finite element (FE) analysis of the torsional behaviour of GFRP-RC decks, focusing on key design parameters like concrete compressive strength, cutout geometry, reinforcement distribution, bar diameter, and reinforcement spacing. The study found that the pre-cracking torsional behaviour is heavily influenced by concrete compressive strength, which also significantly affects the cracking torque. Interestingly, the cutout geometry did not impact the pre-cracking behaviour, with cracking in decks with various cutout shapes consistently initiating at edge of the cutout and progressing to the opposite end. Decks with more than four sets of diagonal bars, large bar diameters, and dense reinforcement spacing showed improved post-cracking rigidity and narrower cracks. Additionally, equations proposed in the study can reliably predict pre-cracking torsional strength and rigidity, taking into account the decks' concrete strength and geometric properties.

The FE simulation results closely match the actual torsional behaviour of GFRP-RC decks. Future studies are suggested to investigate other vital parameters like cutout dimensions and locations, aiming to refine the model’s precision in evaluating the impact of cutout on cracking torque and to deepen understanding of the torsional capacity of GFRP-RC pontoon deck with an edge cutout. The significant findings from this chapter as well as Chapters 3 and 4 are highlighted in the Conclusion section.

CHAPTER 6: CONCLUSION

The use of GFRP reinforcement in reinforced concrete pontoon decks is recognized as an effective corrosion-resistant solution in marine environments. However, understanding their structural performance under torsional stress from wave action remains unclear in the engineering field. This thesis has comprehensively examined the torsional behaviour of GFRP-RC pontoon decks, both with and without edge cutout, through a combination of experimental and numerical methods. Large-scale specimens were rigorously tested in a custom-designed torsion setup, integrated with digital image correlation techniques. This approach facilitated a detailed investigation of the effects of cutout, reinforcement distribution, diagonal reinforcements around cutout, and grid spacing on the decks' torsional rigidity pre- and post-cracking, cracking torque, failure mechanisms, and post-cracking strength. The research further expanded into the numerical realm, where 27 variable finite element models were created and analysed using an adjusted Concrete Damaged Plasticity (CDP) model in ABAQUS. These models, closely calibrated with experimental data, showed excellent alignment with real-world scenarios, enhancing the reliability of the findings. This modelling phase allowed for a thorough exploration of factors such as concrete compressive strength, cutout geometry, and reinforcement configuration, significantly enriching the understanding of their impact on GFRP-RC decks' torsional behaviour. Additionally, this study successfully developed equations for accurately estimating pre- and post-cracking torsional rigidity and cracking torque. These equations consider the role of GFRP reinforcement and the reduction effect of cutout, contributing valuable predictive tools for future design and analysis. The study yielded insightful and high-quality results, which are meticulously summarized and detailed in the

subsequent sections, marking a significant advancement in the field of marine structural engineering.

6.1. Torsional behaviour of GFRP-reinforced concrete pontoon decks with and without an edge cutout

This study experimentally examined the torsional behaviour of GFRP-reinforced concrete pontoon decks, with a focus on the influences of edge cutout, reinforcement-bar distribution, and rotation direction. A novel design equation was also formulated to characterize the post-cracking torsional behaviour of these decks. Key findings from this research include:

- Bar configuration played a pivotal role in the failure behaviour of the pontoon decks under torsion. Decks with double-layer reinforcement exhibited remarkable resilience, showing no failure signs up to the maximum torque. Conversely, single-layer reinforced decks were prone to excessive cracks and large torsional deformation. Decks featuring an edge cutout typically failed due to shear cracks originating at the cutout corner.
- The direction of rotation significantly influenced the cracking pattern and stress distribution, particularly affecting pre-cracking torsional rigidity by up to 17%, depending on the deck's continuity. However, it had no impact on cracking torque or post-cracking behaviour.
- The reinforcement distribution did not considerably affect initial cracking strength or pre-cracking rigidity. It was however crucial in the post-cracking stage. Double-layer reinforcement led to slower crack growth and increased torsional rigidity, with enhanced performance observed in both decks with and without edge cutout.

- The presence of edge cutout resulted in a reduction of cracking torque by about 17%, attributable to the reduced effective width and concentrated stress at the cutout corners. Additionally, decks with double-layer reinforcement and a cutout showed lower pre-cracking rigidity due to the reduction in the torsional constant.
- The ACI 318-19 equation provided conservative yet effective predictions for cracking torque, while the proposed method focusing solely on the GFRP bars' contribution accurately estimated post-cracking torsional rigidity.

It is important to note that these conclusions are based on the specific specimens and failure modes observed in this study. Further research involving larger datasets is recommended to develop a more comprehensive prediction equation, which could reliably guide the design and engineering of GFRP-reinforced concrete structures in practical applications.

6.2. Torsional behaviour of GFRP-RC pontoon decks with an edge cutout and diagonal reinforcement

This study details the key findings from pure torsion tests on GFRP-RC pontoon decks with edge cutout, focusing on various GFRP bar arrangements, diagonal bars, and grid spacing. The experimental observations and analysis of test results led to several conclusions:

- Edge cutout induced concentrated stress, causing decks to fail shortly after initial cracking due to extensive cracks or concrete crumbling. However, decks with double-layered reinforcement, diagonal bars, and dense grid spacing exhibited significantly enhanced torsional capacity, withstanding maximum load strokes without failure.

- Diagonal bars improved pre-cracking torsional behaviour, but their impact post-cracking was minimal. When combined with double-layer reinforcement, diagonal bars increased pre-cracking torsional rigidity by 26%, effectively bridging crack openings and restraining shear crack expansion.
- Decks with double-layered reinforcement demonstrated up to 100% stronger post-cracking torsional rigidity compared to single-layer reinforced decks. This improvement was due to the increased vertical distance of bars from the cross-section centroid, resulting in a higher torsional constant.
- Denser grid spacing bolstered post-cracking torsional behaviour and crack control, attributed to a greater number of continuous longitudinal bars providing additional torsional resistance and limiting crack expansion.
- Densely reinforced decks with double diagonal bars matched the torsional performance of double layer reinforced solid decks within the tested deformation range. However, their ultimate torsional capacity was lower, as the edge cutout induced high stress levels not fully mitigated by the diagonal bars and denser reinforcement.
- The ACI 318-19 equation accurately predicted deck cracking torque with a 12% standard deviation, considering the offsetting effect of diagonal bars on edge cutout influence. Additionally, a new method to predict post-cracking behaviour, including torsional rigidity and failure, was introduced, considering reinforcement specifics.

Future research should explore other parameters affecting the torsional design of GFRP-RC planks. Given the time and safety constraints of physical experiments, numerical modelling like FEA in Abaqus presents a viable alternative. Further

theoretical work is also needed to predict the ultimate torsional capacity for GFRP-RC planks without enclosed shear reinforcement, providing practical design guidance.

6.3. Study of critical design parameters on the torsional behaviour in GFRP-RC pontoon decks with edge cutout

A comprehensive finite element (FE) analysis of the torsional behaviour of GFRP-RC decks was implemented, delving into the impact of key design parameters like concrete compressive strength, cutout geometry, reinforcement distribution, bar diameter, and reinforcement spacing. The FE model was rigorously validated against experimental results from large-scale GFRP-RC deck tests. From the gathered data, several conclusions can be highlighted:

- Concrete compressive strength significantly influences the pre-cracking torsional behaviour of GFRP-RC decks, with higher strength leading to increased initial and pre-cracking torsional rigidity and cracking torque. The GFRP bars also play a role in determining the cracking torque.
- Cutout geometry does not affect the pre-cracking torsional behaviour. Regardless of the cutout shape (chamfer, fillet, or half-round), cracking consistently initiates at the edge of the top surface near the cutout and progresses towards the fixed end.
- While GFRP reinforcements, including diagonal bars, larger bar diameters, and dense reinforcement spacing, have a minor impact on the initial cracking torque, they significantly contribute to post-cracking behaviour. Configurations with more than four sets of diagonal bars, larger bar diameters, and dense reinforcement spacing enhance the post-cracking torsional rigidity and result in narrower cracks after cracking.

- The developed equations can effectively predict the pre-cracking torsional strength and rigidity of GFRP-RC decks by considering concrete compressive strength and deck geometry.

The accuracy of the FE simulations has been confirmed through comparison with actual GFRP-RC deck torsional behaviour. Future studies are recommended to investigate other critical design aspects, such as the size and placement of cutout. These investigations aim to refine the model's accuracy in depicting the impact of cutout on cracking torque and to offer a deeper understanding of the torsional capacity of GFRP-RC decks.

REFERENCES

ABAQUS, H 2014, 'ABAQUS standard user's manual, version 6.14', *Providence, RI, USA: Dassault Systèmes*.

Ahmed, EA, Settecasi, F & Benmokrane, B 2014, 'Construction and testing of GFRP steel hybrid-reinforced concrete bridge-deck slabs of Sainte-Catherine overpass bridges', *Journal of Bridge Engineering*, vol. 19, no. 6, p. 04014011.

AlAjarmeh, OS, Manalo, AC, Benmokrane, B, Karunasena, W & Mendis, P 2019, 'Axial performance of hollow concrete columns reinforced with GFRP composite bars with different reinforcement ratios', *Composite Structures*, vol. 213, pp. 153-64.

Ameli, M, Ronagh, HR & Dux, PF 2007, 'Behavior of FRP strengthened reinforced concrete beams under torsion', *Journal of Composites for Construction*, vol. 11, no. 2, pp. 192-200.

Andersen, P 1937, 'Rectangular concrete sections under torsion', *Journal Proceedings*, pp. 1-12.

Anil, Ö, Kina, T & Salmani, V 2014, 'Effect of opening size and location on punching shear behaviour of two-way RC slabs', *Magazine of concrete research*, vol. 66, no. 18, pp. 955-66.

Anumolu, S, Abdelkarim, OI & ElGawady, MA 2016, 'Behavior of hollow-core steel-concrete-steel columns subjected to torsion loading', *Journal of Bridge Engineering*, vol. 21, no. 10, p. 04016070.

Below, KD, Rangan, BV & Hall, AS 1975, 'Theory for concrete beams in torsion and bending', *Journal of the Structural Division*, vol. 101, no. 8, pp. 1645-60.

Benmokrane, B, Manalo, A, Bouhet, J-C, Mohamed, K & Robert, M 2017, 'Effects of diameter on the durability of glass fiber–reinforced polymer bars conditioned in alkaline solution', *Journal of Composites for Construction*, vol. 21, no. 5, p. 04017040.

Benmokrane, B, Sanni Bakouregui, A, Mohamed, HM, Thébeau, D & Abdelkarim, OI 2020, 'Design, construction, and performance of continuously reinforced concrete pavement reinforced with GFRP bars: Case study', *Journal of Composites for Construction*, vol. 24, no. 5, p. 05020004.

Bernardo, L & Teixeira, M 2018, 'Modified softened truss-model for prestressed concrete beams under torsion', *Journal of Building Engineering*, vol. 19, pp. 49-61.

Bernardo, LF & Lopes, SM 2008, 'Behaviour of concrete beams under torsion: NSC plain and hollow beams', *Materials and structures*, vol. 41, no. 6, pp. 1143-67.

Broo, H, Lundgren, K & Engström, B 2005, 'Shear and torsion interaction in prestressed hollow core units', *Magazine of Concrete Research*, vol. 57, no. 9, pp. 521-33.

Cao, X, Wu, L & Li, Z 2020, 'Behaviour of steel-reinforced concrete columns under combined torsion based on ABAQUS FEA', *Engineering Structures*, vol. 209, p. 109980.

Chai, H, Majeed, AA & Allawi, AA 2015, 'Torsional analysis of multicell concrete box girders strengthened with CFRP using a modified softened truss model', *Journal of Bridge Engineering*, vol. 20, no. 8, p. B4014001.

Chen, S, Peng, W & Yan, W 2018, 'Experimental study on steel reinforced concrete columns subjected to combined bending–torsion cyclic loading', *The Structural Design of Tall and Special Buildings*, vol. 27, no. 11, p. e1479.

Chiu, H-J, Fang, I-K, Young, W-T & Shiau, J-K 2007, 'Behavior of reinforced concrete beams with minimum torsional reinforcement', *Engineering Structures*, vol. 29, no. 9, pp. 2193-205.

Collins, M, Walsh, P, Archer, F & Hall, A 1968, 'Ultimate strength of reinforced concrete beams subjected to combined torsion and bending', *Special Publication*, vol. 18, pp. 379-402.

Cowan, HJ 1951, 'Tests of Torsional Strength and Deformation of Rectangular Reinforced Concrete Beams', *Concrete and constructional engineering*, vol. 46, no. 2, pp. 51-9.

Darwin, D, Dolan, CW & Nilson, AH 2016, *Design of concrete structures*, vol. 2, McGraw-Hill Education New York, NY, USA:.

de Saint-Venant, M 1856, *Mémoire sur la torsion des prismes: avec des considérations sur leur flexion ainsi que sur l'équilibre intérieur des solides élastiques en général: et des formules pratiques pour le calcul de leur résistance à divers efforts s' exerçant simultanément*, Imprimerie nationale.

Deifalla, A, Hamed, M, Saleh, A & Ali, T 2014, 'Exploring GFRP bars as reinforcement for rectangular and L-shaped beams subjected to significant torsion: An experimental study', *Engineering structures*, vol. 59, pp. 776-86.

Derkowski, W & Surma, M 2015, 'Torsion of precast hollow core slabs', *Czasopismo Techniczne*.

DTMR 2015, *Design Criteria for Floating Walkways and Pontoons*, Queensland Department of Transport and Main Roads, https://www.tmr.qld.gov.au/business-industry/Technical-standards-publications/Design-criteria-Marine>.

El-Nemr, A, Ahmed, EA & Benmokrane, B 2013, 'Flexural Behavior and Serviceability of Normal-and High-Strength Concrete Beams Reinforced with Glass Fiber-Reinforced Polymer Bars', *ACI Structural Journal*, vol. 110, no. 6.

El-Nemr, A, Ahmed, EA, El-Safty, A & Benmokrane, B 2018, 'Evaluation of the flexural strength and serviceability of concrete beams reinforced with different types of GFRP bars', *Engineering Structures*, vol. 173, pp. 606-19.

Fang, I-K & Shiau, J-K 2004, 'Torsional behavior of normal-and high-strength concrete beams', *Structural Journal*, vol. 101, no. 3, pp. 304-13.

Floruţ, S-C, Sas, G, Popescu, C & Stoian, V 2014, 'Tests on reinforced concrete slabs with cut-out openings strengthened with fibre-reinforced polymers', *Composites Part B: Engineering*, vol. 66, pp. 484-93.

Genikomsou, AS & Polak, MA 2017, 'Effect of openings on punching shear strength of reinforced concrete slabs-finite element investigation', *ACI Structural Journal*, vol. 114, no. 5, p. 1249.

Hadhood, A, Gouda, MG, Agamy, MH, Mohamed, HM & Sherif, A 2020, 'Torsion in concrete beams reinforced with GFRP spirals', *Engineering Structures*, vol. 206, p. 110174.

Hassoun, MN & Al-Manaseer, A 2020, *Structural concrete: theory and design*, John wiley & sons.

Hsu, TT 1968, 'Torsion of structural concrete-behavior of reinforced concrete rectangular members', *Special Publication*, vol. 18, pp. 261-306.

Hsu, TTC 1968, 'Torsion of Structural Concrete - A summary on Pure Tension', *PCA Development Department Bulletin*, vol. 18, pp. 165-78.

Hsu, TTC 1984, *Torsion of reinforced concrete*.

Humphreys, R 1957, 'Torsional properties of prestressed concrete', *The Structural Engineer*, vol. 35, no. 6, pp. 213-24.

Hussein, G & Eid, N 2019, 'Torsional Behavior of Irregular Structures during Earthquakes', *IOSR J. Mech. Civ. Eng*, vol. 16, no. 5, pp. 40-55.

Ibrahim, MS, Gebreyouhannes, E, Muhdin, A & Gebre, A 2020, 'Effect of concrete cover on the pure torsional behavior of reinforced concrete beams', *Engineering Structures*, vol. 216, p. 110790.

Jeng, C-H, Peng, S-F, Chiu, H-J & Hsiao, C-K 2014, 'New torsion experiment on large-sized hollow reinforced concrete beams', *ACI Structural Journal*, vol. 111, no. 6, p. 1469.

Joh, C, Kwahk, I, Lee, J, Yang, I-H & Kim, B-S 2019, 'Torsional behavior of high-strength concrete beams with minimum reinforcement ratio', *Advances in Civil Engineering*, vol. 2019.

Ju, H, Lee, D, Kim, JR & Kim, KS 2020, 'Maximum torsional reinforcement ratio of reinforced concrete beams', *Structures*, Elsevier, pp. 481-93.

Khajehdehi, R & Panahshahi, N 2016, 'Effect of openings on in-plane structural behavior of reinforced concrete floor slabs', *Journal of Building Engineering*, vol. 7, pp. 1-11.

Kim, M-J, Kim, H-G, Lee, Y-J, Kim, D-H, Lee, J-Y & Kim, K-H 2020, 'Pure torsional behavior of RC beams in relation to the amount of torsional reinforcement and cross-sectional properties', *Construction and Building Materials*, vol. 260, p. 119801.

Lampert, P 1971, 'Postcracking stiffness of reinforced concrete beams in torsion and bending', *Symposium 1971*.

Lampert, P & Thürlimann, B 1972, 'Ultimate strength and design of reinforced concrete beams in torsion and bending', in *Ultimate Strength and Design of Reinforced Concrete Beams in Torsion and Bending/Résistance et dimensionnement des poutres en béton armé soumises à la torsion et à la flexion/Bruchwiderstand und Bemessung von Stahlbetonbalken unter Torsion und Biegung*, Springer, pp. 107-31.

Lee, H-H 2017, *Finite element simulations with ANSYS Workbench 17*, SDC publications.

Lee, J-Y & Kim, S-W 2010, 'Torsional strength of RC beams considering tension stiffening effect', *Journal of structural engineering*, vol. 136, no. 11, pp. 1367-78.

Lei, Y, Jin, L, Li, D, Zhu, H & Du, X 2023, 'Comparison of torsional damage and size effects of BFRP-and steel-reinforced concrete beams with different stirrup ratios', *Engineering Structures*, vol. 285, p. 116042.

Lessig, N 1959, 'Determination of the load-bearing capacity of reinforced concrete elements with rectangular cross-section subjected to flexure with torsion', *Beton i Zhelezobeton*, no. 3.

Lopes, AV, Lopes, SM & do Carmo, RN 2014, 'Stiffness of reinforced concrete slabs subjected to torsion', *Materials and structures*, vol. 47, no. 1, pp. 227-38.

Lopes, S & Bernardo, L 2009, 'Twist behavior of high-strength concrete hollow beams–formation of plastic hinges along the length', *Engineering Structures*, vol. 31, no. 1, pp. 138-49.

Manalo, A, Mendis, P, Bai, Y, Jachmann, B & Sorbello, C 2021, 'Fiber-Reinforced Polymer Bars for Concrete Structures: State-of-the-Practice in Australia', *Journal of Composites for Construction*, vol. 25, no. 1, p. 05020007.

Mansur, MA, Ting, SK & Lee, S-L 1983, 'Torsion tests of r/c beams with large openings', *Journal of Structural Engineering*, vol. 109, no. 8, pp. 1780-91.

Maranan, G, Manalo, A, Benmokrane, B, Karunasena, W & Mendis, P 2015, 'Evaluation of the flexural strength and serviceability of geopolymer concrete beams reinforced with glass-fibre-reinforced polymer (GFRP) bars', *Engineering Structures*, vol. 101, pp. 529-41.

Mohamed, HM & Benmokrane, B 2014, 'Design and performance of reinforced concrete water chlorination tank totally reinforced with GFRP bars: Case study', *Journal of Composites for Construction*, vol. 18, no. 1, p. 05013001.

Mohamed, HM & Benmokrane, B 2015, 'Torsion behavior of concrete beams reinforced with glass fiber-reinforced polymer bars and stirrups', *ACI Structural Journal*, vol. 112, no. 5, p. 543.

Mohamed, HM & Benmokrane, B 2016, 'Reinforced concrete beams with and without FRP web reinforcement under pure torsion', *Journal of Bridge Engineering*, vol. 21, no. 3, p. 04015070.

Mohamed, HM, Chaallal, O & Benmokrane, B 2015, 'Torsional moment capacity and failure mode mechanisms of concrete beams reinforced with carbon FRP bars and stirrups', *Journal of Composites for Construction*, vol. 19, no. 2, p. 04014049.

Mondal, TG & Prakash, SS 2016, 'Nonlinear finite-element analysis of RC bridge columns under torsion with and without axial compression', *Journal of Bridge Engineering*, vol. 21, no. 2, p. 04015037.

Mostafa, IT, Mousa, S, Mohamed, HM & Benmokrane, B 2023, 'Behavior of high-strength concrete (HSC) box girders reinforced with GFRP bars, ties, and spirals under torsion', *Engineering Structures*, vol. 294, p. 116726.

Navier, C 1826, *Resume des lecons donnees a l'ecole Royale des Ponts et Chaussees sur l'application de la mecanique a l'etablissement des constructions et des machines. Premiere partie contenant les leçons sur la resistance des materiaux et sur l'etablissement des constructions en terre en maçonnerie et en charpente; par M. Navier*.

Nguyen, M & Pham, P 2017, 'An investigation on the behaviour and stiffness of reinforced concrete slabs subjected to torsion', *IOP Conference Series: Materials Science and Engineering*, IOP Publishing, p. 012017.

Nylander, H 1945, *Vridning och vridningsinspänning vid betongkonstruktioner: Torsion and torsional restraint by concrete structures*.

Okay, F & Engin, S 2012, 'Torsional behavior of steel fiber reinforced concrete beams', *Construction and Building Materials*, vol. 28, no. 1, pp. 269-75.

Pachalla, SKS & Prakash, SS 2017, 'Load resistance and failure modes of GFRP composite strengthened hollow core slabs with openings', *Materials and Structures*, vol. 50, no. 1, pp. 1-14.

Pajari, M 2004, 'Pure torsion tests on single hollow core slabs', *Espoo VTT Tiedotteita, Research Notes*, vol. 2273, pp. 29-8.

Popescu, C, Sas, G, Blanksvärd, T & Täljsten, B 2017, 'Concrete walls with cutout openings strengthened by FRP confinement', *Journal of composites for construction*, vol. 21, no. 3, p. 04016106.

Rahal, KN 2013, 'Torsional strength of normal and high strength reinforced concrete beams', *Engineering Structures*, vol. 56, pp. 2206-16.

Ramesht, MH & Tavasani, MAM 2013, 'A Case Study on Corrosion in Concrete Floating Docks in Qeshm Port', *Procedia Engineering*, vol. 54, pp. 109-16.

Raza, A, El Ouni, MH & Berradia, M 2021, 'Structural Assessment of Eccentrically Loaded GFRP Reinforced Circular Concrete Columns: Experiments and Finite Element Analysis', *Composite Structures*, p. 114528.

Sfikas, IP, Ingham, J & Baber, J 2018, 'Simulating thermal behaviour of concrete by FEA: state-of-the-art review', *Proceedings of the Institution of Civil Engineers–Construction Materials*, vol. 171, no. 2, pp. 59-71.

Shayan, A & Xu, A 2016, 'Realising 100-year bridge design life in an aggressive environment: review of the literature'.

St. Onge, J & Fam, A 2021, 'Torsional Behavior of Circular Concrete-Filled FRP Tubes', *Journal of Composites for Construction*, vol. 25, no. 3, p. 04021013.

Xu, J, Diao, B, Guo, Q, Ye, Y, Mo, Y & Zhou, T 2018, 'Parametric Study on Mixed Torsional Behavior of U-Shaped Thin-Walled RC Girders', *Advances in Civil Engineering*, vol. 2018.

Young, C, Sagar, S & Hughes, C 1922, *Torsional strength of rectangular sections of concrete, plain and reinforced*, University of Toronoto.

Yousef, AM, El-Metwally, SE, Askar, HH & El-Mandouh, MA 2019, 'Behavior of high-strength concrete interior slab-column connections with openings under seismic loading', *Construction and Building Materials*, vol. 214, pp. 619-30.

Zhou, C, Li, L & Wang, L 2019, 'Improved softened membrane model for prestressed composite box girders with corrugated steel webs under pure torsion', *Journal of Constructional Steel Research*, vol. 153, pp. 372-84.

Zia, P 1961, 'Torsional strenth of prestressed concrete members', *Journal Proceedings*, pp. 1337-60.

APPENDIX A: REVIEW OF TORSION TEST SETUP

A.1.1. Torsion test setup for beams

Fang and Shiau (2004) develop a test set-up (Figure. 8.1) to evaluate the torsion behaviour of concrete beams, which have been adapted by a number of researchers (Fang & Shiau 2004; Chiu et al. 2007; Okay & Engin 2012; Jeng et al. 2014; Joh et al. 2019; Ibrahim et al. 2020). The torsion test setup eliminates the frictional resistance by using a spherical seat under the fixed beam end. Meanwhile, the rollers beneath the two beam supports allowed the beam to move and elongate freely when deformed. This setup was designed to ensure that the RC beam is subject to pure torsion. However, the free moving roller bars can dramatically increase the difficulty of maintaining the specimen in a fixed position.

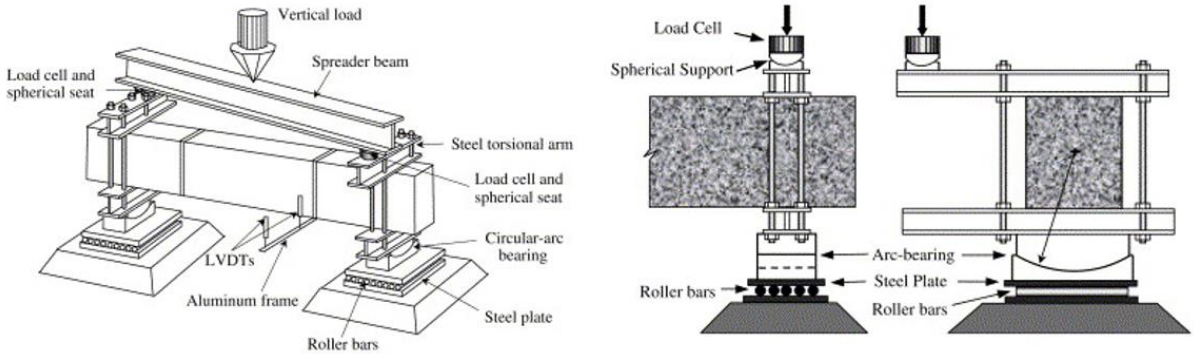

Figure A.1. Schematic torsion test setup for beam (Chiu et al. 2007)

A.1.2. Torsion test setup for reinforced square slab

Lopes, Lopes & do Carmo (2014) tested reinforced square slab under pure torsion by using the test setup shown in Figure A.2. In this test set-up, four corners of the slab are simply supported before testing. Torsion load is simulated by loading on one of the corners downward while the opposite corner's upward vertical movement was constrained. This is a relatively simple design which can easily be set in most

laboratories, but it is not suitable for large scale concrete pontoon decks since it could not diminish the stress reduction effect caused by the planks' self-weight.

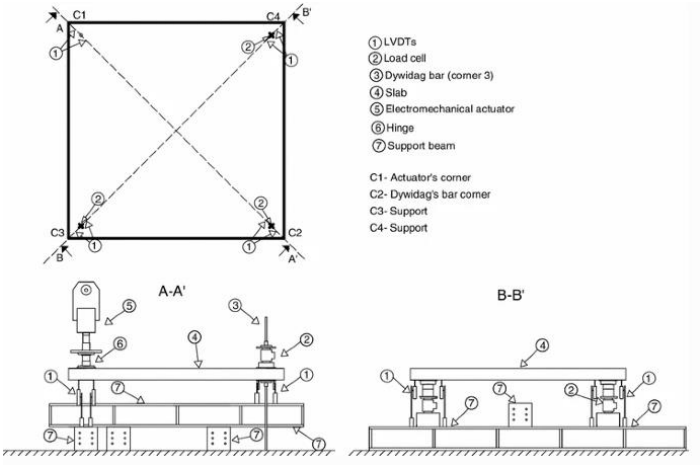

Figure A.2. Torsion test setup for reinforced square slab (Lopes et al. 2014)

A.1.3. Torsion test setup for hollow concrete slabs

Derkowkis & Surma (2015) introduced a pure torsion test for hollow concrete slabs in Figure A.3. In this test set-up, two special supports were designed to allow the two ends of the slab to move as a rigid body without additional restrictions. The active end allowed the plank to rotate around a longitudinal axis below the plank and slightly rotate around the axis perpendicular to the active end. Vertical, lateral and longitudinal movements were all restricted in the active end. On the other hand, the passive end constrained the vertical movement and rotation about the longitudinal axis of the plank. Torsion in the plank was achieved by loading eccentrically on active end. This torsion test setup is adapted to evaluate the torsion behaviour of concrete planks reinforced with GFRP bars. Detailed information of the developed test set-up will be provided in the materials and method section.

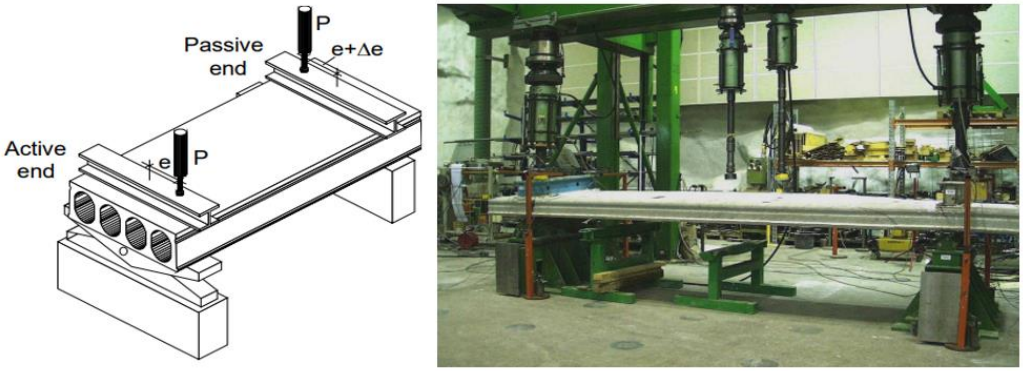

Figure A.3. Torsion test setup for hollow concrete plank (Pajari 2004; Derkowski & Surma 2015)

APPENDIX B: CONFERENCE PAPER AND RELATED PUBLICATIONS

B1.1. Concrete 2023, the Biennial Conference hosted by the Concrete Institute of Australia

Torsional behavior of GFRP-RC pontoon decks with edge cutout

Xian Yang[1], Allan Manalo[2], Omar Alajarmeh[3], Brahim Benmokrane[4], Charels-Dean Sorbello[5], Senarath Weekrakoon[6]

[1]PhD candidate, *Centre for Future Materials (CFM), School of Civil Engineering and Surveying, University of Southern Queensland, Toowoomba 4350, Australia*

[2]Professor, *Centre for Future Materials (CFM), School of Civil Engineering and Surveying, University of Southern Queensland, Toowoomba 4350, Australia*

[3]Senior researcher and teaching fellow, *Centre for Future Materials (CFM), School of Civil Engineering and Surveying, University of Southern Queensland, Toowoomba 4350, Australia*

[4]Professor, *Department of Civil Engineering, University of Sherbrooke, Sherbrooke, Quebec, Canada*

[5]*Project manager, Boating Infrastructure Unit, Department of Transport and Main Roads, Brisbane, 4000, Australia*

[6]*Principal engineer, Boating Infrastructure Unit, Department of Transport and Main Roads, Brisbane, 4000, Australia*

Abstract:

Glass fiber reinforced polymer (GFRP) bars reinforced concrete (RC) structures have attracted interests from the design engineers and infrastructure owners in Australia due to their structural efficiency and significant durability that are free from regular maintenance. However, understanding on the torsional behavior of GFRP-RC pontoon decks when subjected to wave actions is still limited. This study presented the experimental results for four large-scale GFRP-RC pontoon decks with and without a square edge cutout. The parameters investigated included edge cutout and reinforcement distribution (single and double layer). The results showed the edge cutout reduced the decks cracking torque by 17% and post-cracking torsional rigidity by 50%. ACI 318-14 equation was found reliable to predict the cracking torque of the decks.

Keywords: GFRP, pontoon deck, edge cut-out, reinforcement distribution, torsional rigidity.

1. Introduction

Structural deterioration caused by steel corrosion in reinforced concrete structures has become a serious issue around the world. In Australia, approximately AU$ 13 billion per year is required for repair or replacement associated with steel corrosion(Cassidy et al. 2015). Therefore, there is an urgent demand from the infrastructure owners for durable reinforced concrete structures requiring less regular maintenance. This has increased the interest in using glass fiber reinforced polymer (GFRP) bars as reinforcement for concrete structures especially in aggressive coastal and marine environment. Although plenty of research works have been implemented on the flexural(Al-Rubaye et al. 2020), shear (Nguyen-Minh & Rovňák 2013)and compression behavior (AlAjarmeh et al. 2019) and some design criteria for GFRP-RC structures (CSA 2012; ACI 2015) have been established, the understanding about GFRP-RC structures under torsion is still very limited. Torsional behavior is particularly crucial for structures working in the marine environment such as pontoon decks as wave actions can induced a significant torsion force. If not designed properly, early torsional cracks will happen to the pontoon decks and steel corrosion is inevitable since the crack opening provides ingress for aggressive seawater. GFRP reinforcement is an effective solution for corrosion, but more research efforts are required in the study of torsional behavior of GFRP-RC decks.

Researchers studying the torsional behavior of rectangular RC structures have primarily focused on either GFRP-RC beams or steel-reinforced slabs, with torsional behavior found to be related to concrete strength, reinforcement distribution, reinforcement properties, and the cross-sectional aspect ratio. There has been little research done on the torsional behavior of GFRP-RC decks under pure torsion. Hsu (1968) found that reinforcement has a little influence on pre-cracking torsional behavior, hence reinforced concrete acts quite

B1.2. Journal of Structure, Flexural behaviour of GFRP-reinforced concrete pontoon decks under static four-point and uniform loads

Structures 59 (2024) 105796

Contents lists available at ScienceDirect

Structures

journal homepage: www.elsevier.com/locate/structures

Flexural behaviour of GFRP-reinforced concrete pontoon decks under static four-point and uniform loads

Shahrad Ebrahimzadeh [a], Xian Yang [a], Allan Manalo [a], Omar Alajarmeh [a,*], Zaneta Senselova [a], Charles Dean Sorbello [b], Senarath Weerakoon [b], Brahim Benmokrane [c]

[a] Centre for Future Materials (CFM), School of Engineering, University of Southern Queensland, Toowoomba 4350, Australia
[b] Maritime Safety Queensland, Department of Transport and Main Roads, Brisbane, Qld 4000, Australia
[c] University of Sherbrooke, Sherbrooke, Quebec J1K 2R1, Canada

ARTICLE INFO

Keywords:
Cutout
Flexural behaviour
Four-point bending
GFRP bars
Reinforced concrete decks
Uniform distributed loading

ABSTRACT

Concrete pontoon decks are subject to flexural loading actions under concentrated and uniform loads caused by self-weight, live loads, and wave actions. This study investigated the structural behaviour of concrete pontoon decks reinforced with glass fiber-reinforced polymer (GFRP) bars under static four-point and uniform loading conditions. Five large-scale GFRP-reinforced concrete decks with a length of 2400 mm, width of 1500 mm, and thickness of 125 mm were tested to evaluate their moment capacity, strain behaviour, cracking propagation, and failure mechanism. The effects of the loading configurations, reinforcement arrangement, and cutout simulating the piles' location were evaluated. The edge cut-out initiated flexural-shear cracks, causing the pontoon decks to fail at an effective bending stress 10% lower than the solid decks. Decreasing the span-to-depth ratio from 5.6 to 4.0 increased the induced shear stress of a section and caused the deck to fail by shear compression. Uniform loading resulted in an even load distribution and minimized the stress concentration around the cutout. An increase in the effective depth improved all deck flexural characteristics. The equations in ACI 4401. R-15 and CSA S806–12 provided an accurate prediction for solid decks but overestimated the ultimate flexural strength of the GFRP-reinforced concrete decks with a cutout.

Nomenclature

a	Shear span
b	Width of rectangular cross-section
c	Distance from the extreme compression fiber to the neutral axis
d	Distance from the extreme compression fiber to the centroid of the tension reinforcement
d_v	Effective shear depth
E_c	Modulus of elasticity of concrete
E_f	Modulus of elasticity of FRP
E_{fv}	Modulus of elasticity of the FRP shear reinforcement
f'_c	Specified compressive strength
f_f	Stress in the FRP reinforcement under a specified load
f_{fu}	Design tensile strength of FRP, considering reductions for service environment
f_r	Modulus of rupture of concrete
I_g	Gross moment of inertia
k	Neutral-axis factor
K_{el}	Initial stiffness
V_c	Shear strength resistance provided by the concrete
y_t	Distance from the centroidal axis of the cross-section to the extreme fiber in tension
α_1	The ratio of the average stress of the equivalent rectangular stress block to f'_c
β_1	Factor taken as 0.85 for concrete strength up to 28 MPa. Above that, the factor was reduced at a rate of 0.05 for every 7 MPa to a minimum of 0.65
ε_{cu}	Ultimate strain in the concrete
λ	Factor to account for concrete density
ϕ_c	Resistance factor of the concrete
ρ_f	Reinforcement ratio

* Corresponding author.
E-mail address: omar.alajarmeh@usq.edu.au (O. Alajarmeh).

https://doi.org/10.1016/j.istruc.2023.105796
Received 20 August 2023; Received in revised form 30 November 2023; Accepted 19 December 2023
Available online 28 December 2023

B1.3. Journal of Structure, Development and mechanical performance evaluation of a GFRP-reinforced concrete boat-approach slab.

Structures 46 (2022) 73–87

Contents lists available at ScienceDirect

Structures

journal homepage: www.elsevier.com/locate/structures

Development and mechanical performance evaluation of a GFRP-reinforced concrete boat-approach slab

Allan Manalo [a,*], Omar Alajarmeh [a], Xian Yang [a], Wahid Ferdous [a], Shahrad Ebrahimzadeh [a], Brahim Benmokrane [b], Charles-Dean Sorbello [c], Senarath Weerakoon [c], Darren Lutze [d]

[a] University of Southern Queensland, Centre for Future Materials, West Street, Toowoomba, QLD 4350, Australia
[b] University of Sherbrooke, Sherbrooke, Quebec J1K 2R1, Canada
[c] Maritime Safety Queensland, Department of Transport and Main Roads, Brisbane, Qld 4000, Australia
[d] Inconmat, Marion, SA 5043, Australia

ARTICLE INFO

Keywords:
Approach slab
GFRP bars
Boating infrastructure
In-situ loading test

ABSTRACT

The use of glass fiber-reinforced polymer (GFRP) composite bars as internal reinforcement in concrete structures exposed to marine and aggressive environments has gained popularity in recent years. The fact that designers and workers are unfamiliar with the design and handling of GFRP bars contributes to GFRP bars being used less often than traditional steel reinforcement bars. This case study presents the construction and loading test for GFRP-reinforced concrete boat-approach slab. Two types of reinforcement mesh stemmed from a similar design requirement were implemented: 16 mm diameter bars spaced 150 mm apart in both directions and 24 mm diameter bars spaced 300 mm apart in both directions to evaluate the fabrication and installation efficiency with GFRP bars. Loading tests and monitoring were employed to evaluate the field performance of the GFRP-reinforced slab. The results show that a slab reinforced with 16 mm diameter GFRP bars can be durable and reliable, and can increase worker productivity during handing and installation. Moreover, considering the appropriate subgrade modulus for the supporting ground in the design and analysis can lead to a more cost-effective design of GFRP-reinforced concrete approach slabs. Lastly, this case study demonstrates the durability and resilience of GFRP-reinforced concrete as boating infrastructure.

1. Introduction

Most of the widespread corrosion deterioration of reinforced concrete infrastructure is due to direct contact with and exposure to seawater in coastal environments [15]. Sulfate damage is also a typical problem for reinforced concrete (RC) structures exposed to extreme environmental conditions [2]. Cadenazzi et al. [9] estimated that the most costly repairs to coastal structures were due to the corrosion of the reinforcing steel in concrete. Maritime Safety Queensland of the Department of Transport and Main Roads is spending at least $10 million per year in Queensland alone to repair and maintain boating and marine infrastructure [12]. On average, the corrosion of steel reinforcement costs the Australian economy at least $13 billion per year [13]. Moreover, the cost of steel corrosion will significantly increase if, as Wang et al. [22] predict, even in inland parts of Australia due to climate change increasing temperatures and humidity, which would accelerate steel corrosion. There are therefore significant economic benefits in using noncorroding reinforcing bars to minimize if not eliminate the corrosion of steel in reinforced concrete structures.

Using glass fiber-reinforced polymer (GFRP) bars instead of steel in marine environments and aggressive soil conditions could be more economical since GFRP is noncorroding. In recent years, GFRP bars have become more common as internal reinforcement in concrete structures because they are noncorroding, exhibit high tensile strength, and have light weight properties. Moreover, there have been advances in GFRP materials and manufacturing processes [13] which also result in the increase of its resistance against in-service elevated temperature. This has been demonstrated in a study where it was found that the tensile strength and modulus of GFRP bars were not significantly affected even after heating to temperature close to 100 °C [23]. Recent studies have also confirmed that the surrounding concrete cover extended the durability of GFRP bars in actual structures [14]. Further, the light weight of GFRP bars reduces the transportation, handling, and installation costs [12]. GFRP bars have been successfully used in durable bridge

* Corresponding author.
E-mail address: manalo@usq.edu.au (A. Manalo).

https://doi.org/10.1016/j.istruc.2022.10.040
Received 12 August 2022; Received in revised form 11 September 2022; Accepted 10 October 2022
Available online 22 October 2022